

Transport of Macromolecules Across Microvascular Walls: The Two-Pore Theory

BENGT RIPPE AND BÖRJE HARALDSSON

*Departments of Nephrology and Physiology, University Hospital, Lund; and Department of Physiology,
University of Göteborg, Göteborg, Sweden*

I. Introduction	163
II. Vesicle Controversy	164
A. Transcytosis hypothesis	164
B. Evidence in support of passive transport of plasma proteins across large pores in continuous endothelia	165
III. Assessment of Transvascular Large-Solute Transport: Theoretical Considerations	167
A. General outline of homoporous models	167
B. Homoporous approaches for assessing permeability-surface area product and reflection coefficient in lymphatic protein flux analyses	169
C. Heteroporous models of transvascular large-solute transport	174
D. Effect of vascular wall charge on large-solute transport	177
IV. General Behavior of a Two-Pore System	180
A. Computer-simulated results for two-pore membranes	180
B. Evaluation of transcapillary large-solute transfer at low lymph flow states: pore modeling ..	188
V. Brief Survey of Techniques for Assessing Transvascular Macromolecular Passage	192
A. General overview	192
B. Critique of lymphatic protein flux analyses	194
C. Critique of tissue uptake studies in intact animals	195
VI. Protein Transport in Various Vascular Beds at Low and High Transvascular Filtration Rates: Application of Two-Pore Equations	197
A. General considerations	197
B. Continuous capillaries	198
C. Fenestrated capillaries	200
VII. Structure-Function Correlations: Transport Pathways	202
A. Continuous capillaries	202
B. Fenestrated capillaries	204
VIII. Modulation of Vascular Large-Solute Permeability	205
A. Effects of some autacoids	205
B. Protein effect and albumin effect	206
C. Orosomucoid effect	207
D. Effects of neutral dextran on microvascular permselectivity	208
E. Effect of high vascular pressures on vascular permeability	208
IX. Summary	209

I. INTRODUCTION

The walls of the exchange vessels in the circulation, i.e., the capillaries and postcapillary venules, offer routes for a nearly unimpeded diffusion of lipophilic species and of small-molecular-weight hydrophilic substances between blood and tissue, yet they are nearly impermeable to macromolecules. This relative impermeability of microvascular walls to large molecules is a prerequisite for the establishment and maintenance of a fluid equilibrium between the intravascular and extravascular fluid compartments according to the classical Starling hypothesis. On the other hand, antibodies, protein-bound hormones, opsonins, cytokines, and a large

number of other macromolecular substances must continually have access to the interstitial space to be ultimately returned to the plasma via the lymphatic system. This is of particular importance in inflammatory conditions.

The mechanisms that account for the transfer of macromolecules across microvascular endothelia under normal conditions are poorly understood and have been a matter of much controversy over the last few decades. In particular, the possibility that proteins may be "shuttled" back and forth across the endothelial cells by plasmalemmal vesicles, so-called transcytosis, as originally proposed by Palade (215), has aroused much interest. That transcytosis is a major mechanism responsible

for the bulk transport of proteins across vascular walls is a view presently held by many morphologists (305, 306).

However, from a functional perspective, transvascular large-solute transport shows many characteristics that do not comply with transcytosis. From such perspectives, passive transport of macromolecules through aqueous channels, i.e., through pores or other size-selective structures (slits or pores with a matrix of fibers) in the blood-tissue barrier, would rather be the appropriate transfer mode for large solutes. This has become even more obvious over the last few decades, since we have obtained tools to make rather detailed descriptions of protein transport across the conceivably heteroporous microvascular barrier.

In the early 1950s, Pappenheimer et al. (217) formulated the pore theory of capillary permeability. It predicted the diffusion across capillary walls of small hydrophilic solutes through water-filled channels or pores of radius $\sim 40 \text{ \AA}$, which were assumed to be morphologically represented (in continuous endothelia) by the clefts between the endothelial cells. Later Grotte (102) and Mayerson and co-workers (181, 182) presented evidence for a dual ("bimodal") size selectivity of the barrier partitioning blood from lymph. Grotte (102) found that large molecular size dextrans appeared in canine leg lymph in a concentration that decreased rapidly as a function of molecular size for molecules being $<40-45 \text{ \AA}$ in radius. Larger macromolecules still appeared in the lymph, but at low lymph-to-plasma concentration (L/P) ratios, which were only slightly affected by molecular size. Grotte (102) therefore suggested that a few "large pores" or "capillary leaks" (1/30,000 of the small pores) with a radius of 250–300 \AA would account for the transcapillary passage of plasma proteins. Such a bimodal capillary selectivity concerning molecular size has now been amply confirmed in numerous tissues and species as previously reviewed (325).

Over the last two decades considerable conceptual advances have been made as to the mechanisms of transport across heteroporous membranes (100, 101, 122, 229, 252, 274, 279, 346). Although experimental data on blood-tissue transport of proteins have earlier been interpreted in two-pore or multiple-pore models, the calculations were generally based on homoporous (single pathway) formalism. The major purpose of this review is to partly reevaluate previously published data on transvascular macromolecule transport using heteroporous transport concepts and equations. In that respect, the present review may be regarded as an extension of previously published reviews on capillary transport of macromolecules (42, 47, 48, 181, 248, 252, 254, 256, 267, 324, 325). We shall try to demonstrate that it is possible in a majority of vascular beds to perform a complete analysis of the capillary wall selectivity to macromolecules from, for example, lymphatic protein sieving data without the sometimes complicating procedure of elevating venous pressure, which has hitherto been the established approach for determining the capillary barrier characteristics in terms of pore sizes and numbers (325).

II. VESICLE CONTROVERSY

A. *Transcytosis Hypothesis*

One conspicuous feature of endothelial cells, when investigated using routine electron microscopy, is the abundant presence in their cytoplasm of "vesicles" (radius $\sim 250 \text{ \AA}$) of plasmalemmal origin, so-called plasmalemmal vesicles. Ever since their discovery (215), they have been postulated to take part in the bulk transport of large solutes across the endothelial barrier by cytopempsis (200), i.e., transcytosis (28, 131, 306, 307) as previously extensively reviewed (305–307, 309, 336). Electron microscopic investigations have demonstrated how large solutes (e.g., ferritin) or particles (such as colloidal gold particles or gold-albumin complexes) (92) enter the plasmalemmal vesicles or invaginations from the lumen either to remain in the fluid phase ("true" fluid-phase transcytosis) or to be bound to the plasmalemmal membranes receptors (receptor-mediated transcytosis) and subsequently appear in the interstitial space. This can no doubt give the impression that transcytosis is a quantitatively important transfer mode. However, the interpretation can in many cases be that the transfer of large solutes to the interstitium has occurred through nearby large pores (148) or through pathways established across endothelial cells by random confluences of plasmalemmal vesicles (311). Thus the appearance of tracer within abluminal vesicles or membrane invaginations may be a secondary phenomenon. Recent dynamic electron microscopic studies of capillaries in the rete mirabile of the eel, using terbium as an electron-dense macromolecular marker, have demonstrated the presence of abluminal patches of intravascularly given tracer at a considerable distance away from the intercellular junctions (337). These patches that were bounded by pericytes, thereby hindering the dissipation of tracer in the interstitium, regularly showed higher tracer concentrations than plasmalemmal vesicles. This suggests that tracer transfer may have occurred through channels formed by transiently fused plasmalemmal vesicles.

A different model of the processing of large molecules across the endothelium than the classical transcytosis hypothesis has been proposed by Clough and Michel (39, 40) based on the uptake kinetics of ferritin into vesicles communicating with the endothelial cell surfaces, the so-called "fusion-fission" model. In this model, vesicles, or actually invaginations of the plasmalemmal membrane, communicating with the cell surface, are rapidly labeled with the molecular probe to later fuse with either "free" vesicles or with invaginations from the opposite cell surface. If free vesicles are engaged, the latter may eventually fuse with cavities communicating with either of the endothelial cell surfaces.

Because of the possible involvement of molecular binding sites for molecules on the vesicle membranes (91, 92, 146, 293, 294, 305), transcytosis would be satura-

ble, i.e., it would follow Michaelis-Menten kinetics. Conceivably, transcytosis should exhibit a temperature coefficient that is larger than that characterizing passive transport (146) by diffusion/convection, since it may involve active components. In addition, membrane fluidity and cytoplasmic viscosity is expected to be more reduced for any given temperature reduction than is water viscosity. Also, transcytosis should be regarded more or less as a dissipative (diffusive) transport mechanism (248, 249).

In an *in vitro* system of cultured endothelial cells from large (porcine) arteries grown to confluence on a polycarbonate Micropore filter, Shasby and Shasby (298) reported that the interstitial to lumen transport rate of radiolabeled albumin was twice that occurring from lumen to interstitium. In this system albumin was reported to be transported against a concentration gradient, and furthermore, its transport could be inhibited by NaCN, indicating active transport. However, subsequent investigators (303) have not been able to reproduce these findings using similar large-vessel endothelial cell cultures. The latter authors concluded that albumin is not actively transported from the abluminal to the luminal side or vice versa in cultured endothelium from bovine and sheep pulmonary arteries. Anyway, cultures of large vessel endothelia grown out after several passages and subjected to, for example, ethanol and trypsin treatment may not be representative of normal capillary endothelium *in vivo*. Actually, the fluxes of albumin reported in the mentioned studies were ~50-fold higher than those measured in, for example, isolated perfused rat hindquarters (105, 279), supporting this contention.

Physiologists who have analyzed large-solute transport generally have found little or no positive evidence in favor of transcytosis as an important mechanism for the transport of plasma proteins across microvascular walls (276, 325). Bulk transport of proteins from blood to interstitium (or lymph) thus seems to follow first-order kinetics and not Michaelis-Menten kinetics. Furthermore, in studies on whole organs, transvascular large-solute transport seems to exhibit a temperature coefficient not very different from that characterizing passive transport (279). Capillary protein transport also appears to be highly dependent on the level of capillary pressure and in part on the rate of net transcapillary filtration (105, 279, 325). The evidence supporting the notion that plasma proteins are passively transported across microvascular walls is summarized in section II.B.

B. Evidence in Support of Passive Transport of Plasma Proteins Across Large Pores in Continuous Endothelia

1. General considerations

Since large pores are predicted to be very rare, constituting only 1 part per 10,000–30,000 of the total popu-

lation of pores, the chance for their visualization in electron micrographs is so minor that, if seen, they may easily be dismissed as artifacts. It is then hardly to be expected that the large-pore system could be revealed by ultramicroscopic techniques. The evidence in support of large-pore transport is thus partly indirect and based on physiological studies on the sieving characteristics of the blood-interstitial barrier or the blood-lymph barrier in a variety of microvascular beds. For example, lymphatic protein flux analyses in general support the observations originally made by Grotte (102). Passive convection of large solutes across the rare large pores can readily account for the bulk transfer of the major plasma proteins from the blood to tissue, although albumin and smaller macromolecules can be predicted to also permeate the capillary membrane by diffusion through the interendothelial clefts (small pores).

In practically all previous lymphatic protein flux analyses there is a coupling of large-solute transport to transcapillary volume flow (47, 48, 252, 259, 262, 325) at any given plasma colloid osmotic pressure. This seems to hold even for macromolecules as large as fibrinogen (221, 259). Hence, normal transvascular protein transport would be mostly convective and, hence, largely unidirectional as demonstrated by several authors (18, 71–73, 106, 161, 208, 279, 289, 350). Altering the transvascular volume flow by changing plasma colloid osmotic pressure should, however, lead to uncoupling of protein transfer from fluid flow. Recent studies in intact rats suggest, however, that coupling of protein flux to volume flow, even when induced by capillary pressure elevations, may be less pronounced in skin and muscle *in vivo* than generally found in lymphatic flux analyses *in vitro* (243, 258). We return to this issue in section V.

2. Volume recirculation concept

As is discussed at some length below, the fraction of diffusion (or vesicular transport) contributing to the total transcapillary transport of macromolecules under conditions when the transvascular filtration rate is high must be insignificant (47, 48, 252, 325). Results from studies by Rippe et al. (279) using serum-perfused rat hindquarters indicate that convection across large pores must be the principal mechanism whereby macromolecules pass continuous capillary walls even at zero lymph flows.

Rippe et al. (279) investigated the rat hindquarter microvascular bed during maximal arteriolar dilatation (using isoprenaline or low doses of papaverine). The experiments were designed as paired, parallel perfusions of one test hindquarter preparation and one control, using oxygenated heparinized horse serum or mixtures of horse serum and bovine serum albumin (sometimes diluted with Tyrode solution) as perfusates. The hindquarters were arranged for a gravimetric technique, allowing continuous monitoring of tissue weight and of arterial and venous pressures and perfusate flow. The control animal was usually kept at 36°C, whereas the

test animal was cooled via its perfusate to a rectal temperature of 14–16°C. Tissue weight could be held constant over time (isogravimetric conditions), or the preparations could be arranged for conditions of steady weight gain over time by raising venous pressure and hence capillary pressure. When all hemodynamic parameters and the capillary filtration coefficient (L_pS) were stable, radiolabeled serum albumin [^{125}I -albumin (RISA)] was added to the perfusate, and perfusion was continued for 40–60 min. After this RISA perfusion, tracer-free perfusate was employed to wash the hindquarter vasculature free from tracer during 6–8 min. Muscle tissue samples were then taken and analyzed with respect to their content of fluid (from wet to dry weight ratios) and RISA. Blood-to-tissue RISA clearance was calculated as the transvascular mass transfer of RISA per unit time and unit tissue weight divided by the plasma RISA concentration prevailing during tracer perfusion.

In these experiments there was a significant coupling between RISA flux and net transcapillary fluid filtration, the coupling coefficient being 0.063 and 0.079 at 14 and 37°C, respectively. Cooling the hindquarters from 36 to 14°C did not reduce the transcapillary RISA flux more than in proportion to the increased viscosity, as discussed in section II B3. The most striking finding in the experiments was, however, that the RISA clearance during isogravimetric conditions proved to be dependent on the plasma (perfusate) colloid osmotic pressure (π_p). Since “clearance” (Cl) represents the rate of mass transfer divided by the plasma (tracer) concentration, it should be completely independent of the latter parameter. However, the dependence of clearance on π_p during, for example, isovolumetric conditions can be understood if the concept of volume recirculation in heteroporous (two-pore) membranes is introduced.

If large pores exist in the vascular wall, there will always be a bulk filtration of plasma across these pores along the local capillary-to-interstitial hydrostatic pressure gradient, regardless of the direction and magnitude of the volume flow occurring across the small pores. This is because the effective colloid osmotic pressure gradient across large unselective pores is much too low to balance out the normal blood-tissue hydrostatic pressure gradient prevailing here. If the hydrostatic capillary pressure in a vascular bed is lowered slightly, so that net filtration and hence lymph flow ceases, absorption of fluid across small protein-sieving pores will be in perfect balance with the continuous large pore bulk filtration. In this transient isovolumetric state of the tissue, protein-rich fluid leaves the microvasculature across large pores, but this fluid filtration is exactly balanced by an equally large absorption into the microvessels of protein-poor fluid across the small pores. Hence, due to volume recirculation, there is a net convective flux of proteins by solvent drag in the absence of a net convection. This transient situation may prevail for approximately an hour in muscle (118, 279), but cannot be maintained during steady-state conditions. During steady state, fluid filtration is usually approxi-

mately equally partitioned between small and large pores.

The net convective protein flux by volume recirculation in a heteroporous membrane appears in many respects as a diffusive process. Hence, in previous homoporous analyses of transvascular protein transfer, it has been included in the “dissipative” [or permeability-surface area (PS) product] term. However, volume recirculation seems to make up the major portion of the apparent (homoporous) PS . The rate of volume recirculation is determined by the hydrostatic pressure difference prevailing across the large pores and indirectly by the colloid osmotic pressure difference existing across the small pores ($\Delta\pi$). Hence, Rippe et al. (279) analyzed the relationship between Cl and $\Delta\pi$ in accordance with theoretical predictions for a two-pore membrane (100, 125, 138, 229, 346). Extrapolating their Cl data to a situation where $\Delta\pi$ equals zero enabled them to calculate the true diffusive component of protein (albumin) transfer during isogravimetric conditions. Only ~30% of the total “isogravimetric” albumin clearance was found to be due to diffusion (through small pores), whereas as much as ~70% was found to occur by convection (through large pores) caused by fluid recirculation from large to small pores.

The dependence of Cl on $\Delta\pi$ has been explicitly demonstrated also for the pleural membrane (145) and, retrospectively, by Rippe and Haraldsson (272, 274) for the macromolecular sieving data published by Renkin and co-workers (259, 262) from the dog’s paw. This behavior is characteristic of all heteroporous membranes and is discussed at some length in section III C. Thus, whenever it is possible to demonstrate a dependence of protein clearance on transvascular colloid osmotic pressure gradient at or near “isovolumetric” states, this should be taken as evidence in favor of protein transport through large pores and not by vesicles. Heteroporous transport may, at least partly, explain why the apparent microvascular PS to albumin appears to be reduced after plasmapheresis (359) or increased after plasma volume expansion using colloids (261).

3. Effects of temperature reductions on large-solute transport

Rippe et al. (279) showed that tissue cooling from 36 to 14°C reduced the transcapillary RISA flux in due proportion to the increased viscosity, but not at all to the marked extent that the tissue metabolism was reduced. This seems to favor the notion that transcapillary albumin transport is completely passive in nature. Even though the movement of vesicles across the cytoplasm would not require very much energy, the process of fusion/fission of membranes or binding of molecules to plasmalemmal membrane receptors in the vesicles would be dependent on the cellular metabolism. Furthermore, the fluidity of membranes and/or the cytoplasm would be highly temperature dependent. Thus results from the mentioned experiments do not support the transcytosis hypothesis.

4. Effects of chemical fixation of endothelium on large-solute transport

Haraldsson and Johansson (108) were able to produce a light to moderate chemical fixation of vascular endothelium by short-term (3 min) perfusion fixation of the rat hindquarter vasculature using glutaraldehyde. After washout of the fixative (using dextran-Tyrode solution), the hindquarters could again be perfused with serum. In such fixed, but perfused, vascular beds RISA transport was reduced, but only to the extent that the capillary hydraulic conductance and the small-solute diffusion capacities (PS for Cr-EDTA and cyanocobalamin) were altered. Thus the permeability of the microvascular walls with regard to RISA was apparently not reduced; only the capillary surface area had decreased.

5. Morphological data challenging the transcytosis hypothesis

With the use of ultrathin ($\sim 140 \text{ \AA}$) serial sectioning of endothelial cells from various capillaries, it has been demonstrated that free plasmalemmal vesicles in fact are not as frequent as previously thought (29, 32, 33, 80–84). Virtually all of the apparently free vesicles seen in routine electron micrographs appear to be parts of racemose invaginations from the cell surfaces as originally postulated by Bundgaard et al. (32). This has been demonstrated using both conventional chemical fixation as well as rapid fixation using slam freezing (84). Thus, if the vesicular system is partly involved in transvascular exchange of macromolecules, this transport must probably occur through rare temporary connections between the luminal and abluminal set of invaginations forming channels (311). However, such patent transcellular channels are almost never found by electron microscopists, at least not in true capillaries (83, 132, 351, 352).

The evidence cited above thus supports the notion that passive filtration (convection) across large pores (radius 200–400 \AA) must be the principal mechanism responsible for the bulk passage of macromolecules from blood to tissue and that transcytosis plays only a minor role in this transport (274, 276). On the other hand, transcytosis may be a transport mode allowing highly selective passage of, for example, hormones, such as insulin (146, 124a), and possibly lipoproteins (310, 336) across the endothelium, whereas the bulk passage of plasma proteins is most likely a passive phenomenon.

III. ASSESSMENT OF TRANSVASCULAR LARGE-SOLUTE TRANSPORT: THEORETICAL CONSIDERATIONS

A. General Outline of Homoporous Models

1. Linear transport formalism

Based on irreversible thermodynamics, Kedem and Katchalsky (136–138) derived a set of equations describ-

ing the flow of solvent (J_v) and solute (J_s) across homoporous and heteroporous membranes. For fluid flow the following is valid

$$J_v = L_p S (\Delta P - \sigma \Delta \pi) \quad (1)$$

and for solute flux through a homoporous membrane

$$J_s = J_v (1 - \sigma) \bar{C} + PS \Delta C \quad (2)$$

where $L_p S$ represents the hydraulic conductance (the product of hydraulic conductivity and membrane surface area); ΔP is the transmembrane hydrostatic pressure gradient; σ is the reflection coefficient of the membrane to the solute; $\Delta \pi$ is the transvascular osmotic pressure gradient; PS the solute permeability-surface area product; $\Delta C = (C_p - C_i)$, the solute concentration gradient, where C_p and C_i stand for solute concentration in plasma and interstitium, respectively; and \bar{C} is the mean intramembrane solute concentration. The \bar{C} varies in a complex nonlinear fashion as a function of $J_v(1 - \sigma)$ and PS . For high values of PS or low values of J_v , transport is diffusion dominated and \bar{C} approximately equals $(C_p + C_i)/2$. However, for low values of PS or high J_v values, \bar{C} will approach C_p . The permeability coefficient (P) equals the ratio of the apparent transcapillary diffusion coefficient of solute over the diffusion distance, i.e., $D_s/\Delta x$. Thus the second term to the right in Equation 2 contains a differential.

2. Nonlinear transport formalism

Integration of Equation 2 across the membrane and between the boundary conditions C_p and C_i yields the following equation

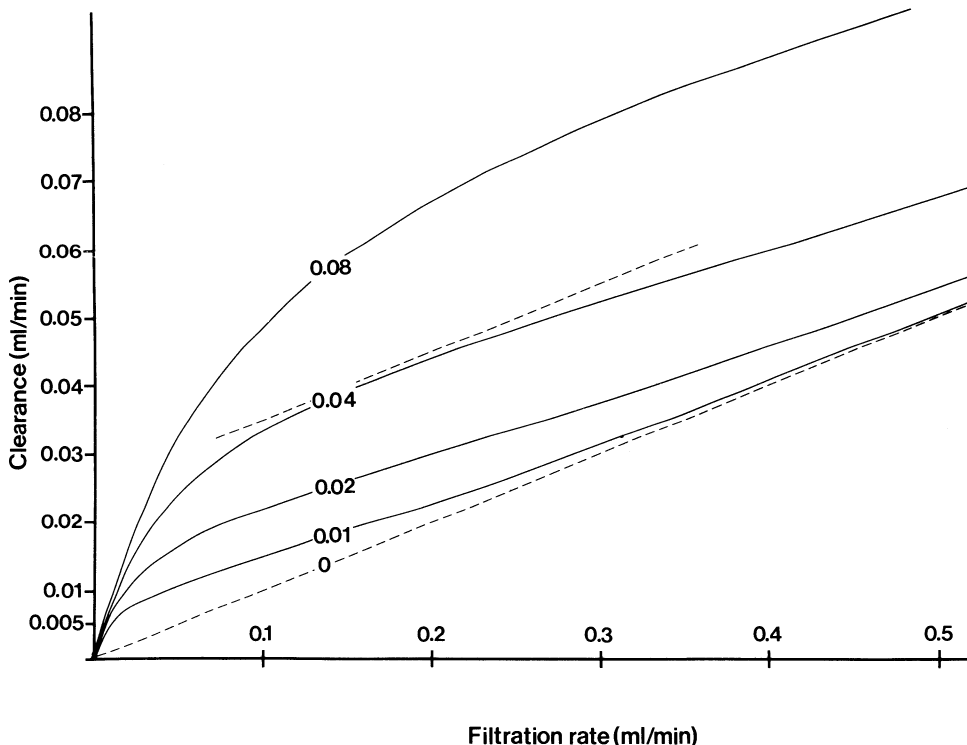
$$J_s = J_v (1 - \sigma) \frac{C_p - C_i e^{-Pe}}{1 - e^{-Pe}} \quad (3)$$

where $Pe = J_v(1 - \sigma)/PS$, i.e., here Pe represents a modified Peclet number (26, 171, 228, 329). Equation 3 is known as the familiar nonlinear global convection/diffusion equation, or in the form written above, as the Patlak equation (228).

Solute clearance (Cl) across the membrane is obtained by dividing both sides of Equation 3 by the plasma concentration of solute

$$Cl = J_v (1 - \sigma) \frac{1 - (C_i/C_p) e^{-Pe}}{1 - e^{-Pe}} \quad (4a)$$

or when the system is in steady state, i.e., when the transcapillary clearance is in equilibrium with the lymphatic clearance of solute (cf. Ref. 97)



$$Cl = J_v \frac{1 - \sigma}{1 - \sigma e^{-Pe}} \quad (4b)$$

This equation may be partitioned in a convective and a diffusive component for conditions when solute enters the membrane

The first term to the right in *Equation 5* approaches zero when Pe is large, and hence, the “diffusive component” of clearance will approach zero at high volume flows. In practice, transport is convection dominated already when Pe is larger than ~ 3 . Figure 1 illustrates steady-state homoporous clearance as a function of J_v . For $\sigma = 0.9$ and $PS = 0.01$ (ml/min) (bottom solid line in Fig. 1), Pe becomes >3 when J_v exceeds 0.3 ml/min. In this situation, (protein) clearance can be approximated by $J_v(1 - \sigma)$. For $PS = 0.08$ (ml/min), Pe becomes >3 first when J_v exceeds 0.24 (ml/min).

The initial serum-to-tissue (unidirectional) clearance of solute can be described as the solute clearance occurring when the interstitial space is considered large and the amount of interstitially accumulated solute (tracer) is small; that is, when tracer $C_i \sim 0$ (cf. Refs. 274, 279). Then Equation 4 reduces to

$$Cl = J_v \frac{1 - \sigma}{1 - e^{-Pe}} \quad (6)$$

The limit of both Equations 4 and 6 when J_v approaches infinity ($\text{Pe} > 3$) is $\text{Cl} = J_v(1 - \sigma)$. Whereas Cl ap-

proaches zero in *Equation 4* when J_v goes to zero, Cl in *Equation 6* goes to PS for $J_v = 0$. *Equation 6* thus fulfills the criteria necessary for describing unidirectional tracer transport.

3. Permeability-surface area product

The capillary diffusion capacity (PS) is defined as

$$PS = \frac{D_s}{\Delta x} A = \frac{D_s}{\Delta x} \frac{A}{A_o} \times A_o = D_o \frac{A_o}{\Delta x} \frac{A}{A_o} \quad (7)$$

where D_s is the free diffusion coefficient of solute, A represents the effective (apparent) pore area available for restricted diffusion (159, 217), and A_o is the total cross-sectional pore area; A/A_o thus represents a factor determining the degree of "restricted" to free diffusion occurring across the permeable pathways under study. The term $A_o/\Delta x$ is the total unrestricted pore area over unit diffusion path length (in cm/100 g tissue) and may be calculated (for cylindrical pores) from the tissue capillary hydraulic conductance (in $\text{ml} \cdot \text{min}^{-1} \cdot \text{mmHg}^{-1}$ · 100 g^{-1}) applying Poiseuille's law (159, 216).

$$\frac{A_o}{\Delta x} = \frac{8\eta L_p S}{r^2 \times 60 \times 1.320} \quad (8)$$

where η is water viscosity, which is here set to 0.007 $\text{dyn} \cdot \text{s}^{-1} \cdot \text{cm}^{-2}$, and 1,320 is a factor converting millimeters of mercury into dynes per square centimeter, while 60 converts minutes to seconds.

The solute diffusion coefficient D_s is defined by

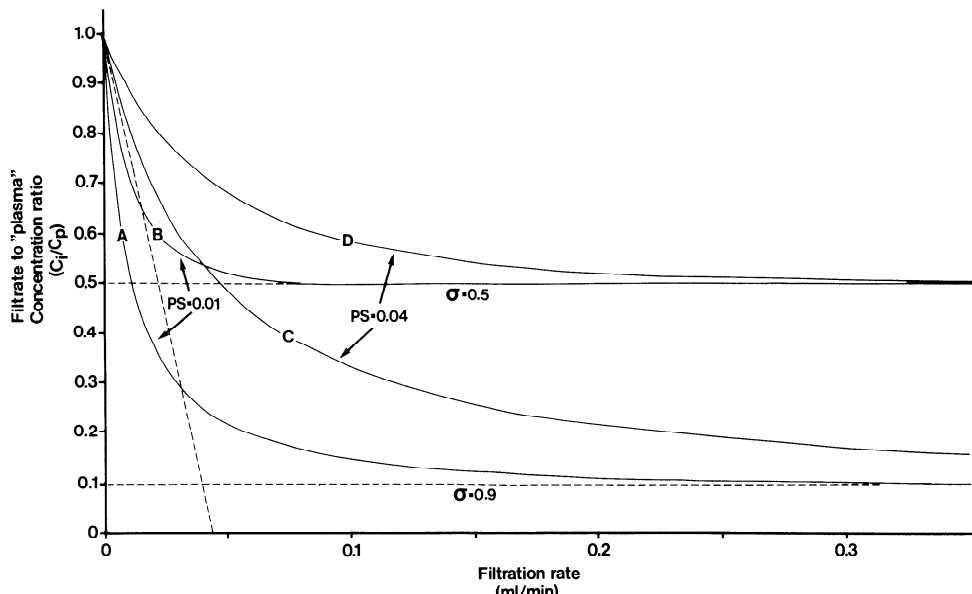


FIG. 2. Filtrate-to-plasma concentration ratio (C_i/C_p) of solute as a function of net J_v in 4 homoporous membranes. Curves A and B are simulated (Eq. 3) for $PS = 0.01$ ml/min, and curves C and D for $PS = 0.04$ ml/min. Curves A and C are simulated from a membrane having $\sigma = 0.9$, and curves B and D from a membrane having $\sigma = 0.5$. Tangent of curve C for $J_v = 0$ intersects abscissa at $J_v = 0.0444$, and slope of this tangent is -22.5 . Thus, for $\sigma = 0.9$, a PS value of 0.04 ml/min can be calculated [from initial slope $= -(\sigma/PS)$] (99). Note that increases in PS (or reductions in σ) reduce initial slope of C_i/C_p vs. J_v function (cf. Ref. 99).

$$D_s = \frac{RT}{6\pi \times N \times a_e \times \eta} \quad (9)$$

where a_e refers to the solute radius, RT is the product of the gas constant and the temperature in degrees Kelvin, and N is Avogadro's number.

Solving for PS in Equation 4b yields (cf. Ref. 23)

$$PS = J_v(1 - \sigma)/\ln \left[\frac{Cl\sigma}{Cl - J_v(1 - \sigma)} \right] \quad (10)$$

Solving for PS in Equation 6 for unidirectional solute transfer yields

$$PS = J_v(1 - \sigma)/\ln \left[\frac{Cl}{Cl - J_v(1 - \sigma)} \right] \quad (11)$$

In lymphatic protein flux analyses, lymph flows and lymph-to-plasma protein concentration ratios (C_L/C_p) are usually measured during conditions close to steady state. If one can assume that C_L/C_p equals C_i/C_p (250, 291), then according to Equation 4b

$$\frac{C_i}{C_p} = \frac{1 - \sigma}{1 - \sigma e^{-Pe}} \quad (12)$$

the C_i/C_p will gradually decrease for increasing lymph flows (J_v) to eventually reach a minimum value that is not further changed by increases in lymph flow. This limiting value for C_i/C_p equals $(1 - \sigma)$ (Fig. 2) (cf. sect. III B4). Once σ is determined, PS can be calculated at any given C_i/C_p and lymph flow (J_v) from a modification of Equation 10

$$PS = J_v(1 - \sigma)/\ln \left[\frac{\frac{C_i}{C_p} \sigma}{\frac{C_i}{C_p} - (1 - \sigma)} \right] \quad (13)$$

Another way of solving for PS when σ is known is to employ the first derivative of the C_i/C_p versus J_v function (Eq. 12) when $J_v = 0$. Thus it can be shown that this function has a slope of $-(\sigma/PS)$ for $J_v = 0$ (99). As a consequence, if PS is relatively small, then the C_i/C_p function will initially fall very steeply when J_v increases, whereas if PS is large, the initial slope of the C_i/C_p J_v function will be much less steep (Fig. 2).

B. Homoporous Approaches for Assessing Permeability-Surface Area Product and Reflection Coefficient in Lymphatic Protein Flux Analyses

The various approaches presented in this section for assessing homoporous PS (PS_{app}) and apparent σ (σ_f) from steady-state lymphatic protein flux data are illustrated by their application to lymph-to-plasma protein concentration ratios (C_i/C_p or R), blood-lymph clearances (LR, see below), and apparent PS values [$LR/(1 - R)$] versus J_v (L) for albumin, immunoglobulin G (IgG), and fibrinogen/macroglobulin (FM) from the dog's paw published by Renkin et al. (259; cf. also 47, 252) as listed in Table 1.

1. Linear flux equation for a semipermeable membrane

Renkin (247) and Garlick and Renkin (90, 257) employing Equation 2 for assessing capillary permeability to macromolecules made the simplifying assumption that $\sigma = 1$. Then, PS is easily solved from C_i/C_p

TABLE 1. Steady-state lymphatic protein flux data from the dog's paw

J _v Level	J _v (L), μl · min ⁻¹ · 100 g ⁻¹	Δπ, mmHg (C _p = 4.6)	C _i / C _p (R)			LR Clearance, μl · min ⁻¹ · 100 g ⁻¹			LR/ 1 - R (PS _{app}), μl · min ⁻¹ · 100 g ⁻¹			1 - R 1 + R			
			Total protein	Albumin	IgG	FM	Albumin	IgG	FM	Albumin	IgG	FM	Albumin	IgG	FM
1	18.48	9.43	0.402	0.469	0.358	0.188	8.67	6.62	3.47	16.32	10.31	4.28	0.3615	0.4728	0.6835
2	53.04	11.22	0.255	0.294	0.203	0.124	15.59	10.77	6.58	22.09	13.51	7.51	0.5456	0.6625	0.7794
3	78.96	11.99	0.187	0.236	0.156	0.098	18.63	12.32	7.74	24.39	14.59	8.58	0.6181	0.7301	0.8215
4	96.00	12.16	0.172	0.223	0.154	0.085	21.41	14.78	8.16	27.55	17.48	8.92	0.6353	0.7331	0.8344
5	147.8	12.53	0.137	0.165	0.121	0.074	24.39	17.89	10.94	29.21	20.35	11.81	0.7167	0.7841	0.8622
6	175.0	12.47	0.143	0.159	0.119	0.074	27.82	20.82	12.95	33.08	23.63	13.98	0.7256	0.7873	0.8622

Steady-state lymphatic protein flux data from dog paw (259; cf. also Refs. 47, 252) obtained at 6 different lymph flows (J_v). All data are recalculated for 100 g paw tissue (assuming 25 g as an average paw tissue weight). Transvascular osmotic pressure gradient (Δπ) values are calculated assuming a plasma total protein concentration of 4.6 g% (46 g/l) and applying Equation 3.5 in Ref. 159. C_i/C_p, lymph-to-plasma protein concentration ratio; IgG, immunoglobulin G; FM, fibrinogen/macroglobulin; PS_{app}, apparent permeability-surface area product. [Data from Renkin et al. (259).]

$$PS = \frac{J_v \times \frac{C_i}{C_p}}{1 - \frac{C_i}{C_p}} \quad (14a)$$

or, denoting C_i/C_p = R and J_v = L

$$PS = \frac{LR}{1 - R} \quad (14b)$$

Note, however, that because this apparent PS value here contains both a convective and a diffusive term, PS (Eq. 14b) will increase with increasing volume flows, as illustrated by the data of Renkin et al. (259) in Figure 3A. At any given volume flow (L), the apparent PS values, however, were shown to decrease with increasing solute radius in a bimodal fashion, supporting the notion of a dual selectivity of the vascular walls in agreement with Grotte's initial prediction. Because the transport for solutes larger than ~50 Å in radius is not likely to be diffusive, this technique for evaluating the selectivity of vascular walls at normal or elevated lymph flow is far from being satisfactory. Above all, the large-pore radius will be greatly overestimated, since the degree of apparent restricted "diffusion" will be very minor for macromolecules larger than ~50 Å in radius. Thus, as described in section III C6, the clearances of solutes >50 Å in radius are likely to decline with increasing molecular radius (a_e) in proportion to the reduction of (1 - σ) with a_e and not due to predictions compatible with restricted diffusion.

2. Linear flux equation: slope method

The next step of development of theory was to include the convective term of Equation 2 in assessments of microvascular selectivity (230, 259, 262). Hence, attempts were made to estimate both PS and σ. It was

then usually assumed that the mean solute concentration in the membrane equals (C_i + C_p)/2, which is, however, true only for diffusion-dominated transport. Under these conditions the following relation for R (=C_i/C_p) is obtained

$$R = \frac{C_i}{C_p} = \frac{PS + \frac{J_v}{2}(1 - \sigma)}{PS + \frac{J_v}{2}(1 + \sigma)} \quad (15)$$

Since Equation 15 contains two unknowns, PS and σ, at least two successive determinations of C_i/C_p and corresponding lymph flows are required for its solution. This can be done graphically by plotting LR/(1 - R) (Eq. 14b) versus the fluid filtration rate (J_v or L). The slope of this relationship can be shown to equal (1 - σ)/2σ and its ordinate intercept equals PS/σ (259), but other graphical solutions are also possible (230). The technique is demonstrated in Figure 3A using a linear regression analysis of LR/(1 - R) (apparent PS) for albumin versus J_v using Table 1 data. A plot of LR (cf. Eq. 15), i.e., albumin clearance, versus J_v is also shown. Further details of the "slope method" have been presented elsewhere (230, 259, 262, 326, 325). The problem of using Equation 15 is that the limiting value of R in this equation is (1 - σ)/(1 + σ) for high J_v values, whereas the correct value is (1 - σ). Thus Equation 15 is not valid unless lymph flows are kept low. Furthermore, Equation 15 is only valid for homoporous membranes and greatly overestimates true PS for heteroporous membranes.

3. Linear flux equation: cross-point method

Taylor et al. (326) came up with a slightly different homoporous and linear technique to solve PS and σ_f from lymphatic protein flux data. Steady-state lymph-to-plasma protein concentration ratios for stepwise increments of J_v are used to calculate both an apparent

PS , setting σ equal to one (from *Eq. 14b*), and an apparent σ , setting PS equal to zero (*Eq. 15*), respectively, when the mean intraporous concentration of solute (\bar{C}) is set to $(C_i + C_p)/2$ (or to C_p). In a diagram with the apparent $PS[LR/(1 - R)]$ on the abscissa and the apparent $\sigma[(1 - C_i/C_p)/(1 + C_i/C_p)]$ or $(1 - C_i/C_p)$ as derived from *Eq. 15* or *Eq. 12*, respectively, setting $PS = 0$ on the ordinate, the coordinates for these extreme points can be connected by a straight line for every set of steady-state J_v and C_i/C_p values. When this is done for successive elevations of J_v , and hence decreases in C_i/C_p , the lines corresponding to each pair of data would theoretically intersect in a specific point for a perfectly homoporous membrane, at least when J_v is relatively low. The coordinates of this point of intersection would be $x = PS$ and $y = \sigma$. The principle is shown in Figure 3B using four successive sets of C_i/C_p versus J_v data for albumin (1-4 in Table 1) from Renkin et al. (259) and setting $\bar{C} = (C_i + C_p)/2$.

From Figure 3B it is evident that there is no unique point of intersection for the experimental data. First, σ_f tends to increase with increasing J_v . At high filtration rates, σ is actually underestimated when $\bar{C} = (C_i + C_p)/2$. Second, the apparent PS (PS_{app}) shows abnormal behavior. Apparent PS first increases with increasing J_v to reach a maximum, to again decline when J_v goes to infinity. The cross-point method works reasonably well for homoporous membranes at low J_v values ($Pe < 1$) similar to the slope method (135), but it is problematic when J_v is high (292). This is of course due to the inadequacy of linear equations to describe nonlinear phenomena. For heteroporous membranes, both techniques markedly overestimate PS (at low volume flows) as compared with heteroporous models, because PS_{app} contains both a dissipative component and a component owing to fluid recirculation in nonisoporous membranes.

4. Nonlinear flux equation: wash-down technique

The most established way at present to assess microvascular large-solute permselectivity is based on the so-called "wash-down" technique (97, 324, 325). This technique rests on the concept that when steady-state lymph-to-plasma protein concentration ratios (L/P) reach minimal and filtration-independent values at high lymph flows, then L/P must equal $(1 - \sigma)$ for the proteins investigated, as predicted from the nonlinear flux equation (228) (Fig. 2). This holds for homoporous as well as heteroporous membranes. In heteroporous (2-pore) membranes, high filtration rates are needed to create a partitioning of fluid flows among the different fluid-conductive pathways in due proportion to the fractional hydraulic conductances (α) accounted for by each pathway. This is a prerequisite for determining a correct compound reflection coefficient. We return to this issue in section III C. We also show that, in fact, transport of macromolecules across large pores is convection dominated in the majority of capillary beds al-

ready at normal transvascular filtration rates. Thus the contribution of diffusion to total large-pore solute transport is minor. In contrast, small-pore transport is usually diffusion dominated also at (moderately) elevated lymph flows. Thus the rationale for increasing the transvascular fluid flow for assessing $(1 - \sigma)$ is both to reduce the diffusional component of small-pore transport and to obtain L/P values that reflect a partitioning of the fluid fluxes among the different fluid pathways in proportion to the fractional hydraulic conductances accounted for by small and large pores (i.e., by α_L and α_S , respectively). Hence, under these conditions

$$L/P = \alpha_L(1 - \sigma_L) + \alpha_S(1 - \sigma_S) = 1 - \sigma \quad (16)$$

where σ_L and σ_S represent the large- and small-pore reflection coefficients for the solutes investigated, respectively. The first term to the right in *Equation 16* represents the fractional large-pore sieving coefficient, and the second term to the right represents the fractional small-pore sieving coefficient obtained at very high filtration rates. By first plotting sieving coefficients experimentally determined at high volume flows for solutes being >50 Å in radius versus a_e (in a semilog diagram) together with theoretical predictions of $(1 - \sigma_L)$ as a function of solute radius over pore radius (a_e/r_L) according to pore theory (see below), it is possible to find a proper α_L and a proper large-pore radius (r_L) fitting to the data. By subtracting the first term to the right in *Equation 16* from the total sieving coefficient (L/P), it is then possible to similarly analyze α_S and the proper small-pore radius (r_S) determining $(1 - \sigma_S)$ employing a "pore-stripping" analysis (47, 251, 262, 324, 325). Furthermore, it should be noted that an apparent (homoporous) PS can be calculated from every set of C_i/C_p (L/P) versus J_v (L) data obtained with the wash-down technique using *Equation 13*, once σ has been determined from filtration-independent L/P values.

5. Nonlinear flux equation: limiting slope technique

If steady-state protein clearance from blood to lymph is plotted versus J_v (Fig. 1), there will, according to *Equations 4* and *5*, be an initial nonlinear convex-upward rise in Cl. The Cl curve later transitions into a relationship taking the properties of a more or less straight line, the slope of which approximately equals $(1 - \sigma)$. For homoporous membranes, the curve slope approaches $(1 - \sigma)$ first when $Pe > 3$. If a sufficient number of data are available, the limiting slope the Cl versus J_v curve, and hence σ , may be assessed. When σ is known, it is then possible, using *Equation 10*, to determine PS for every set of Cl versus J_v data available. From the overall PS , i.e., the average of individual PS values (and from the σ), it is possible to construct a Cl versus J_v curve according to *Equations 3-5*. Such an analysis is shown for albumin (by the hatched line) in Figure 3C based on the data listed in Table 1.

A variant of this technique has recently been intro-

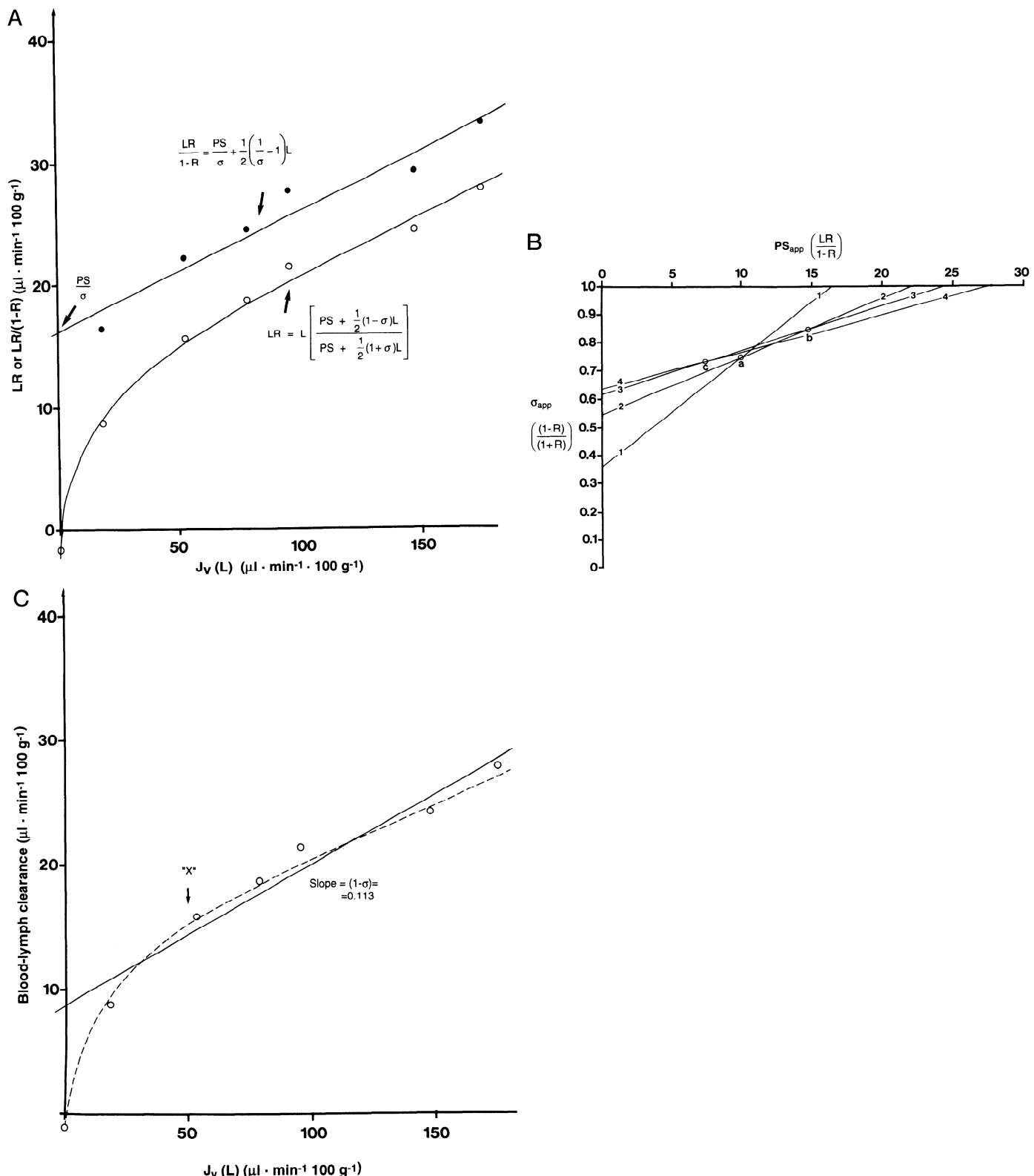


FIG. 3. A: slope technique for assessing homoporous PS and σ . Apparent PS [$LR/(1-R)$] and clearance (LR) of albumin, as calculated according to linear flux formalism (Eq. 15) from data listed in Table 1 (259), are plotted vs. $J_v(L)$. Ordinate intercept and slope of $LR/(1-R)$ vs. $J_v(L)$ line are (according to Eq. 15) PS/σ and $(1-\sigma)/2\sigma$, respectively. Bottom curve is simulated using PS and σ values obtained from top regression line according to expression for R derived in Equation 15. B: cross-point method for assessing homoporous σ (σ_t) and PS . Apparent σ [$(1-R)/(1+R)$] vs. apparent PS (PS_{app}) for albumin at levels 1–4, as listed in Table 1 (259), are interconnected by straight lines. Cross-point between data pairs 1 and 2 (denoted a) yields $PS_{app} = 10$ and $\sigma_t = 0.750$. Cross-point for data pairs 2

duced based on *Equation 5* (245, 246). If the first term to the right in *Equation 5* is regarded as the diffusive component of transport, it may be realized that this component will initially increase for increasing J_v values, when C_i/C_p decreases, to later decrease when Pe becomes large. Thus the first term in *Equation 5* has a maximum at moderately elevated J_v values. Setting the (first) derivative of this term in *Equation 5* at zero yields the following

$$\sigma = \frac{1 - x}{e^{-x}} \quad (17a)$$

where x represents a so-called "unique" Peclet number prevailing when the diffusive component has reached a maximum. The term *unique* was adopted since x is here solely determined by σ . The solution of *Equation 17* is not explicit, but the equation can be easily solved using an ordinary pocket calculator and a trial-and-error approach. For $\sigma = 0.9$, for example, the unique Peclet number is 0.3915, for $\sigma = 0.8$ it is 0.528, and for $\sigma = 0.1$ it is 0.962 (246). (As shown in *Eq. 39b*, the fractional contribution of diffusion to overall clearance during steady state is $\sigma \cdot e^{-Pe}$, and this expression reaches a maximum when J_v approaches 0.)

It has been argued that when the Cl versus J_v function transitions from a nonlinear to a near "linear" portion, the diffusive component of transport reaches a maximum, and for this transition point *Equation 17* can be applied (245, 246). Once the value of J_v for this event and σ from the final slope of the Cl versus J_v relationship are determined, it is possible to obtain a homoporous *PS* using the unique Peclet number (as coupled to the σ determined) from

$$\frac{J_v(1 - \sigma)}{x} = PS \quad (17b)$$

In Figure 3C, a linear regression line is drawn for all albumin Cl versus J_v data from Table 1. The overall albumin reflection coefficient calculated from the regression slope ($1 - \sigma$) was found to be 0.887. Because $\sigma = 0.887$ corresponds to an x of 0.4131, *PS* can be calculated to be $13.6 \mu\text{l} \cdot \text{min}^{-1} \cdot 100 \text{ g}^{-1}$ for a transition point selected at $J_v = 50 (\mu\text{l} \cdot \text{min}^{-1} \cdot 100 \text{ g}^{-1})$. This *PS* value is close to that obtained with the slope technique discussed in section IIIB2), but the σ value obtained using limiting

slopes is more realistic than that obtained by the classical slope method.

Note that the nonlinear flux equation does not predict an absolutely linear Cl versus J_v slope following the initial convex-upward rise in Cl. The initial linear curve portion is actually slightly concave upward. According to homoporous transport theory, the Cl versus J_v curve will approach a strictly linear course, having the slope of $(1 - \sigma)$, first at very high J_v values (Fig. 1). Early portions of the Cl slopes, which may be assessed experimentally, will slightly underestimate $(1 - \sigma)$ and, hence, overestimate the reflection coefficient for homoporous membranes. However, it is demonstrated in section VI A3 that the limiting slope technique may be rather accurate for determining σ for heteroporous membranes, for which the Cl versus J_v relationships are usually linear already following the initial convex-upward bend of the curve.

The approaches mentioned in the previous sections are valid only for homoporous membranes, but as discussed, the wash-down technique and the limiting slope technique may be rather appropriate for determining σ also for heteroporous membranes. Because microvascular membranes in general are not homoporous, the apparent σ and apparent *PS* determined using homoporous techniques will, however, change as a function of lymph flow (cf. cross-point method). Furthermore, homoporous *PS* values will be much larger than the true (heteroporous) *PS* values. In Table 2 are listed the results from all the homoporous techniques discussed here as applied to the protein (albumin) flux data of Renkin et al. (259). The *PS* values for albumin assessed with the various techniques range from ~ 12 to $16.5 \mu\text{l} \cdot \text{min}^{-1} \cdot 100 \text{ g}^{-1}$. Thus they are three- to fourfold higher than the heteroporous (albumin) *PS* determined for the same data later in this review (see sect. IIIC).

For a correct description of transvascular protein transfer, heteroporous concepts must be introduced, and fluid fluxes across each set of pathways must be modeled in parallel. If done correctly, however, linearization of the nonlinear transport equations may work satisfactorily (279). Problems arise when separation of fluid and solute fluxes across the different sets of pores in the membrane is not done, i.e., when a heteroporous membrane is mathematically treated as being homoporous. In section IIIC, we thus focus on heteroporosity effects on transvascular protein transfer, using the nonlinear flux equation for the calculations.

and β (denoted b) yields $PS_{app} = 14.7$ and $\sigma_f = 0.845$. Finally, cross-point for data pairs β and γ (denoted c) yields $PS_{app} = 7.5$ and $\sigma_f = 0.735$ (all *PS* values are expressed in $\mu\text{l} \cdot \text{min}^{-1} \cdot 100 \text{ g}^{-1}$). Theoretically, a unique point of intersection can be obtained only at low J_v values for homoporous membranes. C: limiting slope technique for assessing σ and PS_{app} using nonlinear flux equation (see also Table 2). Albumin clearance [$J_v \cdot (C_i/C_p)$] for the 6 J_v levels listed in Table 1 are plotted vs. filtration rate (lymph flow). Best computer-aided nonlinear least-squares fit (broken line) was obtained for $PS = 16.4 \pm 1.4$ (SE) $\mu\text{l} \cdot \text{min}^{-1} \cdot 100 \text{ g}^{-1}$ and $\sigma = 0.881 \pm 0.011$ according to *Equation 4*. The *PS* and σ can also be assessed by inspection. A limiting slope of 0.11–0.12 is then obtained. Actually, a linear regression line drawn for all data yields a slope of 0.113. This corresponds to a σ of 0.887. In the next step, a *PS* value can be calculated according to *Equation 10* for each individual Cl value, yielding a mean *PS* of $16.5 \pm 1.7 \mu\text{l} \cdot \text{min}^{-1} \cdot 100 \text{ g}^{-1}$ for all data. The J_v value corresponding to the point at which Cl curve transitions from a nonlinear to a "near" linear slope was selected at $50 \mu\text{l} \cdot \text{min}^{-1} \cdot 100 \text{ g}^{-1}$. For $\sigma = 0.877$, the corresponding unique Peclet number (x) is 0.413, yielding a PS_{app} value of $13.6 \mu\text{l} \cdot \text{min}^{-1} \cdot 100 \text{ g}^{-1}$ at $J_v = 50$.

TABLE 2. Homoporous analyses of paw lymphatic albumin flux data

Technique	$PS, \mu\text{l} \cdot \text{min}^{-1} \cdot 100 \text{ g}^{-1}$	σ	Remarks
<i>Linear flux equation</i>			
$PS = \frac{LR}{1-R}; \sigma = 1$	16.3	1	$PS = \frac{LR}{1-R}$ at lowest $J_v(L)$
Slope technique	13.5	0.836	$\frac{LR}{1-R}$ vs. $J_v(L)$; linear regression analysis
Cross-point I	$12.2 \pm 3.1^*$	$0.813 \pm 0.062^\dagger$	$\frac{1-R}{1+R}$ vs. $\frac{LR}{1-R}$
Cross-point II	$14.6 \pm 2.9^*$	$0.910 \pm 0.030^\dagger$	$(1-R)$ vs. $\frac{LR}{1-R}$
<i>Nonlinear flux equation</i>			
Washdown	~ 12.0	~ 0.85	R vs. J_v ; curve fit "by inspection"; $\sigma_{J_{v \rightarrow \infty}} \sim (1-R)$
Washdown (PC fit)	14.9 ± 1.3	0.869 ± 0.013	Cl vs J_v ; nonlinear curve fitting
Limiting slope	$16.5 \pm 1.7^*$	0.887 ± 0.01	Cl vs. J_v ; slope from linear regression, individual PS values from Eq. 10
Limiting slope (PC fit)	16.4 ± 1.4	0.881 ± 0.011	Cl vs. J_v ; nonlinear curve fitting
"Unique" Peclat number ($L = 50$)	13.6	0.89	Cl vs. J_v ; curve fit by inspection, J_v obtained at inflection point

Values are means \pm SE of all individual PS values (*) and of reflection coefficient (σ) values from 3 highest levels of $J_v(L)$ (†). Determination of homoporous $PS(PS_{app})$ and $\sigma(\sigma_f)$ for albumin based on data listed in Table 1 using linear flux equations and nonlinear flux equation. Two of the curve fits (as denoted PC fit) have been performed using InPlot software on a personal computer. Difference between cross-point I and cross-point II is specified under remarks. Slope technique, cross-point technique I, and limiting slope technique (including technique utilizing unique Peclat numbers) are shown in Fig. 3, A-C, respectively. Cl, clearance. [Data from Renkin et al. (259).]

C. Heteroporous Models of Transvascular Large-Solute Transport

1. Partitioning of fluid fluxes among the different fluid pathways in a heteroporous membrane

The general equation of fluid transport for a heteroporous membrane system is

$$J_v = \sum_{i=1}^m J_{v,i} = \sum_{i=1}^m \alpha_i L_p S (\Delta P - \sum_{j=1}^n \sigma_{ij} \Delta \pi_j) \quad (18)$$

where m is the number of different-sized pores, n is the number of solutes in the system which exert an osmotic pressure difference across the membrane, α_i is the fraction of hydraulic conductance attributed to pore type " i ," $L_p S$ is the capillary hydraulic conductance, ΔP is the transendothelial difference in hydrostatic pressure, σ_{ij} is the reflection coefficient for solute j at pore type i , and $\Delta \pi_j$ is the transendothelial osmotic pressure difference of solute j . The complexity of this equation stems from the different properties of each pore with respect to osmotic pressure differences exerted by each solute. Relatively complex models based on this equation have been derived for, for example, peritoneal transport (280, 282), comprising several different fluid conductive pathways [viz. small (paracellular) pores, large pores, and "transcellular" ultrapores] and taking into account crystalloid osmotic pressures exerted by a number of crystalloids in

addition to the Starling forces, i.e., the colloid osmotic and hydrostatic pressure gradients.

In this review we treat the capillary wall as having two main sets of pathways conducting fluid flow and solute fluxes in a fashion originally predicted by Grotte (102). We also assume that there is complete crystalloid osmotic equilibrium across the microvascular walls. In this rather simplistic model, net volume flow across membrane can be described by Equation 1. During conditions when there are no net volume shifts occurring across the membrane ("isogravimetric" or "isovolumetric" conditions), the following is valid

$$\Delta P_{iso} = \sigma \Delta \pi \quad (19)$$

For a two-pore model, σ represents a weighted sum of the large pore protein reflection coefficient (σ_L), and the small pore protein reflection coefficient (σ_S), the weighting factors being the fractions of $L_p S$ accounted for by each set of pores (α_L, α_S), respectively

$$\sigma = \alpha_L \sigma_L + \alpha_S \sigma_S \quad (20)$$

During isovolumetric conditions, that is, when $J_v = 0$, there will be a fluid flow along the blood-tissue hydrostatic pressure gradient across large pores, because here σ_L is near 0, but this fluid filtration will be counterbalanced by fluid absorption across small pores caused by $\sigma_S \cdot \Delta \pi$, because σ_S here is ~ 1 . At least if small and large pores are uniformly distributed along the exchange vessels and the interstitium is reasonably well

mixed (the same $\Delta\pi$ and ΔP across small and large pores), large-pore filtration (J_{vL}) is described by (cf. Eq. 1)

$$J_{vL} = \alpha_L L_p S (\Delta P - \sigma_L \Delta\pi) \quad (21)$$

Note, that since σ_L is ~ 0 , there is always a filtration of fluid and proteins across large pores as long as ΔP is larger than zero.

Inserting

$$\Delta P_{iso} = (\alpha_L \sigma_L + \alpha_S \sigma_S) \Delta\pi \quad (22)$$

for isogravimetric conditions, as obtained from Equations 19 and 20 into Equation 21 and rearranging, yields the large-pore volume flow during isovolumetric conditions ($J_{vL,iso}$)

$$J_{vL,iso} = \alpha_L (1 - \alpha_L) L_p S (\sigma_S - \sigma_L) \Delta\pi \quad (23)$$

Making a similar derivation for small-pore volume flow during isovolumetric conditions ($J_{vS,iso}$) we obtain

$$J_{vS,iso} = -\alpha_L (1 - \alpha_L) L_p S (\sigma_S - \sigma_L) \Delta\pi \quad (24)$$

Furthermore, for net convection, the large-pore volume flow equals

$$J_{vL} = \alpha_L (1 - \alpha_L) L_p S (\sigma_S - \sigma_L) \Delta\pi + \alpha_L J_v \quad (25)$$

and the small-pore volume flow equals

$$J_{vS} = -\alpha_L (1 - \alpha_L) L_p S (\sigma_S - \sigma_L) \Delta\pi + \alpha_S J_v \quad (26)$$

and thus $J_{vL} + J_{vS} = J_v$. Note that σ_S and σ_L here refer to small- and large-pore reflection coefficients for total protein, respectively, which are generally somewhat larger than those for albumin. For the sake of simplicity, σ for total protein in this presentation, however, is set to equal σ for albumin, since albumin is the major serum colloid.

In terms of unrestricted large- and small-pore area [A_{oL} and A_{oS} , respectively (Eq. 7)], the ratio between the fractional large- and small-pore hydraulic conductivity (α_L and α_S , respectively) equals (cf. Poiseuille's law)

$$\frac{\alpha_L}{\alpha_S} = \frac{\alpha_L L_p S}{\alpha_S L_p S} = \frac{n_L \pi r_L^4}{n_S \pi r_S^4} = \frac{A_{oL}}{A_{oS}} \left(\frac{r_L}{r_S} \right)^2 \quad (27)$$

2. Solute fluxes through a heteroporous membrane: linear approximations

Once the fluid fluxes through each of the two sets of pores, J_{vL} and J_{vS} , have been determined according to Equations 25 and 26, it is possible to assess the solute fluxes and clearances across either set of pores using linear flux equations (Eq. 2) or nonlinear equations

(Eqs. 3-5). With the use of linear approximations (Eq. 2), the protein clearance through small pores (Cl_S) becomes

$$Cl_S = PS_S + J_{vS} (1 - \sigma_S) \quad (28)$$

and that through large pores (Cl_L)

$$Cl_L = PS_L + J_{vL} (1 - \sigma_L) \quad (29)$$

or inserting Equation 26 in Equation 28

$$Cl_S = PS_S - \alpha_L (1 - \alpha_L) L_p S (\sigma_{Sa} - \sigma_{La}) \Delta\pi (1 - \sigma_S) + \alpha_S J_v (1 - \sigma_S) \quad (30)$$

and inserting Equation 25 in Equation 29

$$Cl_L = PS_L + \alpha_L (1 - \alpha_L) L_p S (\sigma_{Sa} - \sigma_{La}) \Delta\pi (1 - \sigma_L) + \alpha_L J_v (1 - \sigma_L) \quad (31)$$

where the subscript a refers to albumin or total protein. Total Cl is regarded as the sum of Cl_S and Cl_L , and total PS is supposed to equal PS_S plus PS_L .

Total heteroporous transport is thus dependent on 1) pure diffusive transport (PS), 2) a volume recirculation term, and 3) solute transport coupled to net convection (J_v). Note that the volume recirculation term is dependent on $\Delta\pi$. For albumin (subscript a), the total clearance (Eq. 30 + Eq. 31) can be written as

$$Cl = PS_a + \alpha_L (1 - \alpha_L) L_p S (\sigma_{Sa} - \sigma_{La})^2 \Delta\pi + J_v (1 - \sigma_a) \quad (32)$$

which is the linear two-pore solute flux equation derived by Kedem and Katchalsky (137, 138) and made further explicit by House (125) and later employed by Rippe et al. (279).

Rippe and co-workers (274, 279) and later Haraldsson (105) and Haraldsson and Rippe (118), employing the RISA uptake technique described in section II B 2, analyzed transvascular albumin transfer in plasma perfused rat hindlimb muscle according to these principles. They first determined the sum of the PS term and the volume recirculation term by setting $J_v = 0$. Second, they tried to separate PS from the volume recirculation term by determining Cl for $\Delta\pi = 0$. This could be carried out, since the relationship between Cl and $\Delta\pi$ (actually π_p) was experimentally determined. Extrapolation of this relationship to $\Delta\pi = 0$ would, conceivably, yield an estimate of PS ($PS_S + PS_L$). According to these principles, Rippe et al. (279) found that only 25-30% of total albumin tracer flux occurring in rat muscle when J_v was zero at "normal" plasma colloid osmotic pressures was due to diffusion (across small pores), the remaining portion being due to convection through large pores, which was later confirmed in the same preparation by albumin (tracer) wash-out studies by Haraldsson (106).

*3. Solute fluxes through a heteroporous membrane:
nonlinear transport equations*

Essentially the same procedures for calculating clearances are employed here, except that nonlinear transport formalism is used as described above. Fluid fluxes through either pore system are first separated according to *Equations 25* and *26*, then the resulting fluid flows are inserted into *Equation 3*. Each set of pores is assumed to determine its own “downhill” concentration. Macromolecular solute fluxes through either set of pores are then assumed to be mixed within the interstitium (193). According to *Equation 3* (see sect. IIIA2) we have

$$Cl_s = J_{vS} \frac{1 - \sigma_s}{1 - \sigma_s e^{-Pe_s}} \quad (3b)$$

and

$$Cl_L = J_{vL} \frac{1 - \sigma_L}{1 - \sigma_L e^{-Pe_L}} \quad (3c)$$

and total clearance is ($Cl_L + Cl_s$). For unidirectional tracer transport, *Equation 4* is employed. Furthermore, the lymph-to-plasma protein concentration ratio is calculated as

$$L/P = \frac{Cl_s + Cl_L}{J_v} \quad (33)$$

These principles were recently adopted by Rippe and Haraldsson (272–274) and previously also in reviews by Curry (47) and Renkin (252) and are applied in the following sections.

4. Restricted transport through aqueous channels

Aqueous channels can be pores, slits, or pores filled with a matrix of fibrous macromolecules. In either of these pathways, solute transport will be restricted as compared with the situation when occurring in a free solution. The diffusional restriction in a slit having a width of 50 Å is approximately the same as that occurring in a pore of radius 50 Å, provided that the solute radius is <23 Å. For solutes with a radius larger than the half-slit width (25 Å), there is, of course, no passage at all through the slit. According to the “fiber matrix theory” (47, 51), a matrix of fibrous macromolecules occupying 5% of the total matrix volume (fractional void volume 95%) and having a fiber radius of 5 Å yields approximately the same degree of restricted diffusion of small solutes as 50 Å (radius) cylindrical pores.

We have preferred simple pore theory to model the degree of restricted diffusion as a function of molecular size, i.e., in terms of solute radius (a_e) over a pore radius (r_p), as denoted λ . How D_s varies with a_e is described by

Equation 9. In *Equation 34*, we employ the relationship (179)

$$\frac{A}{A_o} = \frac{(1 - \lambda)^{9/2}}{1 - 0.3956\lambda + 1.0616\lambda^2} \quad (34)$$

to describe the degree of restricted diffusion (A/A_o) occurring in cylindrical pores as a function of solute radius over pore radius.

To model restricted solute convection, i.e., $(1 - \sigma)$ with λ , we employ the relationship (179)

$$(1 - \sigma) = 1 - \frac{(1 - \lambda)^2[2 - (1 - \lambda)^2](1 - \lambda/3)}{1 - \lambda/3 + 2/3\lambda^2} \quad (35)$$

5. Recalculation of homoporous reflection coefficient and permeability-surface area product from heteroporous models

From a heteroporous perspective it is possible to recalculate an apparent (homoporous) overall reflection coefficient for a two-pore membrane for a given solute at any given J_v . This apparent σ (σ_f) can be defined as (22, 47, 262)

$$\sigma_f = \frac{J_{vL}}{J_v} \sigma_L + \frac{J_{vS}}{J_v} \sigma_S \quad (36)$$

Furthermore, inserting σ_f into *Equation 10* or *11* (and solving for PS) gives a homoporous estimate of PS . It is also possible to calculate an apparent (homoporous) PS assuming that σ is known, after calculating ($Cl_L + Cl_s$) according to *Equations 3b* and *3c* then solving for PS using (the homoporous) *Equation 10*.

In heteroporous transport models, macromolecular transport is thus to a great extent determined by the balance of fluid fluxes occurring through protein-selective and unselective transcapillary fluid conductive pathways, respectively. At high filtration rates, σ_f in *Equation 36* will approach the true value of σ as described in *Equation 20*, because in that situation C_i/C_p approaches α_L and C_i/C_p approaches α_S . The rationale for experimentally elevating J_v in, for example, lymphatic protein flux analyses is primarily to get a realistic estimate of the composed (heteroporous) reflection coefficient for this reason. Second, the diffusive component of total transport will become negligible at high volume flows.

6. Fractional contribution of diffusion and convection to total large solute flux

The (modified) Pe number for a specific solute (x) for large pores is obtained by substituting J_{vL} by the expression in *Equation 24*, and PS_{Lx} by *Equation 7* in $J_{vL}(1 - \sigma_{Lx})/PS_{Lx}$, yielding

$$\text{Pe}_L = \frac{J_{vL}(1 - \sigma_{Lx})}{PS_{Lx}} = \frac{\alpha_L L_p S(1 - \alpha_L)}{D_x(A/A_o)_{Lx}(A_o/\Delta x)_L} \\ \times \left[\Delta\pi(\sigma_S - \sigma_L) + \frac{J_v}{(1 - \alpha_L)L_p S} \right] (1 - \sigma_{Lx}) \quad (37)$$

But according to Poiseuille's law (cf. *Equation 8*)

$$\text{Pe}_L = \frac{(1 - \alpha_L)r_L^2 1,320}{D_x(A/A_o)_{Lx} 8\eta} \\ \times \left[\Delta\pi(\sigma_S - \sigma_L) + \frac{J_v}{(1 - \alpha_L)L_p S} \right] (1 - \sigma_{Lx}) \quad (38)$$

Small-pore Pe can be derived in a similar manner.

Peclet number is here independent of the absolute value of $A_o/\Delta x$ (cf. Ref. 69) but dependent on r_L , a_e (*Equations 7* and *9*), α_L , and the expression within the square brackets. For most organs the first term within the square brackets of *Equation 15* lies within the range of 8–12 mmHg (270, 323) and the second ($\sim J_v/L_p S$) is ~ 1 mmHg for normal lymph flows (323, 325). For a majority of organs the magnitude of the whole expression in brackets is thus on the order of 10 mmHg.

Rearranging *Equation 4b* yields

$$Cl(1 - \sigma \cdot e^{-Pe}) = J_v(1 - \sigma) \quad (39a)$$

and

$$1 - \sigma \cdot e^{-Pe} = J_v(1 - \sigma)/Cl \quad (39b)$$

The fractional convective portion of total unidirectional homoporous clearance is thus $(1 - \sigma \cdot e^{-Pe})$, and the fractional diffusive portion is $\sigma \cdot e^{-Pe}$. The fractional convective and diffusive portions can also be derived by dividing the diffusive and convective terms in *Equation 5*, respectively, by the expression for Cl given in *Equation 4b*.

For a heteroporous membrane, the fractional diffusional clearance (Diff%) becomes

$$\text{Diff}\% = \frac{Cl_L \cdot \sigma_L e^{-Pe_L} + Cl_S \cdot \sigma_S e^{-Pe_S}}{Cl_L + Cl_S} \quad (40)$$

and the fractional diffusion clearance occurring through large pores (Diff_L%) will be

$$\text{Diff}_L\% = \sigma_L \cdot e^{-Pe_L} \quad (41)$$

According to this expression it can be shown that the diffusional steady-state transport across large pores is very small for all solutes, provided that the large-pore radius $> 200 \text{ \AA}$ (274). For a macromolecule as small as albumin there is thus only 2% diffusion across a 200-Å pore as simulated according to *Equations 37* and *40* and modeling A/A_o according to *Equation 34* and σ_L

according to *Equation 35*. The expression within the square brackets of *Equation 37* was then set to 10 mmHg and α_L to 0.10 (274). For solutes larger than albumin, the diffusive component under these premises is negligible. According to this reasoning, the Cl_L of macromolecules can with negligible error at any net J_v be expressed as

$$Cl_L = J_v L(1 - \sigma_L) \quad (42)$$

Hence, the large-pore macromolecular clearance is just a product of $(1 - \sigma_L)$ and the large-pore volume flow. Due to this fact, evaluation of lymph flux data can be done in a rather simplistic manner similar to the previously mentioned pore-stripping analysis (251, 262, 325), as further discussed in section IVB.

According to *Equation 40*, diffusion is the predominating transport process for solutes smaller than 30 Å in radius (105). For solutes of radius between 30 and 50 Å, convection becomes progressively more important with increases in solute radius, and for solutes larger than the small-pore radius, transport is more or less entirely convective. Thus, as a generalization, small-pore transport is mainly diffusive at normal lymph flows, even for solutes as large as albumin, while the transport of small and large solutes across large pores is mainly convective.

D. Effect of Vascular Wall Charge on Large-Solute Transport

The endothelial glycocalyx and the basement membrane of endothelial cells, as well as many components of the interstitial matrix, exhibit binding sites for positively charged tracer substances such as cationic ferritin or ruthenium red (167, 217, 304, 306–309). The capillary wall thus appears to carry a net negative charge as indicated by early measurements of reflection coefficients to neutral and negatively charged dextrans in the perfused rabbit ear (7, 88) and in glomerular capillaries (36). Indeed, tissue uptake studies of differently charged proteins in peripheral capillaries, such as the muscle vascular bed (107), and transcapillary tracer efflux studies in single mesenteric capillaries (4), strongly suggest that fixed negative charges significantly contribute to the molecular selectivity of microvascular walls for large molecules. However, a majority of lymphatic protein flux analyses dealing with this topic have indicated the presence of a positively charged blood-tissue barrier, especially in the lung (94, 160, 236) and the intestine (185, 231). The reason for this discrepancy is not clear. Studies by Parker and co-workers (93, 219) suggest that the interstitial distribution volumes of polycations are generally larger than those of polyanions of comparable size. The interstitium may therefore behave as an ion-exchange chromatographic column. Fixed negative charges in the interstitial matrix may exclude polyanions from the gel phase and/or cause reversible binding of polycations. This will promote the blood-lymph

transfer of polyanions and retard that of polycations. Under non-steady-state conditions, the relative lymph concentration of polyanions (cf. albumin) will then exceed that of polycations or neutral species. Also, as concerns the glomerular permselectivity to dextrans, the much lower urine concentrations of negatively charged dextrans as compared with those of neutral ones in acute experiments have recently been interpreted as reflecting binding (and cellular uptake) of negatively charged dextrans by mesangial cells at the blood-urine barrier (322).

1. General phenomena associated with capillary wall charge

The major impact of negative charge in the capillary wall on the transport of small negatively charged macromolecules is that it causes solute partitioning effects in negatively charged pores, i.e., an increased diffusion restriction of negative charged solutes as compared with neutral ones. Another implication of negative capillary wall charge is that it causes a Donnan distribution of small ions and a Donnan potential across the capillary wall. Still other phenomena associated with charged macromolecule transport are shown in Table 3, as expressed in so-called phenomenological "equations" (136-138). When solute charge is taken into account, solute flux is no longer due to just diffusion and convection but also due to electrophoresis driven by an electrical potential (see below) which tends to promote the transport of polyanions from blood to tissue. Furthermore, hydraulic flow will now be affected by electroosmotic pressure in addition to hydrostatic and colloid osmotic pressures. Electroosmosis will tend to counteract fluid movement through charged membrane pores. Moreover, a current flow across the microvascular membrane will be created. This current flow is not only due to the tissue-to-blood electrical potential gradient causing an electric current, but there will also appear a component owing to the hydrostatic pressure-driven flow of ions, a "streaming current," and a component owing to the ionic diffusion as driven by the ionic concentration difference, a "diffusion current." All these phenomena associated with charged solute-membrane transport interactions appear, however, to be quite small in comparison with the Donnan effect and solute-

partitioning effects on transvascular transport caused by electrical charges on membrane and solute.

2. Donnan distribution and Donnan potential

Because albumin and other polyanions show lower interstitial than plasma concentrations, there is a Donnan distribution of small ions across the microvascular walls with a higher concentration of mobile cations and a lower concentration of mobile anions in plasma than in the interstitium. All in all, the unequal distribution of large polyanions causes the concentration of osmotically active particles to be higher in plasma than in the interstitial fluid, which at least partly explains why macromolecules show much higher plasma osmotic pressures in the capillaries than expected from their molar concentrations alone. The unequal distribution of ions also produces a Donnan potential of approximately -0.5 to -1 mV (47) across the capillary wall with the capillary lumen negative. The Donnan distribution and its importance for transvascular transport has recently been discussed at some length elsewhere (47, 48).

3. Partitioning of molecules in charged membranes: double-layer model

One approach to model charge-dependent sorting of solutes in charged biological membranes, namely employing the double-layer hypothesis, is outlined here. Consider a particle with a surface charge that is uniformly spread over the particle's surface. A diffuse cloud of counterions balances the particle's charge. The combination of particle charge plus counterion cloud is called the "double layer," the thickness of which is on the order of one so-called Debye screening length (l_D). The l_D can be assumed to be the length constant by which the local space charge falls off in a direction away from the particle's surface. Thus it is approximately correct to think of the space charge falling off to 0.368 ($=e^{-1}$) of its original value for every l_D away from the surface.

The l_D (in Å) is inversely proportional to the square root of the ionic strength of the solution by

TABLE 3. Phenomenological "equations" (138) describing membrane transport of charged solutes

Solvent flow	= hydraulic flow	+ osmotic flow	+ electroosmotic flow
Solute flux	= ultrafiltration	+ diffusion	+ electrophoresis (ion migration)
Current flow	= streaming current	+ diffusion current	+ electric current

For a homogeneous membrane, solute permeability, membrane hydraulic conductivity, and reflection coefficient are the practical membrane coefficients necessary to describe transmembrane flux of an uncharged solute. If the solute is charged, 3 new practical coefficients must be included, namely electric conductance, transport number (τ_c), and electroosmotic permeability (β). Electric conductance (reciprocal of electrical resistance) can be determined by recording electrical current in response to an applied electric field while transmembrane pressures ($\Delta_p - \Delta\pi$), and solute concentration differences are held at 0. Under these specific conditions ($\Delta_p - \Delta\pi = 0, \Delta C = 0$), β represents volume flow, and τ_c represents salt flux associated with current flow. From a practical point of view, electrical phenomena across capillary walls are of little significance, however, other than causing charge-dependent solute partitioning and, hence, restricted (or facilitated) solute transport across the membrane.

$$l_D = \sqrt{\frac{RT\epsilon}{8\pi F^2 C}} \quad (43)$$

where F is the Faraday constant, ϵ is the dielectric constant, and C is the molar concentration (in mM) of solvent many Debye lengths away from the charged surfaces. Substituting appropriate values for the mentioned constants yields

$$l_D = \frac{97.1}{\sqrt{C}} \quad (44)$$

Thus for a 0.15 M salt solution, l_D is ~ 8 Å.

According to the Debye-Hückel theory of ion-ion interactions, l_D is the typical distance over which charge effects are exerted. In principle, the probability that two equally charged particles will be separated from each other by more than their double layers ($2l_D$) is close to unity. Hence, the movement of a charged particle in an equally charged cylindrical pore will be restricted to a space within the center of the pore, and the particle will be excluded from a space at a distance of approximately two l_D away from the pore wall.

Munch et al. (202) suggested that transport restriction due to equal solute and membrane charges may be modeled by increasing the solute radius (a_e) by one l_D and decreasing the pore radius (r_p) by one l_D . The modified solute radius-to-pore radius ratio (λ^*) then becomes

$$\lambda^* = \frac{a_e + l_D}{r_p - l_D} \quad (45)$$

Munch et al. (202) found a surprisingly good agreement between data and theory using this modified solute radius-to-pore radius ratio to model reflection coefficients to albumin across artificial membranes containing track-etched pores (of radius 220 Å) at various ionic strengths of the solvent (NaCl). Curry (47) compared this rather crude model with a more exact description given by Smith and Deen (312) of rejection of charge solutes from pores with charged walls. The model given by Munch et al. (202) and the more exact model were in excellent agreement for solutes ranging from 10 to 70 Å in radius and pores of radius 100 Å for equal solute and membrane charge (-20 mM).

4. Partitioning of molecules in charged membranes: modified Nernst-Planck equation

A more complete approach to model transport of charged particles through charged membranes based on the Nernst-Planck equation has been employed by Deen et al. (57) as applied to the glomerular filter. This approach rests on the assumption that fixed negative membrane charges are uniformly distributed across the whole membrane. The intramembrane electrical potential will then be negative with respect to plasma, which

will tend to restrict the entry of anions and enhance that of cations into the membrane. Within the relatively thin glomerular membrane, the transmembrane electrical potential gradient developed here will be quite small, so electrophoretic transport will be negligible. However, the partitioning of solutes due to electrical charge will be quite substantial. For an equivalent pore radius of the glomerular filter of ~ 50 Å and an intramembrane concentration of fixed negative charges (C_m) of 165 meq/l, generating an intramembrane potential of -13 mV, Deen et al. (57) were able to obtain a good fit of theory to their measured urine-to-plasma concentration ratios in Munich-Wistar rats of different-sized negatively charged (sulfated) dextrans, neutral dextrans, and positively charged (diethylaminoethyl) dextrans.

The streaming potential generated within the membrane by pressure-driven transport of ions tends to retard the transmembrane fluid flow. A greater transmural hydraulic pressure gradient will be required to produce a given filtration rate than if the capillary wall were uncharged. In terms of electroosmotic pressure, a pressure gradient of 4-5 mmHg opposing the filtration at normal glomerular filtration rates can be calculated for a uniformly charged membrane with an intramembrane charge concentration of 165 meq/l for the data of Deen et al. (57). In renal peritubular capillaries, Öjteg et al. (209-211), using a similar model as Deen et al. (57), calculated an electroosmotic pressure of 3-5 mmHg for "large" pores in the microvascular membrane, whereas the electroosmotic pressure gradient across "small" pores was found to be negligible.

The main theoretical problem with the approaches employed by Deen et al. (57) and Öjteg et al. (209, 211) is the assumption that the capillary membrane has a homogeneous distribution of fixed negative charges, yet is "porous." For this assumption to be valid, the equivalent pore radius has to be smaller than the double layer thickness ($1 l_D$), i.e., smaller than 8 Å, at a normal plasma ionic composition. Only if this condition is met will there be an approximately uniform charge distribution within the pores. In fact, the pores will then show a uniform space distribution of counterions, i.e., of cations. Because the equivalent small-pore radius in most capillary walls appears to be much larger than 8 Å ($\sim 45-60$ Å), the validity of the approaches outlined above can be questioned. The cited studies, however, demonstrate that 1) the solute-partitioning effects of transport due to charge may be considerable, 2) the electrophoretic transport of negatively charged macromolecules from blood to tissue (ion migration) is negligible, and 3) the plasma compartment is slightly negative (0.7-1.5 mV) in comparison with the interstitium. In addition, the mentioned studies indicate a possible, albeit rather insignificant, role for electroosmosis in transvascular protein transport.

5. Application of the double-layer model to experimental data

We have employed the double-layer model (202) together with the two-pore theory to model blood-tissue

clearances and σ of negatively charged and neutral solutes in the muscle vascular bed of rat hindquarters (105, 274, 275). The best fit of experimental data on initial blood-tissue clearances of albumin and two differently charged isoenzymes of lactate dehydrogenase (LDH: LDH-1 and LDH-5) to our theoretical simulations occurred for r_s equal to 64 Å, r_L equal to 310 Å, and α_L equal to 0.055 as calculated using *Equation 45*, since the "equivalent" small-pore radius was estimated to be 45 Å and the equivalent large-pore radius was estimated to be 225 Å when charge interactions were not explicitly accounted for.

Because albumin in a majority of capillary exchange studies is the critical molecular probe for estimating the small-pore radius, the latter will usually be underestimated (by ~15–20 Å) by not taking charge interactions into account. Because the structural small-pore radius is a major determinant of $A_o/\Delta x$ as calculated from L_pS (*Eq. 8*), this parameter will be overestimated if the equivalent r_s instead of the structural one is used in the calculations (cf. *Eq. 8*). Furthermore, uncharged species that are just slightly larger than the (negatively charged) albumin molecule, such as IgG, will erroneously be treated as being impermeant through small pores if charge is not accounted for. The clearance of such uncharged macromolecules will thus be underestimated by employing the concept of equivalent pores, especially when the transcapillary fluid flow is high. It should be emphasized, however, that the small-pore component of overall IgG transport is still rather small. All in all, the errors of using equivalent pore modeling are thus rather marginal. For the sake of simplicity and to be able to compare the present pore radius estimates with those in previous models (324, 325), we have adopted the equivalent pore concept for computer simulations of macromolecule clearances across membranes of varying composition.

IV. GENERAL BEHAVIOR OF A TWO-PORE SYSTEM

A. Computer-Simulated Results for Two-Pore Membranes

To illustrate the behavior of a heteroporous (2-pore) system, fluid and solute fluxes in three kinds of uncharged membranes having differing size selectivity are computer simulated according to the principles outlined in section III C. The particular membranes chosen are listed in Table 4. Two membranes are quite selective, having the small-pore radius set to 43 Å and 45 Å, respectively (denoted *membranes A* and *B*, respectively), with the fractional large-pore hydraulic conductances (α_L) set to 0.02 and 0.05, respectively. The third membrane investigated has a rather low sieving capacity, with a small-pore radius of 55 Å and α_L set to 0.05 (denoted *membrane C*). For all three membranes, the large-pore radius is set to 250 Å and the hydraulic conductance to 8 ml · min⁻¹ · mmHg⁻¹ · 100 g tissue⁻¹. The $A_o/\Delta x$ value was calculated from L_pS (*Eq. 8*) for membranes *A* and *B* yielding ~30,000 cm/100 g and 26,582 cm/100 g, respectively. For *membrane C*, $A_o/\Delta x$ was set to 30,000 cm/100 g and was not calculated from L_pS to be similar in magnitude as $A_o/\Delta x$ for *membranes A* and *B*.

1. Partitioning of fluid flows among the two major fluid conductive pathways: non-steady-state conditions

Fluid fluxes across a two-pore membrane will be partitioned according to the fractional hydraulic conductances accounted for by each pore system (α_S and α_L , respectively) only at extremely high (infinite) filtration rates. As seen from *Equations 25* and *26*, the fractional filtration flows across either pore system at low filtration rates will be offset owing to the magnitude of the "volume recirculation" term, which is to a great extent governed by the $\Delta\pi$. Furthermore, the latter will itself vary with the prevailing filtration rate at steady state. As mentioned in section III C 1, it is possible to transiently create a situation with fluid recirculation between the different pore systems, and *in vivo* this may occur by lowering the capillary hydrostatic pressure. This may transiently cause net fluid absorption from the interstitium across small pores counterbalancing at $J_v = 0$, the fluid filtration continually occurring across large pores. This situation may last for minutes to hours depending on the organ and tissue under study (274).

In Figure 4, the partitioning of fluid fluxes between small and large pores is depicted for *membrane B*, having small pores of radius 45 Å ($\alpha_S = 0.95$) and large pores of radius 250 Å ($\alpha_L = 0.05$), when $\Delta\pi$ is kept constant at 14.06 mmHg, corresponding to a C_i/C_p value (L/P) for total proteins (albumin) of 0.5 at a plasma protein concentration of 6.5 g/l ($\pi_p = 22.88$ mmHg for total proteins). Such conditions of a constant $\Delta\pi$ may prevail during, for example, tracer experiments in which the changes in $\Delta\pi$ over time may be small (negligible). Colloid osmotic pressures are calculated according to the classical Pappenheimer formulation (*Eq. 3.5* in Ref. 159). As seen from Figure 3, both small- and large-pore

TABLE 4. *Membrane parameters used to model transvascular fluid and protein transport in a heteroporous system*

	Equivalent Pore Model		
	Membrane A	Membrane B	Membrane C
Small-pore radius, Å	43	45	55
Fractional large-pore L_pS	0.02	0.05	0.05
$\frac{A_o}{\Delta x}$, cm/100 g	30,000*	26,582*	30,000

Capillary hydraulic conductance (L_pS) = 8 µl · min⁻¹ · mmHg⁻¹ × 100 g⁻¹; plasma protein concentration = 6.5 g/l; plasma colloid osmotic pressure = 22.88 mmHg; and interstitial colloid osmotic pressure = variable with C_i/C_p for albumin. Large-pore radius = 250 Å; mol radius of albumin = 35.5 Å; mol radius of IgG = 54 Å; and mol radius of IgG = 120 Å. * Calculated from L_pS (*Eq. 8*).

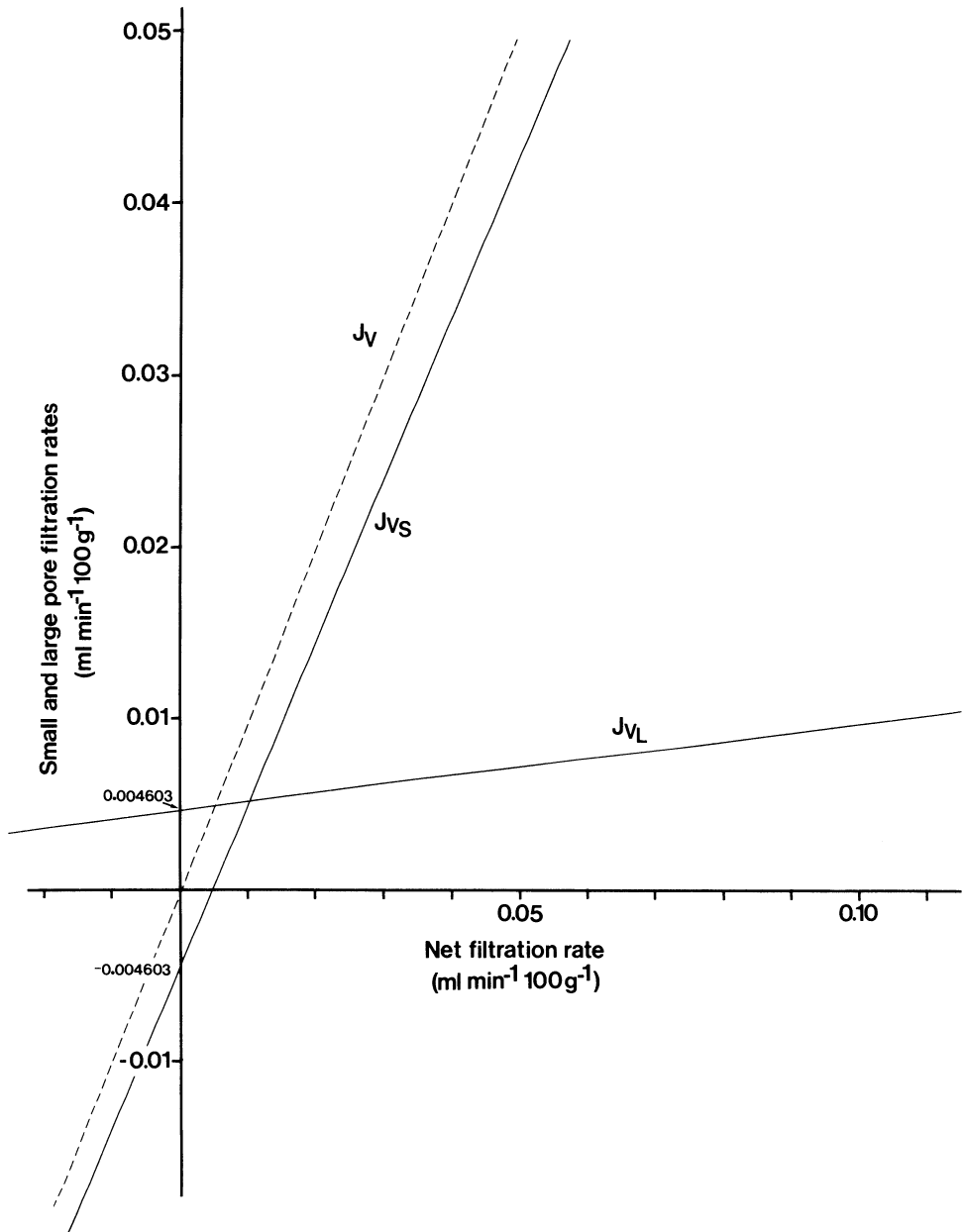


FIG. 4. Total (net) filtration rate (broken identity line) and small- (J_{vs}) and large-pore filtration rates ($J_{v,L}$) are plotted against J_v , simulated using data characterizing membrane B (Table 4) and assuming a constant colloid osmotic pressure difference ($\Delta\pi$) (14.06) for the whole range of J_v values. At zero net filtration, there will be a volume recirculation of $0.004603 \text{ ml} \cdot \text{min}^{-1} \cdot 100 \text{ g}^{-1}$.

volume flows are offset by the volume recirculation term when net filtration rate is zero and $\Delta\pi$ has not been affected (reduced) by the manipulation (reduction) of capillary hydrostatic pressure carried out to establish an isovolumetric state. Under these semi-steady-state conditions, fluid will recirculate from large to small pores.

2. Partitioning of fluid flux among the two major fluid conductive pathways: steady-state conditions

During steady-state conditions, there is no protein transport at zero net transvascular volume flow, because any protein concentration gradients formerly present between plasma and interstitium have then completely dissipated. In steady state, $\Delta\pi$, which determines

the partitioning of fluid flows between small and large pores, will increase as a function of J_v to reach a maximum first at high (infinite) J_v values. With increasing $\Delta\pi$ values, J_v will be progressively diverted from the large-pore system toward the small-pore system. At near zero net filtration rates, the fractional volume flow through large pores will thus be close to 100%, but C_i/C_p will fall progressively with increasing J_v values to asymptotically approach α_L for very high filtration rates.

Figure 5 shows net (total) filtration rate as well as small- and large-pore steady-state filtration rates simulated using the parameters listed in Table 4 for membrane B. Here $\Delta\pi$ is not constant as in Figure 3 but varies as a function of filtration rate. The $\Delta\pi$ (for total proteins) was assumed to be determined by the C_i/C_p value calculated for albumin, and it was assessed using

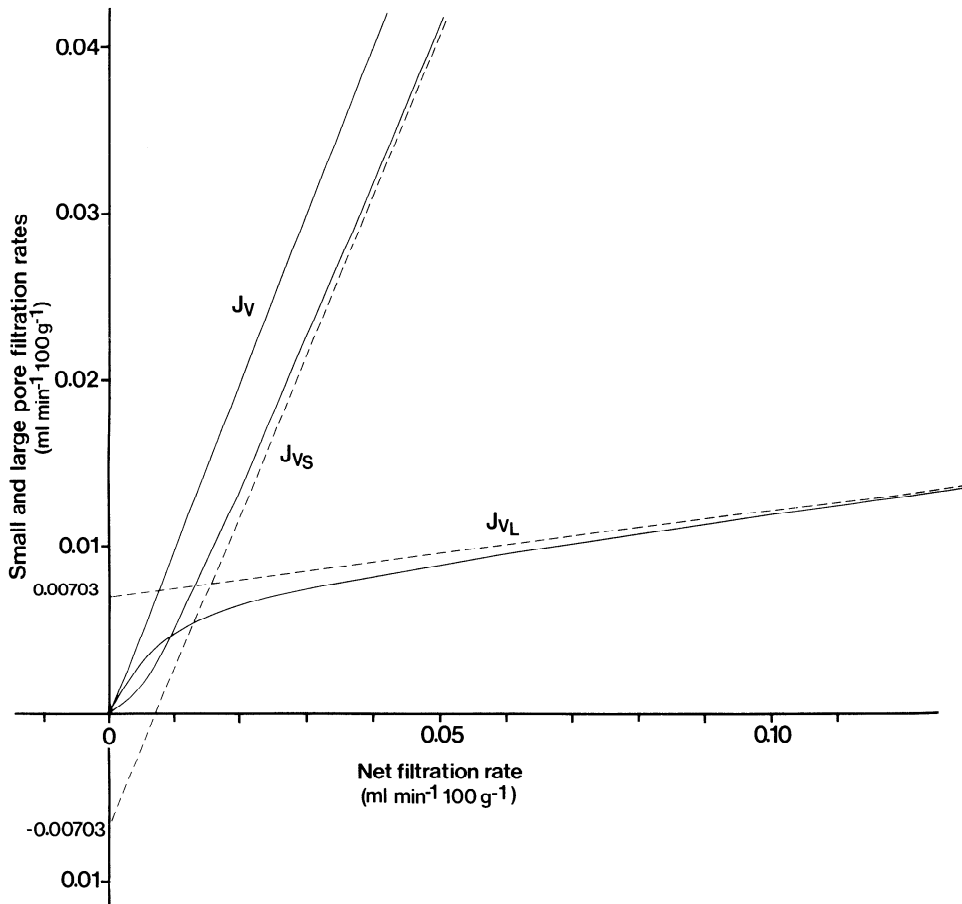


FIG. 5. Small- and large-pore volume flows as a function of net filtration rate, J_v (identity line), simulated for steady state and using data for membrane B (cf. Tables 4 and 5). Here $\Delta\pi$ is not constant but varies as a function of filtration rate; $\Delta\pi$ is calculated for steady-state conditions using an iterative procedure. Note that during steady-state conditions, volume recirculation is no longer possible. Large- and small-pore filtration rates due to “recirculation term” (cf. Eqs. 23 and 24) at infinite J_v values are indicated by ordinate intercepts of broken lines.

an iterative procedure. First, a tentative C_i/C_p value (albumin) was employed for the computation of C_i/C_p for albumin according to Equation 33. The initial estimate of C_i/C_p was then corrected toward the calculated value, and so on until the tentative and calculated values agreed (to a correspondence by more than 99.99%). Note that the J_v intercepts of the tangents of the functions depicted in Figure 4 (Eqs. 25 and 26) obtained for high (infinite) filtration rates approach the isogravimetric volume flows, $J_{v,L,iso}$ and $J_{v,S,iso}$, at the maximum possible $\Delta\pi$ for the minimum possible C_i/C_p , here equaling $(1 - \sigma) = 0.0988$. For a maximum $\Delta\pi$ of 21.47 mmHg, $J_{v,L,iso}$ (and $-J_{v,S,iso}$) became $0.0070 \text{ ml} \cdot \text{min}^{-1} \cdot 100 \text{ g}^{-1}$, to be compared with $0.0046 \text{ ml} \cdot \text{min}^{-1} \cdot 100 \text{ g}^{-1}$ for a $\Delta\pi$ of 14.06 mmHg (in Fig. 3).

3. Steady-state large-solute clearances and sieving coefficients in a two-pore membrane

Calculated large-pore and total (large pore plus small pore) steady-state solute clearances of albumin (mol radius 35.5 Å), IgG (mol radius 54 Å), and immunoglobulin M (IgM; mol radius ~120 Å) together with Pe numbers and fractional small- and large-pore fluid flows are simulated as a function of net steady-state filtration rate for the three model membranes (listed in Table 4) in Table 5. The Cl versus J_v relationships for the three molecules are depicted for membrane B in Figure

6. The unidirectional albumin tracer flux (interstitial tracer concentration ~ 0) for $\Delta\pi = 14.06$ is also shown (dotted line). The large-pore volume flow ($J_{v,L}$) curve versus J_v of slope (β) 0.05 is shown as a hatched line. Note that all curves are approximately linear at net volume flows exceeding $0.04 \text{ ml} \cdot \text{min}^{-1} \cdot 100 \text{ g}^{-1}$. Thus, unlike homoporous Cl versus J_v relationships (Fig. 1), which are generally concave upward for “moderately” to markedly elevated J_v values, the heteroporous Cl versus J_v curve is nearly linear for these relatively low flow ranges. This linearization probably occurs mainly because of the volume recirculation term acting as a continually increasing dissipative term at low J_v values. Note also that the IgG and IgM curves largely follow the large-pore volume flow curve according to the function $Cl_L = J_{v,L}(1 - \sigma_L)$ and that, in fact, all curve slopes (including that for albumin) yield realistic estimates of $(1 - \sigma)$. Identity line ($\beta = 1.0$) is also indicated (dotted line) in Figure 6. In this context it is worth emphasizing that the “offset” of the linear portion of the Cl versus J_v relationships from the abscissa only to a very minor degree reflects diffusive transport. Therefore, large errors arise when PS is determined from clearance at or near $J_v = 0$.

Let us take a closer look at the heteroporous albumin Cl versus J_v curve in Figure 6. It is generated using a total PS of $0.0023 \text{ ml} \cdot \text{min}^{-1} \cdot 100 \text{ g}^{-1}$. If instead the Cl versus J_v curve were simulated according to homopor-

TABLE 5. Computer-simulated solute clearance data for albumin, IgG, and IgM as a function of steady-state lymph flow for membranes A-C (cf. Table 4)

J_v , $\mu\text{l} \cdot \text{min}^{-1} \cdot 100 \text{ g}^{-1}$	$\Delta\pi$, mmHg	J_{vS}/J_v	J_{vL}/J_v	C_i/C_p	Albumin				IgG				IgM	
					Cl , $\mu\text{l} \cdot \text{min}^{-1} \cdot 100 \text{ g}^{-1}$	Cl_L , $\mu\text{l} \cdot \text{min}^{-1} \cdot 100 \text{ g}^{-1}$	Pe_S	Pe_L	Cl , $\mu\text{l} \cdot \text{min}^{-1} \cdot 100 \text{ g}^{-1}$	Cl_L , $\mu\text{l} \cdot \text{min}^{-1} \cdot 100 \text{ g}^{-1}$	Pe_S	Pe_L	Cl_L	Pe_S
<i>Membrane A</i>														
1	5.00	0.297	0.706	0.847	0.846	0.664	0.02	1.24	0.591		2.54	0.279	18.9	
2	8.65	0.386	0.614	0.719	1.439	1.138	0.06	2.16	1.015		4.43	0.486	32.8	
4	13.27	0.528	0.472	0.539	2.155	1.738	0.37	3.33	1.556		6.82	0.747	50.4	
10	18.03	0.731	0.269	0.305	3.052	2.470	0.58	4.71	2.205		9.66	1.058	71.4	
20	20.08	0.841	0.159	0.187	3.739	2.911	1.34	5.56	2.601		11.4	1.248	84.3	
50	21.34	0.921	0.079	0.107	5.359	3.621	3.68	6.92	3.234		14.2	1.552	104.8	
100	21.73	0.950	0.050	0.081	8.088	4.588	7.58	8.76	4.098		18.0	1.967	132.9	
200	21.93	0.965	0.035	0.068	13.554	6.447	15.4	12.3	5.759		25.2	2.764	186.7	
500	22.04	0.974	0.026	0.060	29.901	11.967	33.9	22.9	10.688		46.8	5.129	346.5	
<i>Membrane B</i>														
1	2.25	0.212	0.788	0.935	0.936	0.759	0.01	0.55	0.688		1.13	0.312	8.37	
2	4.20	0.262	0.738	0.873	1.747	1.394	0.03	1.03	1.240		2.11	0.583	15.67	
4	7.43	0.342	0.658	0.764	3.057	2.448	0.08	1.84	2.179		3.78	1.041	27.98	
10	13.15	0.519	0.481	0.540	5.409	4.422	0.29	3.37	3.960		6.89	1.900	51.06	
20	16.78	0.675	0.325	0.366	7.319	5.964	0.75	4.55	5.351		9.32	2.568	69.00	
50	19.61	0.822	0.178	0.214	10.718	8.186	2.29	6.25	7.350		12.80	3.527	94.78	
100	20.55	0.883	0.117	0.157	15.716	10.760	4.92	8.22	9.662		16.83	4.637	124.6	
200	21.00	0.916	0.084	0.129	25.695	15.484	10.23	11.83	13.905		24.23	6.673	179.3	
500	21.28	0.936	0.064	0.111	55.426	29.329	26.13	22.41	26.338		45.89	12.640	339.7	
<i>Membrane C</i>														
1	1.02	0.660	0.340	0.970	0.970	0.336	0.01	0.14	0.322	0.322	22.6	0.29	0.145	2.14
2	2.02	0.664	0.336	0.940	1.884	0.658	0.02	0.27	0.615	0.615	45.5	0.57	0.268	4.24
4	3.68	0.691	0.309	0.889	3.555	1.193	0.04	0.51	1.086	1.085	94.8	1.05	0.489	7.80
10	7.55	0.737	0.263	0.759	7.601	2.483	0.10	1.09	2.212	2.210	252.7	2.24	1.041	16.6
20	11.4	0.789	0.211	0.615	12.260	3.917	0.21	1.75	3.489	3.484	541.5	3.58	1.664	26.5
50	16.0	0.859	0.141	0.410	20.537	6.464	0.57	2.92	5.796	5.781	1,474	5.98	2.773	33.7
100	18.1	0.898	0.101	0.302	30.213	9.293	1.18	4.21	8.357	8.327	3,082	8.62	4.000	63.8
200	19.1	0.923	0.077	0.243	48.766	14.139	2.44	6.42	12.754	12.691	6,329	13.1	6.093	97.2
500	19.5	0.939	0.061	0.219	109.835	27.997	6.19	12.7	25.305	25.146	16,099	26.0	12.066	194.5

For membrane A, $r_s = 43 \text{ \AA}$, $r_L = 250 \text{ \AA}$, $A_o/\Delta x = 30,000 \text{ cm}$, $A_{oL}/A_o = 6.03 \times 10^{-4}$, $\alpha_L = 0.02$, $PS_{\text{alb}} = 0.985$, $PS_{\text{IgG}} = 0.230$, $PS_{\text{IgM}} = 0.015$, $\sigma_{\text{alb}} = 0.9456$, $\sigma_{\text{IgG}} = 0.9835$, $\sigma_{\text{IgM}} = 0.9921$. For membrane B, $r_s = 45 \text{ \AA}$, $r_L = 250 \text{ \AA}$, $A_o/\Delta x = 26,582 \text{ cm}$, $A_{oL}/A_o = 1.70 \times 10^{-3}$, $\alpha_L = 0.050$, $PS_{\text{alb}} = 2.307$, $PS_{\text{IgG}} = 0.574$, $PS_{\text{IgM}} = 0.037$, $\sigma_{\text{alb}} = 0.9012$, $\sigma_{\text{IgG}} = 0.9588$, $\sigma_{\text{IgM}} = 0.9802$. For membrane C, $r_s = 55 \text{ \AA}$, $r_L = 250 \text{ \AA}$, $A_o/\Delta x = 30,000 \text{ cm}$, $A_{oL}/A_o = 0.00254$, $\alpha_L = 0.05$, $PS_{\text{alb}} = 15.394$, $PS_{\text{IgG}} = 0.967$, $PS_{\text{IgM}} = 0.063$, $\sigma_{\text{alb}} = 0.7888$, $\sigma_{\text{IgG}} = 0.9585$, $\sigma_{\text{IgM}} = 0.9802$.

ous principles, a PS of $0.01 \text{ ml} \cdot \text{min}^{-1} \cdot 100 \text{ g}^{-1}$ will approximately fit the heteroporous curve for J_v values below 0.07 ml/min . At higher J_v values, the apparent PS has to be progressively increased with increasing volume flows to match the simulated data. Thus we can conclude that the apparent (homoporous) PS is markedly larger than the heteroporous PS and that the apparent PS will change as a function of volume flow. This abnormal behavior of homoporous PS is due to the fact the apparent PS is partly coupled to $\Delta\pi$ (cf. Eqs. 30 and 31), which increases as a function of net (total) volume flow and continues to do so (to some extent) even at relatively high net filtration rates. For the same reason, heteroporosity causes a considerably delayed washdown of C_i/C_p as a function of J_v in comparison with the situation for homoporous membranes.

In Figure 7, the albumin C_i/C_p values for membrane B ($r_s = 45 \text{ \AA}$, cf. Table 2) are plotted versus J_v (curve a).

Figure 7, curve b (hatched line), depicts a membrane having the same σ as our heteroporous membrane (membrane B) but where PS is $0.01 \text{ ml} \cdot \text{min}^{-1} \cdot 100 \text{ g}^{-1}$. Figure 7 also shows the simulated result of using $PS = 0.0023 \text{ ml} \cdot \text{min}^{-1} \cdot 100 \text{ g}^{-1}$, which is the theoretical PS of membrane B as calculated from L_pS (Eq. 8), denoted curve c. The deviation of curve a from curve b is dependent on the volume recirculation term, which affects the data even at very high filtration rates. Thus heteroporosity makes it difficult to wash down C_i/C_p values to $(1 - \sigma)$ even when very high filtration rates are produced.

4. Differential steady-state albumin fluxes in small and large pores: relationships between diffusive and convective fluxes

As seen from Table 5, the large-pore Pe is 3 for albumin when transmembrane filtration rate is on the

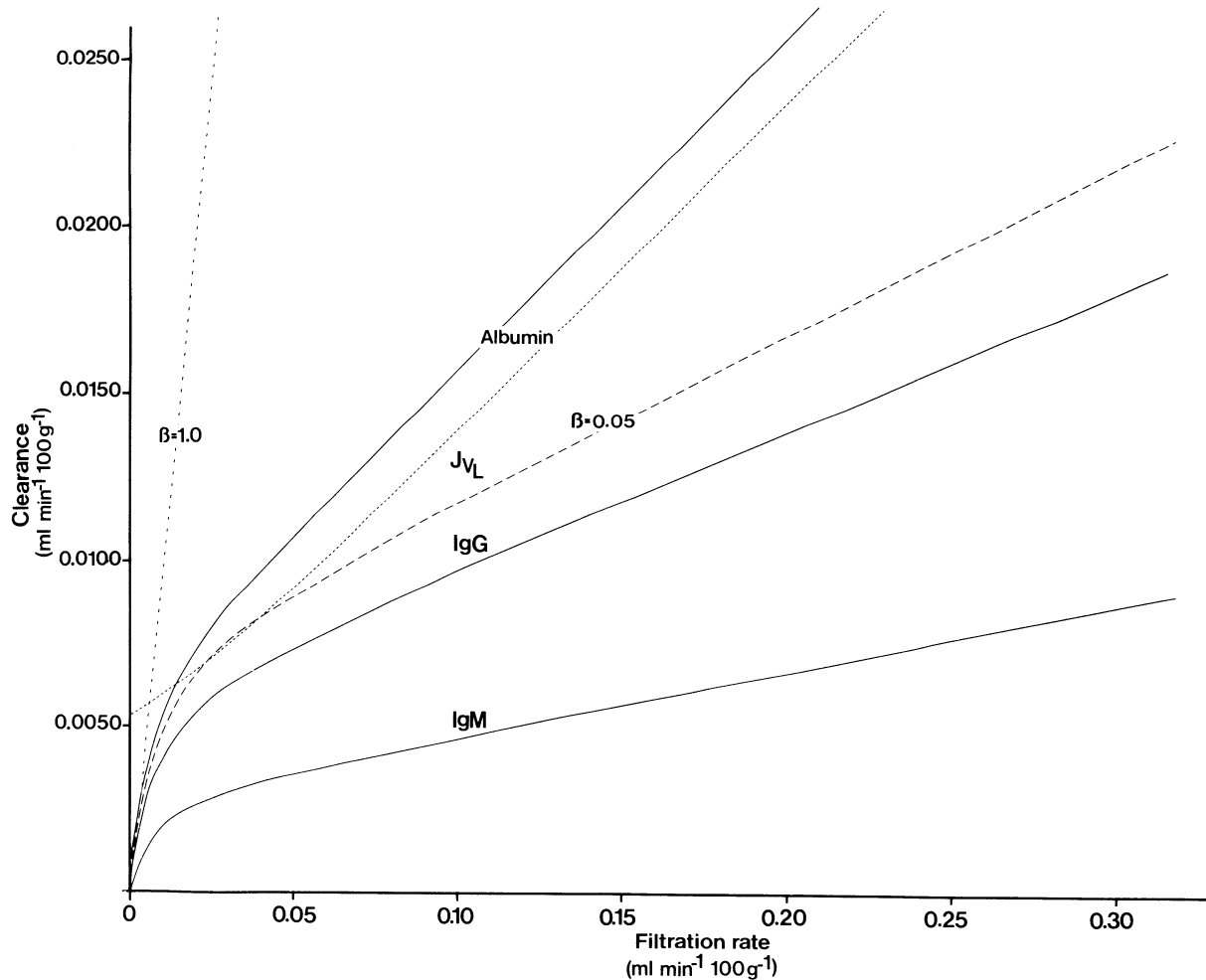


FIG. 6. Computer-simulated steady-state solute clearances for albumin, IgG, and IgM are plotted vs. filtration rate in heteroporous *membrane B* (Table 5). Dotted line represents unidirectional albumin tracer flux, and dashed line depicts large-pore volume flow vs. J_v . Note that all curves are approximately linear at net volume flows exceeding $0.04 \text{ ml} \cdot \text{min}^{-1} \cdot 100 \text{ g}^{-1}$ and that curve slopes (β) for solute clearance vs. filtration rate curves are close to $(1 - \sigma)$. Note also that "offset" of all slopes away from abscissa is only to a very small extent determined by diffusive component (PS) of solute transport.

order of magnitude yielding L/P values (albumin) of 0.5, as approximately prevailing in, for example, skin and muscle (250). Thus large-pore transport is mainly convective even for low volume flows. To obtain $Pe > 3$ for albumin in small pores, J_v has to be increased approximately fivefold above the lymph flow level yielding $C_i/C_p = 0.5$ (albumin) at control. Albumin transport through small pores is thus mainly diffusive at physiological lymph flows.

The partitioning of albumin fluxes between small and large pores, and hence, the degree of diffusive versus convective albumin transport depends on pore dimensions. If the small-pore radius is $< 50 \text{ \AA}$, then large-pore convective transport dominates at physiological lymph flows. If the small-pore radius is $> 50 \text{ \AA}$, then small-pore diffusive transport predominates at low transvascular volume flows. In Figure 8, the fractional contribution to total albumin transport of diffusion and convection in either pore system is plotted as a function of the small-pore radius when net filtration rate is ad-

justed to a level yielding C_i/C_p equal to 0.5 for albumin and $A_o/\Delta x$ is set to 30,000 cm. In other respects, the membrane has the properties of *membrane B* or *C* ($r_L = 250 \text{ \AA}$, $\alpha_L = 0.05$). Steady-state data are simulated using the iterative procedure presented above, that is, C_i/C_p for albumin determines the partitioning of fluid fluxes between small and large pores according to Equations 25 and 26. Note that large-pore albumin diffusion is negligible at lymph flows yielding lymph-to-plasma concentration ratios of albumin of 0.5. Large-pore convection is the predominating transport mode for albumin when $r_s < 48 \text{ \AA}$. Diffusion across small pores predominates when $50 < r_s < 60$, but for larger small-pore radii, convective transport through small pores will dominate the overall transport of albumin across this heteroporous membrane.

Fractional steady-state diffusive and convective albumin fluxes as well as fractional albumin fluxes occurring in either small or large pores are simulated as a function of net J_v for *membrane A* in Figure 9. Note

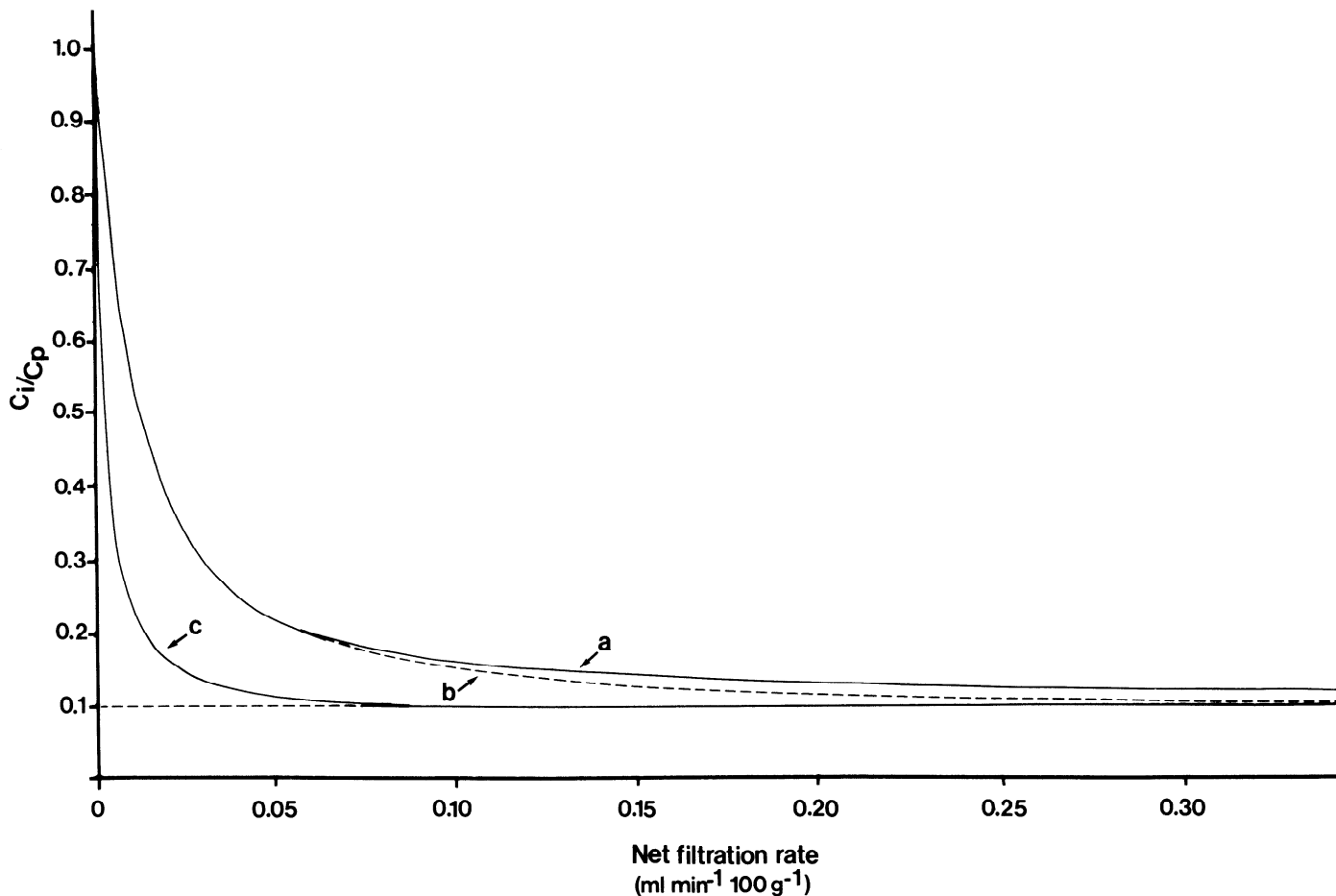


FIG. 7. Simulated C_i/C_p as a function of net filtration rate in membrane B (curve a). Curve b represents a membrane having the same σ for albumin as membrane B, but where $PS = 0.01 \text{ ml} \cdot \text{min}^{-1} \cdot 100 \text{ g}^{-1}$. Simulated result of using $PS = 0.0023 \text{ ml} \cdot \text{min}^{-1} \cdot 100 \text{ g}^{-1}$, which is the theoretical PS of membrane B as calculated from hydraulic conductance ($L_p S$) (Eq. 8) is also shown as curve c. Note that heteroporosity has same effect as increasing homoporous $PS \sim 4$ -fold (curve b vs. curve c). Heteroporosity, in addition, causes a delayed "washdown" of C_i/C_p as a function of J_v (curve a).

again that the large-pore diffusive transport (darkened area) is significantly contributing to overall transport only when J_v is $<0.008 \text{ ml} \cdot \text{min}^{-1} \cdot 100 \text{ g}^{-1}$, i.e., when it is lower than the calculated normal lymph flow (i.e., a J_v yielding C_i/C_p for albumin of 0.5). Note also that small-pore albumin transport is diffusion dominated at these normal filtration rates. With increasing J_v values, the convective portion of small-pore transport increases and diffusive transport eventually disappears. The ultimate partitioning of fluxes between large and small pores is determined by $\alpha_L(1 - \sigma_L)/\alpha_S(1 - \sigma_S)$ as seen from Equations 30 and 31. In the particular case shown in Figure 8, the small-pore (convective) transport will predominate over the large-pore (convective) transport first at extremely high filtration rates.

As concerns IgG and IgM, these molecules can theoretically only permeate the capillary membrane through large pores, for an equivalent small-pore radius being set $<54 \text{ \AA}$. Under these conditions, transport of these large macromolecules will be entirely convective even at low volume flows. At elevated J_v values, the diffusive component of the transport of these solutes is

definitely zero. However, because IgG is a largely uncharged species (at neutral pH) and the "structural" (uncharged) small-pore radius may be $\sim 65 \text{ \AA}$, there would be some diffusion of IgG across small pores even when the equivalent pore radius is as low as 45 \AA , as discussed above. This diffusive component is, however, small.

5. Coupling of solute flux to transcapillary volume flow in heteroporous membranes: effects of increases in capillary hydrostatic pressure versus effects of hemodilution

Depending on whether increases in fluid flow are induced by hydrostatic pressure elevations or by plasma dilution (reductions in plasma oncotic pressure), there is a fundamental difference as to the degree of coupling of solute flux to fluid flow in a two-pore system. If fluid filtration is induced by reducing $\Delta\pi$, keeping capillary hydrostatic pressure constant, then volume flow will be diverted toward the small-pore system. This will, in

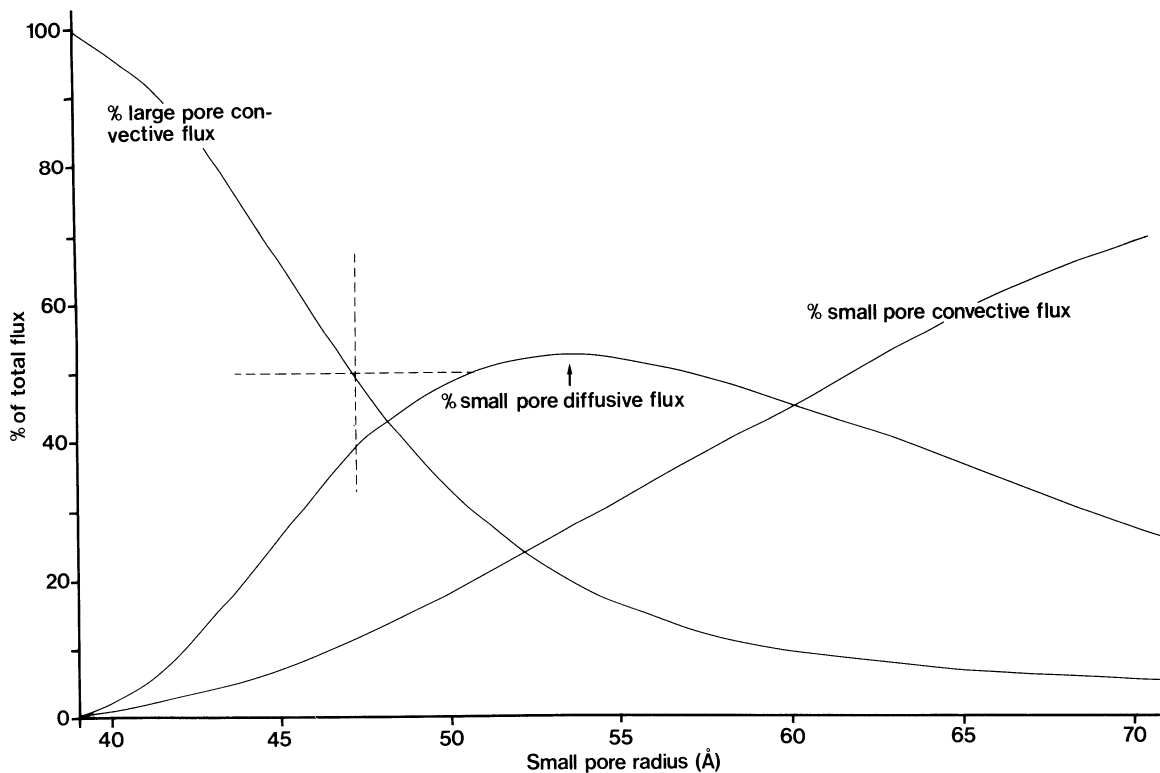


FIG. 8. Differential steady-state albumin fluxes in small and large pores and corresponding diffusive and convective components as a function of small-pore radius (cf. Eqs. 39b-41) in a membrane, where $A_o/\Delta x$ has been set constant at $30,000 \text{ cm}^2/100 \text{ g}$ over the whole range of r_s values and where $\alpha_L = 0.05$ and $L_p S = 0.008 \text{ ml} \cdot \text{min}^{-1} \cdot \text{mmHg}^{-1} \cdot 100 \text{ g}^{-1}$. The C_v/C_p for albumin is set at 0.5. Note that large-pore albumin diffusion is negligible at any r_s . Large-pore convection is the predominating transport mode for albumin for $r_s < 48 \text{ \AA}$, and small-pore diffusion predominates for $50 \text{ \AA} < r_s < 60 \text{ \AA}$. For larger small-pore radii ($> 60 \text{ \AA}$), convective transport through small pores will dominate overall transport of albumin across membrane.

turn, tend to (somewhat) increase the total solute flux for solutes permeating the small-pore system (cf. albumin). In this situation, the convective large-pore transport will, however, remain largely unchanged, insofar as ΔP is unaltered. For moderate initial reductions in $\Delta\pi$, the interstitial colloid osmotic pressure will eventually fall so as to counteract the initial perturbation of the Starling equilibrium. The overall reduction in $\Delta\pi$ at steady state will thus be very small when the initial drop in $\Delta\pi$ at steady state was moderate. In *curve Ia* in Figure 10, the simulated transmembrane clearance of albumin across membrane A is plotted versus J_v following elevations of capillary pressure when C_v/C_p varies as a function of steady-state net volume flow. The "initial" clearance when $\Delta\pi$ is set constant at 14.06 over the whole J_v interval is represented by *curve Ib* in Figure 10. The steady-state albumin clearance simulated following hemodilution is represented by *curve II* in Figure 10. During hemodilution, the hydrostatic pressure difference across the membrane is kept constant at 14.4 mmHg. Whether fluid filtration is induced during steady-state conditions (with counterregulatory changes in interstitial oncotic pressure) or "acutely" ($\Delta\pi$ remaining at its initially perturbed values), the Cl versus J_v curve (*curve II* in Fig. 10) will be identical for J_v values > 0.005 . Note that hemodilution seems to uncouple

solute flux from volume flow. The slope of Cl versus J_v in *curve II* in Figure 10 is thus initially only 0.025 (to 0.03) in comparison with 0.04 for the slopes of *curves I* and *Ib* in Figure 10, the latter two being close to $(1 - \sigma)$ (0.045). Note that a complete uncoupling of protein transfer from volume flow occurs during hemodilution for macromolecules larger in radius than the small-pore radius.

6. Heteroporosity effects on the Starling fluid balance: coupling of net steady-state fluid flow to capillary hydrostatic pressure

When capillary hydrostatic pressure is raised causing increases in transcapillary fluid filtration, then, as a consequence, $\Delta\pi$ increases, which tends to buffer the initial increment in fluid filtration. A similar buffering effect is caused by a concomitant rise in interstitial hydrostatic pressure (P_i). Under the simplifying assumptions that changes in P_i are small and that the microvascular membrane can be treated as a homoporous membrane, Michel (1993) derived a simple homoporous relationship between the capillary hydrostatic pressure and the steady-state filtration rate based on the nonlinear (228) solute flux equation. Provided that PS for total proteins is rather small, it could be shown that hydro-

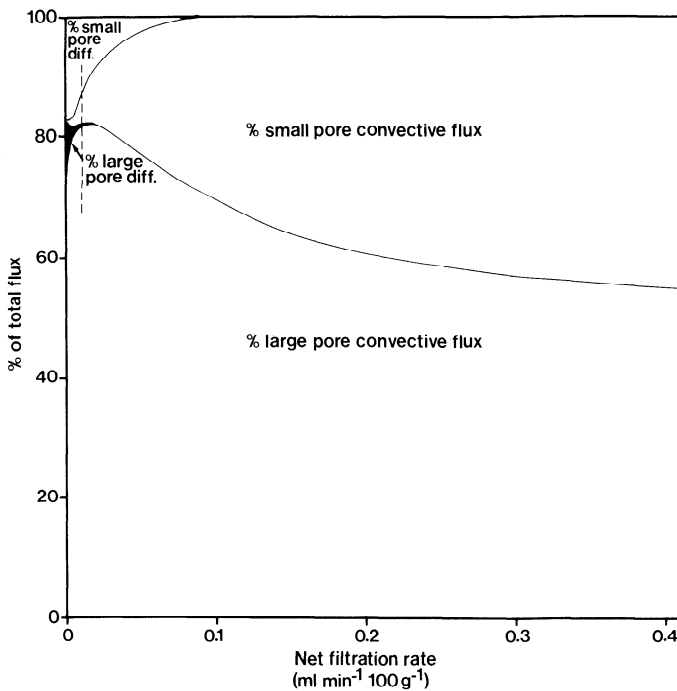


FIG. 9. Fractional contribution of large-pore convection and diffusion as well as of small-pore convection and diffusion to total steady-state transvascular clearance of albumin for *membrane A* as a function of net filtration rate. Vertical dashed line indicates level of J_v yielding a C_i/C_p for albumin of 0.5. Fractional convective flux of albumin through large pores reaches a maximum at approximately twice this J_v value.

static pressure increments, ranging in magnitude between zero and $\sigma^2 \cdot \pi_p$, where π_p is the plasma colloid osmotic pressure, cause only minor perturbations in the net steady-state fluid filtration rate. When the buffering capacity due to changes in $\Delta\pi$ is "exhausted" at pressures above $\sigma^2 \cdot \pi_p$, then the steady-state relationship between J_v and capillary hydrostatic pressure will be governed by the capillary hydraulic conductance. The expression introduced by Michel (193) was later more explicitly derived by Michel and Phillips (197a) and successfully applied to experimental data in single capillary experiments where ΔP was found to approximately equal the capillary hydrostatic pressure (P_c). It was pointed out that when $\Delta\pi$ is exhausted as "safety factor" against edema formation, the effective oncotic pressure opposing filtration will be $\sigma^2 \cdot \pi_p$. For skeletal muscle and skin, for which σ for total proteins may be 0.95 (see sect. VI B), this effective oncotic pressure corresponds to $0.9\pi_p$. In the lung, however, where σ for total proteins may be as low as 0.75, this corresponds to only $\sim 0.56\pi_p$ (cf. Ref. 253).

In a heteroporous membrane, the buffering effects of increases in fluid filtration following hydrostatic pressure increments will be less pronounced than in a homoporous membrane, both membranes having the same PS (for albumin) as demonstrated in Figure 11 (273). Here the relationship between steady-state J_v and transmembrane hydrostatic pressure gradient suggested by Michel and Phillips (193, 197a) for a homoporous

membrane with a PS for albumin of $0.985 \mu\text{l} \cdot \text{min}^{-1} \cdot 100 \text{ g}^{-1}$ (cf. Table 5; dotted curve in Fig. 11) is compared with that of a membrane having the same PS (albumin) but showing the heteroporous properties of *membrane A* ($r_s = 43 \text{ \AA}$, $A_o/\Delta x = 30,000$, $\alpha_L = 0.02$), shown by a solid curve in Figure 11. The computations have been made according to the iterative procedure mentioned above, matching input and output C_i/C_p values (albumin) for steady-state conditions and letting $\Delta\pi$ (total proteins) vary as a function of C_i/C_p . Note that the heteroporous relationship can be mimicked by increasing the PS of the homoporous membrane by a factor two to three.

In the example shown in Figure 11 (for *membrane A*), the normal steady-state filtration rate is $0.005 \text{ ml} \cdot \text{min}^{-1} \cdot 100 \text{ g}^{-1}$ at a P_c of 14.4 mmHg , a π_p of 22.88 mmHg , and a C_i/C_p for albumin of ~ 0.5 . Raising the P_c by 8 to 22.4 mmHg will initially increase J_v by $8 \times L_p S$ ($0.008 \times 8 = 0.064 \text{ ml} \cdot \text{min}^{-1} \cdot 100 \text{ g}^{-1}$ (hatched line and arrow in Fig. 11) to $0.069 \text{ ml} \cdot \text{min}^{-1} \cdot 100 \text{ g}^{-1}$. At steady state, due to increases in $\Delta\pi$ following the continual dilution of the ultrafiltrate at high ΔP values, J_v will, however, decrease to 0.025 ml/min (vertical hatched line and arrow in Fig. 11). Note that if $L_p S$ is calculated from the steady-state relationship between J_v and P_c , then $L_p S$ will be underestimated by nearly 70% ($2.5 \text{ vs. } 8 \mu\text{l} \cdot \text{min}^{-1} \cdot \text{mmHg}^{-1} \cdot 100 \text{ g}^{-1}$). Note also that during normal conditions, fluid balance alterations will occur continuously due to vasomotion and variations in P_c (cf. Ref. 193) along lines parallel to the oblique hatched lines in Figure 11.

7. Heteroporosity effects on the Starling fluid balance: coupling of net steady-state fluid flow to plasma colloid osmotic pressure

In Figure 12, the net steady-state filtration rate is computer simulated for *membrane A* when π_p is varied from 4 to 54 mmHg (solid line). Control π_p is set to 22.88 mmHg , and P_c is set to zero ($P_c = 14.4 \text{ mmHg}$). The steady-state relationship between J_v and π_p is also calculated using the homoporous transport formulation by Michel and Phillips (193, 197a), setting PS equal to $0.985 \mu\text{l} \cdot \text{min}^{-1} \cdot 100 \text{ g}^{-1}$ (hatched line, Fig. 12; Table 5). Note again that during steady state, it is not possible to absorb fluid to the plasma from the interstitium (253). Furthermore, fluid filtration will approach zero only for very high plasma oncotic pressures. At π_p values lower than P_c/σ^2 (where σ is the overall reflection coefficient for the membrane), the J_v versus π_p relationship will approach a straight line, the slope of which is $-L_p S \sigma^2$. If π_p suddenly drops from 22.9 to 14.9 mmHg (i.e., by 8 mmHg), then J_v will initially increase from 0.005 to $0.0662 \text{ ml} \cdot \text{min}^{-1} \cdot 100 \text{ g}^{-1}$ (hatched oblique line and arrow in Fig. 12). Again, due to dilution of the interstitial proteins, the steady-state J_v will approach a much lower value ($0.0167 \text{ ml} \cdot \text{min}^{-1} \cdot 100 \text{ g}^{-1}$) (vertical hatched line and arrow in Fig. 12). Thus, if $L_p S$ is determined by initially reducing $\Delta\pi$ by 8 mmHg, and hence the driving

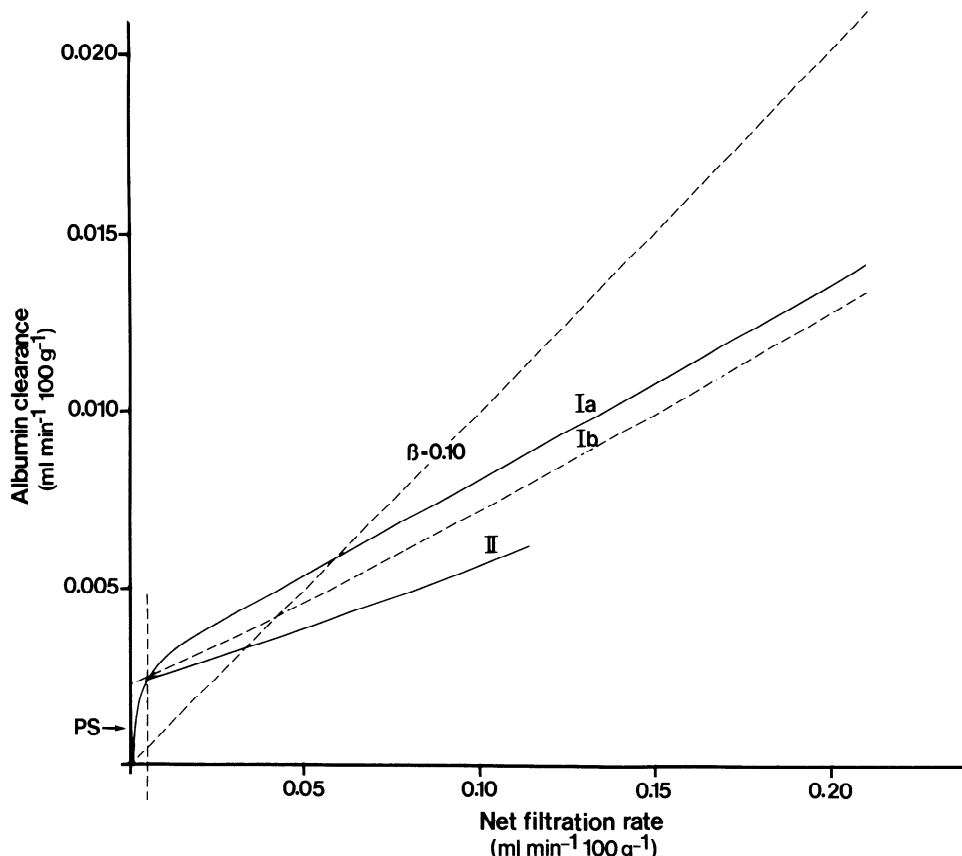


FIG. 10. Steady-state transmembrane clearance of albumin across membrane A (Table 5) is plotted vs. J_v following elevations of capillary pressure (curve Ia) and after hemodilution (curve II). Initial albumin clearance for hydrostatic pressure elevations when $\Delta\pi$ is set constant at 14.06 mmHg over whole J_v range is also indicated (curve Ib). Note that PS represents a very small fraction of total offset of Cl vs. J_v curve slopes. During hemodilution, hydrostatic pressure difference across membrane is kept constant at 14.4 mmHg, and J_v is increased by reducing $\Delta\pi$. Whether system is in steady state, or changes in J_v have occurred by acutely changing $\Delta\pi$, Cl vs. J_v curve will be identical (for J_v values >0.005), here represented by curve II. Note that hemodilution seems to partly uncouple solute flux from volume flow. The upper limit of curve II is determined by the largest fall in $\Delta\pi$ that could be possibly induced in this system. Vertical dashed line indicates level of J_v at which C_i/C_p for albumin is 0.5. Slope (β) of 0.10 is also indicated.

force for fluid filtration is reduced by $\sigma \cdot \Delta\pi$ (7.56 mmHg), and if the concomitant alterations in the steady-state fluid filtration rate are assessed for the calculations, then L_pS is underestimated by $\sim 80\%$ (1.54 vs. $8 \mu\text{l} \cdot \text{min}^{-1} \cdot \text{mmHg}^{-1} \cdot 100 \text{ g}^{-1}$).

B. Evaluation of Transcapillary Large-Solute Transfer at Low Lymph Flow States: Pore Modeling

In this section we discuss how to make determinations of small- and large-pore radii and fractional small- and large-pore L_pS (and hence σ) when steady-state C_i/C_p values have been determined for a number of different-sized macromolecules at specific steady-state lymph flows (transcapillary filtration rates). The procedure is first described in general terms and later applied to the experimental steady-state protein flux data of Renkin et al. (259).

First one has to calculate the solute clearance for each substance as $J_v(C_i/C_p)$. The next step in the present two-pore analysis is to plot these macromolecule clearances against the solute radii (a_e) on a semilogarithmic scale. Theoretical large-pore lines for differing large-pore radii, relating $J_{vL}(1 - \alpha_L)$ to a_e are then fitted to the clearances of the largest solutes measured ($a_e > 50 \text{ \AA}$) according to the method of Renkin et al. (262) (cf. Refs. 47, 251, 252, 324, 325; Eq. 35). This can be done since the large-pore transport is nearly exclusively due to convection. Under such circumstances, the Cl intercept of the

best fitting $(1 - \alpha_L)$ curve represents J_{vL} (cf. Equation 42). The small-pore filtration rate can now be obtained from $(J_v - J_{vL})$. With the use of a modified pore-stripping analysis (251, 262, 324, 325), the small-pore solute clearances (Cl_s) are obtained by subtracting the solutes' large-pore Cl values from their measured total Cl values. The best fit of theoretical curves relating Cl_s to a_e at each J_{vS} to a specific equivalent small-pore radius can now be determined using the nonlinear flux equation and specific models for restricted diffusion and for $(1 - \sigma)$ as a function of solute radius over pore radius (Eqs. 34 and 35, respectively) as described in section III C. The $A_o/\Delta x$ and r_s can thus be estimated if clearances of at least two solutes of radius $< 50 \text{ \AA}$ have been determined for a single steady-state level of J_v . The pore fit can be performed on a programmable pocket calculator using a trial-and-error approach (275), or using a curve-fitting program utilizing a nonlinear least-squares fit procedure on a personal computer (PC), as is performed in this review. If data from only one single steady-state lymph flow are available, two solutes of radius $< 50 \text{ \AA}$ and two solutes of radius $> 50 \text{ \AA}$ are needed for estimating the four unknowns, i.e., r_s , r_L , J_{vL} (or α_L), and $A_o/\Delta x$ (or alternatively L_pS). If data are collected for a number of different J_v values, then the number of solutes required for the analysis can be reduced.

In the next step we can assess α_L and $(1 - \alpha_L)$ to calculate the total σ for the membrane. For that reason we need to know the values of or to calculate $\Delta\pi$ and L_pS (from $A_o/\Delta x$). Then, α_L and $(1 - \alpha_L)$ can be easily solved

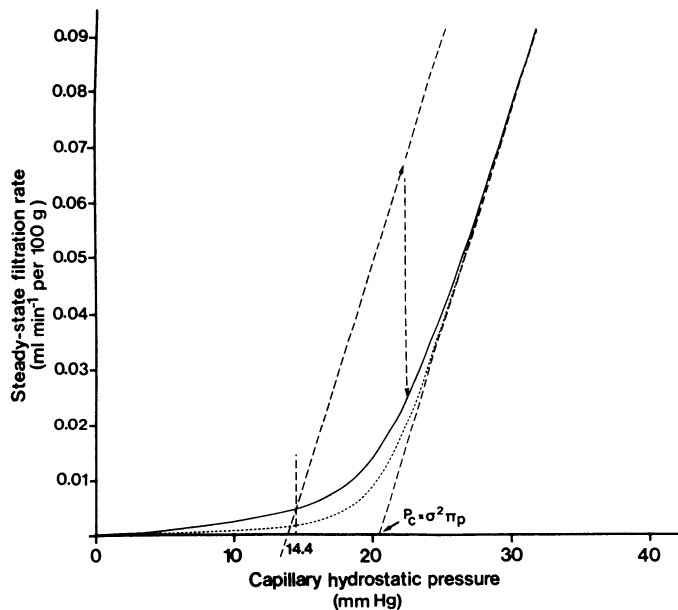


FIG. 11. Steady-state relationship between J_v and capillary hydrostatic pressure (P_c) for a homoporous (dashed line and bottom curve) and a heteroporous membrane (solid line and top curve) having identical values of "overall" total σ and PS . Top curve has properties of membrane A (Table 5). Heteroporosity affects J_v vs. P_c relationship in a fashion similar to that obtained by increasing PS of homoporous membrane 2- to 3-fold. Note also difference between initial fluid filtration occurring upon increasing capillary hydrostatic pressure by 8 mmHg (oblique hatched lined and arrow) and steady-state relationship between fluid filtration and increased P_c .

from the quadratic expressions of Equation 25 or 26, and total σ can be calculated from the small- and large-pore σ for the solute as related to r_L and r_S using α_L and α_S , respectively (Eq. 20). One problem arises when α_L or

$A_o/\Delta x$ (and $L_p S$) varies with net J_v , as indicated, for example, by reduced Cl values with increasing J_v values. In that case we have usually set α_L constant (usually determined for the highest J_v investigated) when vascular "permeability" has been considered stable, and we have allowed for variations in $L_p S$ (and $A_o/\Delta x$). In other cases, the value of $L_p S$ (or $A_o/\Delta x$) yielding the lowest variability of α_L has been accepted as that representing the best "fit" of the model to experimental data.

Rippe and Haraldsson (274) reanalyzed the data of Renkin et al. (259) according to these principles. The procedure adopted is exemplified in Figure 13A. Four steady-state levels of J_v are here selected from Table 1 (levels 1, 2, 5, and 6). First, Cl for albumin, IgG, and FM are plotted versus molecular radius in a semilogarithmic diagram. Next, the best curve fit of Cl for IgG and FM, i.e., molecules that are assumed to pass only through the large pores, is found to a $J_{vL}(1 - \sigma_L) (= Cl_L)$ versus a_e curve by applying Equation 35 (and Eq. 42). Each curve is determined by a unique set of values for J_{vL} (=ordinate intercept) and r_L (which determines the degree of curve "bending"). The best curve fit can be found by a trial-and-error approach (or using curve-fitting on a PC). For the lower curve, r_L is found to be 206.3 Å and J_{vL} equals $8.946 \mu\text{l} \cdot \text{min}^{-1} \cdot 100 \text{ g}^{-1}$. Values of J_{vL} and r_L for all curves investigated are given in Table 6, and some of the data are also depicted in Figure 13A. For curve 1 in Figure 13A, the total fluid flow (J_v) was $18.48 \mu\text{l} \cdot \text{min}^{-1} \cdot 100 \text{ g}^{-1}$, and thus the small-pore volume flow was $(18.48 - 8.95) = 9.53 \mu\text{l} \cdot \text{min}^{-1} \cdot 100 \text{ g}^{-1}$. At this stage we turn to the albumin clearance. Albumin is passing through both small and large pores. From the lower large-pore clearance curve (curve 1), we can determine the large-pore albumin clearance (at $a_e = 35.5$) to be $7.90 \mu\text{l} \cdot \text{min}^{-1} \cdot 100 \text{ g}^{-1}$. We can now calculate Cl_s from (Cl –

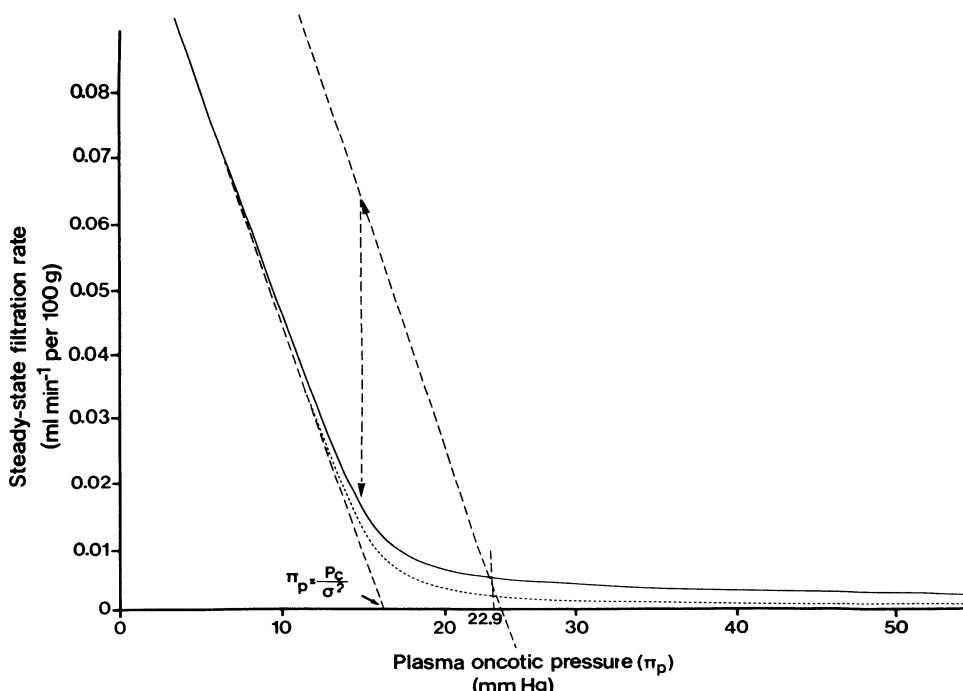


FIG. 12. Coupling of net steady-state J_v to plasma colloid osmotic pressure (π_p) calculated for membrane A. Capillary hydrostatic pressure was set to 14.4 mmHg, and control π_p was set to 22.88 mmHg. Solid line indicates relationship for heteroporous membrane A, and dashed line represents relationship for a homoporous membrane having identical values of overall σ and PS as membrane A. Note that increasing π_p will not cause net fluid absorption during steady-state conditions. Note also difference between initial fluid filtration occurring upon acute reductions in π_p by 8 mmHg and steady-state fluid filtration occurring upon same reduction in π_p (cf. Fig. 11).

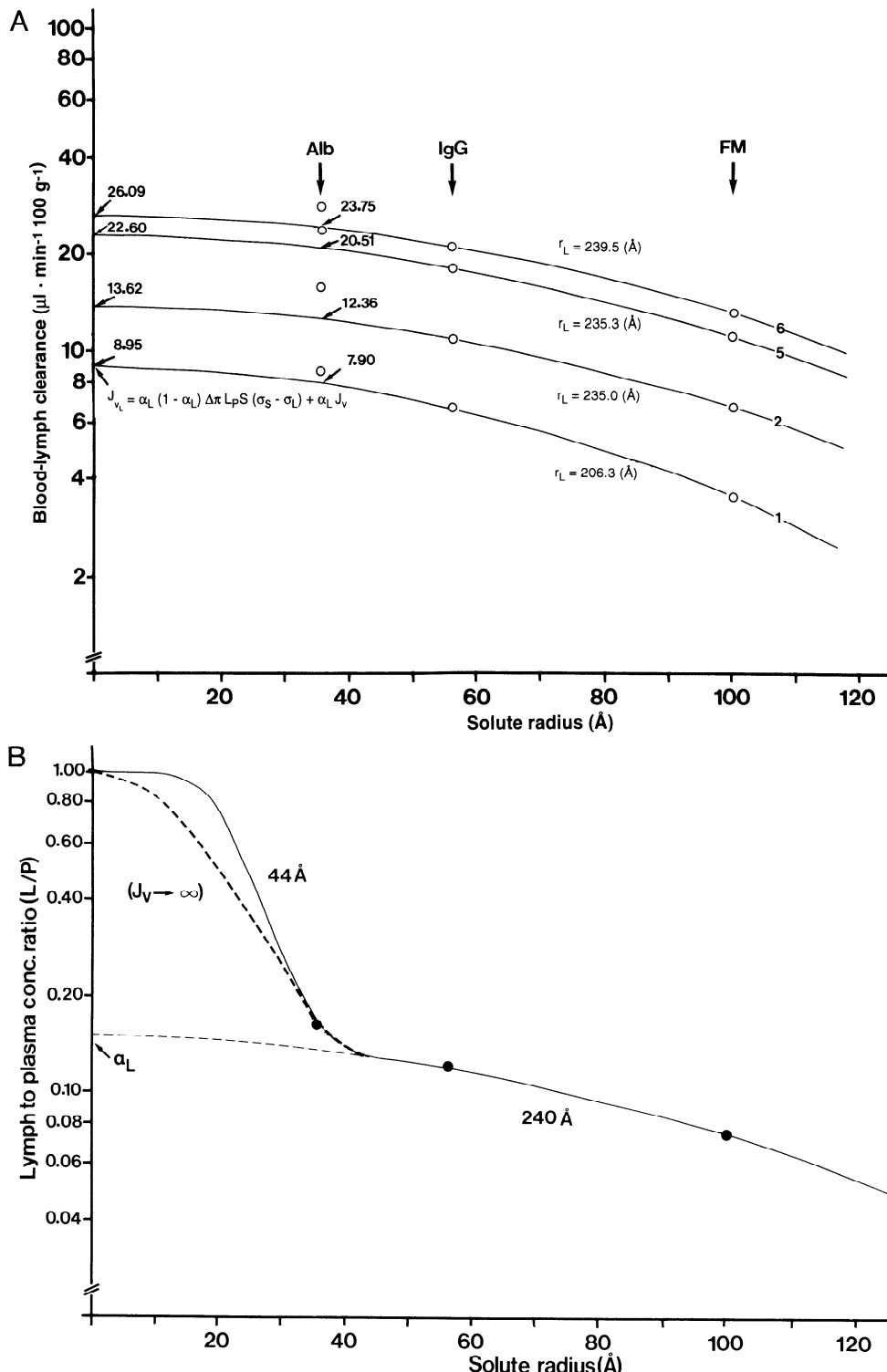


FIG. 13. **A:** semilogarithmic plot of blood-lymph clearances of albumin, IgG, and fibrinogen/macroglobulin (FM) for J_v levels 1, 2, 5, and 6 in Table 1 vs. solute radius (a_e) together with theoretical large-pore lines relating $J_{vL}(1 - \sigma_L)$ to a_e for each specific large-pore radius (r_L) and J_{vL} . Values for large-pore Cl at $a_e = 35.5$ (albumin) and $a_e = 0$ ($=J_{vL}$) are shown. Note that α_L and r_s can be solved for every curve intercept, provided that L_pS (or corresponding $A_o/\Delta x$) and $\Delta\pi$ are known. **B:** lymph-to-plasma concentration ratios (L/P) vs. solute radius at highest J_v in study of Renkin et al. (259) simulated according to present 2-pore model (solid line) and according to classical wash-down technique (thick dashed line). Difference between the 2 analyses mainly lies in the fact that the present model takes into account diffusive transport of solutes across small pores and that α_L is here calculated from J_{vL} and not obtained from sieving data for highest J_v level. Furthermore, in present analysis, all J_v levels are utilized. Thus α_L according to present heteroporous model is 0.10 and not 0.15 as obtained using wash-down principle.

Cl_L), yielding a value of $0.76 \mu\text{l} \cdot \text{min}^{-1} \cdot 100 \text{ g}^{-1}$. Furthermore, we know the corresponding value of J_{vS} . To calculate a small-pore radius from Equation 3b, we also need to know the value of albumin PS_S , which is obtained from $A_o/\Delta x$, and the degree of restricted diffusion of albumin ($a_e = 35.5$) according to Equation 34. In addition, we need to apply Equation 35 to calculate $(1 - \sigma_S)$ for albumin. Again, using a trial-and-error approach (or

a computer fit), we can find an exact r_s that fits the small-pore albumin clearance in Equation 3b.

If $A_o/\Delta x$ is not known, it may be calculated from L_pS using Equation 8. For 100 g of paw tissue, $A_o/\Delta x$ should be $\sim 30,000 \text{ cm}$ as calculated from $L_pS \sim 0.01 \text{ ml} \cdot \text{min}^{-1} \cdot \text{mmHg}^{-1} \cdot 100 \text{ g}^{-1}$ (288). Renkin et al. (259), however, derived an approximate L_pS for the dog's paw of $3.9 \mu\text{l} \cdot \text{min}^{-1} \cdot \text{mmHg}^{-1} \cdot 100 \text{ g}^{-1}$ from the steady-state

TABLE 6. Heteroporous analysis of albumin data from Table 1

Curve No.	$\frac{A_o}{\Delta x}$, cm/100 g	$L_p S$, $\mu\text{l} \cdot \text{min}^{-1} \cdot 100 \text{ g}^{-1}$	r_s , Å	r_L , Å	$J_v(L)$, $\mu\text{l} \cdot \text{min}^{-1} \cdot 100 \text{ g}^{-1}$	J_{vL} , $\mu\text{l} \cdot \text{min}^{-1} \cdot 100 \text{ g}^{-1}$	Albumin					
							C_i/C_p , (R)	α_L	$\frac{J_{vL}}{J_v}$	P_e_S	P_e_L	
1	13,000	3.9	44.9	206.3	18.48	8.946	0.76	7.90	2.16	1.11	4.68	0.200
	29,800	9.05	43.1				0.66	8.00	4.05	0.75	2.21	0.107
2	13,000	3.9	47.1	235.0	53.04	13.62	3.23	12.36	2.61	3.04	7.74	0.162
	29,800	9.05	46.0				3.21	12.38	5.12	1.61	3.53	0.105
3	13,000	3.9	46.6	242.0	78.96	15.37	4.63	14.02	2.38	5.34	9.27	0.135
	29,800	9.05	46.1				4.60	14.04	5.10	2.53	4.10	0.095
4	13,000	3.9	44.65	214.5	96.00	19.55	4.00	17.41	2.03	9.39	10.88	0.150
	29,800	9.05	44.56				3.99	17.42	4.59	4.17	4.77	0.109
5	13,000	3.9	42.30	235.3	147.8	22.60	3.87	20.51	1.42	28.28	15.22	0.122
	29,800	9.05	42.30				3.87	20.52	3.27	12.33	6.95	0.096
6	13,000	3.9	41.85	239.5	175.0	26.09	4.06	23.76	1.34	38.87	19.23	0.123
	29,800	9.05	41.85				4.06	23.75	3.07	16.95	8.39	0.099

Heteroporous analysis of the albumin flux data from Table 1 according to procedure described in section IVB. For each J_v level, large-pore volume flow (J_{vL}) and large-pore radius (r_L) were calculated from IgG and FM data. Small-pore radius (r_s) is then adapted (at 2 levels of $L_p S$ and $A_o/\Delta x$) to yield an exact fit of model to experimental data. Pe, Peclet number; subscripts S and L refer to small pore and large pore, respectively. [Data from Renkin et al. (259).]

relationship of J_v versus venous pressure in their experiments, yielding $\sim 13,000$ cm/100 g. This value is probably too low (cf. sect. IV A6). While the level of $A_o/\Delta x$ has a significant impact on the r_s determination for low J_v states (cf. curves 1-3), it can be shown that it is not crucial for determining r_s for high J_v states (cf. curves 4-6), as demonstrated in Table 6. Here $A_o/\Delta x$ is set at either 13,000 or 29,800 (see below). For the upper curves (curves 5 and 6), the level of $A_o/\Delta x$ plays no significant role at all, because at these J_v values, the Pe values are very high in both small and large pores. In conclusion, a low $A_o/\Delta x$ tends to give a slight overestimation of r_s for low J_v values, but not for high J_v values. Because we have data for a number of different J_v levels, the overall r_s will be only slightly overestimated by selecting a low $A_o/\Delta x$ value.

The next step in the analysis is to solve α_L using the quadratic Equation 25 from the six J_{vL} values obtained for the six experimental J_v values. To solve Equation 25, $\Delta\pi$ values are obtained from Table 1, and as a first approximation, $(\sigma_S - \sigma_L)$ is set to ~ 0.85 (as later modified according to updated r_s values). The magnitude of α_L is more critically linked to assumptions regarding $L_p S$ than is $A_o/\Delta x$. Setting $L_p S \sim 3.9 \mu\text{l} \cdot \text{min}^{-1} \cdot \text{mmHg}^{-1} \cdot 100 \text{ g}^{-1}$ yields a maximum α_L of 0.20 for curve 1. Then α_L falls off for increasing J_v values (to 0.12 for curve 6). However, because in the study of Renkin et al. (259) $L_p S$ was unknown, one may actually treat both $L_p S$ and α_L as unknown parameters, which stay constant over the entire J_v range. Then the best-fitting $L_p S$ (and α_L) can be solved for all six J_{vL} values, yielding α_L equal to 0.100, $L_p S$ equal to $9.05 \mu\text{l} \cdot \text{min}^{-1} \cdot \text{mmHg}^{-1} \cdot 100 \text{ g}^{-1}$, and $A_o/\Delta x$ equal to 29,800 cm/100 g.

The overall results from a heteroporous assessment

of the Table 1 data using a computer-aided nonlinear least-squares regression analysis of all data, according to the model described above, are summarized in Table 7. Note that the standard errors of both the large-pore and small-pore estimates are very small. Thus there is a remarkably good fit of the two-pore model to experimental data at every steady-state filtration rate. It is noteworthy that, in principle, a complete analysis of r_s , r_L , α_L , and α_S can be made at any of the low lymph flow states presented, provided that a reasonable estimate of $L_p S$ is available. Thus, with heteroporous analysis, it is not necessary to elevate venous pressure and, hence, lymph flow to obtain the appropriate macromolecular exchange parameters.

TABLE 7. Results of a nonlinear least-squares regression analysis of all data listed in Table 1 from dog's paw according to heteroporous transport theory

	Albumin (35.5 Å)	IgG (56 Å)	FM/Macro (100 Å)
Overall σ	0.868	0.922	0.954
Small-pore σ	0.954	1.000	1.000
Large-pore σ	0.097	0.219	0.537
Total PS, $\mu\text{l} \cdot \text{min}^{-1} \cdot 100 \text{ g}^{-1}$	4.059	1.261	0.176
Small-pore PS, $\mu\text{l} \cdot \text{min}^{-1} \cdot 100 \text{ g}^{-1}$	0.753	0	0
Large-pore PS, $\mu\text{l} \cdot \text{min}^{-1} \cdot 100 \text{ g}^{-1}$	3.306	1.261	0.176
Large-pore Pe at control J_v	2.30	5.21	22.15
Small-pore Pe at control J_v	0.62		

Capillary hydraulic conductance = 0.00905 ± 0.00093 (SE) $\text{ml} \cdot \text{min}^{-1} \cdot \text{mmHg}^{-1} \cdot 100 \text{ g}^{-1}$; large-pore radius = 228.5 ± 8.59 (SE) Å; small-pore radius = 44.05 ± 1.03 (SE) Å; fractional large-pore $L_p S$ (α_L) = 0.100 ± 0.008 (SE); diffusion area over unit path length = $29,802 \pm 2,384$ (SE) cm/100 g; fractional large-pore area $A_{o,L}/A_o = 4.11 \times 10^{-3}$. [Data from Renkin et al. (259).]

Figure 13B illustrates some other aspects of how the present analysis differs from the wash-down technique (325). In Figure 13B, the sieving coefficients for albumin, IgG, and FM obtained at the highest lymph flow of Table 1 are depicted together with the predicted sieving coefficients (L/P) versus a_e curve using the classical wash-down approach (hatched curve). Predictions made using the present two-pore equations (Fig. 13B, solid curve) are also shown. There is no difference in the two analyses regarding the large-pore radius. Moreover, the large-pore curves have essentially the same shape for every J_v investigated (data not shown). However, the depicted large-pore curve extrapolated to zero- a_e yields an apparent fractional large-pore hydraulic conductance (α_L) according to the wash-down principle, which in view of the present analysis is greatly overestimated. Furthermore, in the present analysis, there is a diffusive component of transport affecting the small-pore clearances, which tends to make the C_i/C_{sp} versus a_e curve close to unity for solutes being <15 Å in radius. However, the two curves converge for larger solutes at high J_v levels. Because transport by small-pore diffusion is taken into account in the present analysis, this will tend to make the small-pore radius estimate (slightly) lower than using the classical wash-down technique.

The data of Renkin and co-workers (cf. Refs. 259, 262) for dog paw have previously been reevaluated in terms of a two-pore model by Curry (47) and Renkin (252), but two-pore equations of the kind derived here were not explicitly applied. Neither Curry (47) nor Renkin (252) was able to fit the two-pore model exactly to the experimental data, but had to postulate the existence of "nonhydraulically conductive pathways" in the capillary walls operating at low J_v values to account for the apparent discrepancies between data and the model. One obvious discrepancy between the present analysis and that by Curry (47) and Renkin (252) is that the L_pS values used in our study are about twice their value, the latter being only 40% of that previously determined for skin (288) and dog hindlimb (218). Because the value given by Renkin et al. (259) is just the regression coefficient of the steady-state lymph flow versus the calculated capillary pressure, it must be markedly underestimated (cf. Fig. 11) due to Starling force adjustments occurring as a consequence of the increases in fluid filtration. This was indeed admitted by Renkin et al. (259). Actually, they stated that the "real" L_pS value may have been up to 60% larger than that employed in their calculations. Furthermore, the overall blood-to-lymph filtration coefficient should be smaller than the capillary membrane L_pS due to the presence of serial fluid resistances in the interstitium. For these reasons we consider the "higher" L_pS value as being the appropriate parameter determining the partitioning of fluid fluxes between small and large pores in the membrane. Hence, the recirculation term in *Equation 25* should be governed by the capillary wall L_pS value, since volume recirculation is a membrane event. The blood-lymph transport would, however, be described by the much lower blood-to-lymph filtration coefficient.

V. BRIEF SURVEY OF TECHNIQUES FOR ASSESSING TRANSVASCULAR MACROMOLECULAR PASSAGE

A. General Overview

1. General aspects

The present review mainly deals with lymphatic protein flux data, partly due to the wealth of such data in the literature, but also due to the fact that lymph data usually include a wide spectrum of macromolecular clearances. The lymph sampling technique was discussed in section IVB. Implicit in analyses of lymph data is that lymph largely reflects the composition of free interstitial fluid, which has been supported experimentally for skin (290) and has been discussed elsewhere (250). This contention has recently been seriously questioned (79, 130, 258), and we discuss this at some length in section vB. Another technique that is discussed separately is the tissue uptake technique (6, 16a, 18, 58, 76, 105, 107, 108, 113, 130, 140, 141, 143, 243, 244, 258, 260, 267, 279). Techniques involving measurements of the disappearance of macromolecular tracers added to the plasma, i.e., their transcapillary escape rate, have been reviewed recently (325) and are just briefly referred to in this context (see sect. vA3). This also holds for techniques based on intravital microscopic observations of the microcirculation. Here we briefly review just a few techniques employed rather extensively recently.

2. Single capillary analyses

As recently reviewed (47, 48, 194), single capillary analyses would seem to be the most direct approaches for quantifying and also demonstrating topographically (195) the leakage of macromolecular tracers across microvascular membranes of known surface area. However, single capillary studies have an upper limit of "resolution" for molecules of radius $\sim 30\text{--}35$ Å (128, 129). Actually, the extravasation rates of albumin and macromolecules larger than albumin seem to be too low to be correctly assessed by current single capillary techniques, at least when normal plasma proteins (including orosomucoid) are present in the perfusate (128). For solutes smaller than $\sim 30\text{--}35$ Å, there are now a number of studies showing that the selectivity of mesenteric frog microvascular walls is consistent with a small-pore radius of ~ 50 Å (48–50). In the terms of the so-called fiber matrix theory (51), according to which a matrix of fibrous molecules fills out all spaces in the microvascular walls, the data are also compatible with the presence of fibers being 5 Å in radius and occupying 5–7% of the volume of the intercellular junctions (49, 129). Furthermore, using single capillary techniques in evaluating the clearance of α -lactalbumin and ribonuclease, having approximately the same size but different net charge (α -lactalbumin being negatively charged at normal pH),

the frog mesenteric capillary wall has been shown to act as a negatively charged barrier, as discussed in section III D (4, 53). Single capillary studies have also been particularly useful for demonstrating the albumin effect (see sect. VII B), the orosomucoid effect (see sect. VIII C), and the relative contribution of the "water-only" (transcellular) fluid conductive pathway in continuous capillaries as discussed further in section VI B 2 (cf. Ref. 194).

3. Single injection residue function technique

Measurements of transvascular albumin clearance using the single injection residue function (SIRF) technique (296), as applied to the exchange of albumin in skeletal muscle capillaries (297), yield extremely high albumin extraction fractions (0.02–0.03) and, hence, initial transvascular albumin clearances. The same general results were recently obtained for muscle and a number of other tissues by measuring the initial (0–10 min) plasma disappearance and tissue uptake of macromolecular tracer(s) added to the plasma (16a). In the SIRF technique, a bolus of tracer macromolecules (cf. albumin) is injected into the main artery supplying the tissue (or organ), and the vascular and intratissue uptake and elimination of tracer are recorded externally (by a gamma camera). The use of the SIRF method is based on the assumption that the function defining vascular washout of an intra-arterially injected macromolecular tracer is readily separable from its superimposed tissue-to-blood tracer wash-out function when plotted on a semilogarithmic scale. This assumption is critical for the technique, especially for solutes having low extraction fractions such as albumin (89). Because the vascular wash-out function appears to be a complex function of time, the wash-out tail is, however, not mono-exponential even for a completely homogeneous tissue (13, 232). Indeed, in a heterogeneous tissue, vascular tracer washout is not very likely to follow a single mono-exponential function at all (106). Therefore, attempts to separate the two wash-out functions in the SIRF method may lead to an overestimation of the extraction of radiolabeled albumin for pure methodological reasons. Thus, compared with results obtained in intact rats (see below), the estimated albumin clearance using this technique is larger by almost two orders of magnitude. Indeed, there are both conceptual and technical problems with the SIRF method (89), but alternatively, the high apparent initial albumin clearance obtained with this technique may indicate that tracer albumin be rapidly exchanging with a "stagnant layer" of molecules immediately adjacent to the endothelial cells. Such a layer may reside in the glycocalyx or within the plasmalemmal invaginations. The high initial albumin extraction may also represent some initial binding to and subsequent dissociation of tracer albumin molecules from these structures. Such mechanisms may also be responsible for the rapid initial plasma disappearance of macromolecular tracers suddenly added to plasma, even though this phenomenon is usually regarded as an arti-

fact due to initial inadequate mixing of tracer with plasma (123a).

4. Reversed osmotic transient method

A variant of the osmotic transient technique (334), here referred to as the reversed osmotic transient technique (ROT) (111, 283), is based on assessments (in an isolated organ) of the initial transcapillary fluid filtration rate ($J_{v,i}$) occurring upon a sudden induced reduction in plasma or albumin $\Delta\pi$. If the organ is initially isogravimetric and L_pS has been separately measured, one can assess the reflection coefficient from $\sigma = J_{v,i}/(L_pS \cdot \Delta\pi)$, where σ represents the reflection coefficient for albumin or total proteins, depending on the nature of the osmotic transient. The reversed osmotic transient technique has recently been extensively used for assessing the permselectivity of muscle capillaries to large solutes (111, 150–152, 271). The σ for total proteins in muscle according to this technique usually falls in the range of 0.9–0.98. Ambiguities of the ROT are related to problems associated with assessing the L_pS correctly (cf. Refs. 193, 344).

5. Integral mass-balance technique for assessing reflection coefficient

The integral mass-balance technique for assessing the selectivity of microvascular walls in whole organs to large solutes was first suggested by Weiser and Grande (345) and later adapted by Maron and Pilati (175, 238) for lung and a skeletal muscle preparation. The method has recently been critically reviewed by Wolf et al. (356) and is just briefly outlined here. The technique is suited for isolated organs, perfused from a reservoir. It is based on measurements of the cumulative amounts of macromolecules and water that leave the circulation when fluid filtration is increased. Theoretically, the technique is based on essentially the same assumptions as the wash-down technique, in that high filtration rates are used to minimize the diffusive component of transport and to obtain a partitioning of fluid flows between small and large fluid conductive pathways aiming toward a limiting value, determined by the fractional hydraulic conductances characteristic of each of these pathways (α_L and α_S). In the simplest form, the technique requires only measurements of hematocrits and protein concentrations in plasma (perfusate) before and after a period of transvascular fluid filtration. However, it has later been shown that hemolysis during the course of the perfusion can produce large overestimations of σ for total proteins, especially when plasma protein changes are measured using simple techniques as refractometry. This is probably the reason why the early studies by Maron (175), Parker et al. (224), and Pilati and Maron (238) yielded very high values for σ , close to unity (175) or even exceeding unity (224). If hemolysis

can be excluded and the rate of fluid filtration is high ($P_e > 5$), the σ_f can be estimated using the equation

$$\sigma = 1 - \left(C_2/C^* \left\{ 1 - \left[\frac{(1 - H_1)(1 - C_1/C_2)}{(1 - H_1/H_2)} \right] \right\} \right) \quad (46)$$

where H_1 and H_2 are the initial and final hematocrits, respectively, and C_1 , C_2 , and C^* are the initial, final, and average plasma protein concentrations, respectively. If hemolysis, which decreases red cell volume and increases plasma hemoglobin and, hence, plasma total protein concentration, occurs during the period of increased filtration, a systematic overestimation of σ will usually be the result (178). Wolf et al. (356) have derived an equation to include this possibility. In the isolated blood-perfused cat hindlimb, the latter authors (356) determined the σ_f for albumin and total plasma proteins to be 0.82 and 0.83, respectively. Other measurements have yielded σ values ranging from 0.89 to 0.93 in the blood-perfused dog gracilis muscle (34) and ~ 0.66 in isolated blood-perfused canine lung lobes (332).

B. Critique of Lymphatic Protein Flux Analyses

Both lymphatic protein flux analyses and macromolecule efflux studies in isolated perfused tissues have been criticized on the basis of recent studies in intact rats. In vivo assessments of net fluid flow and tracer albumin clearance in muscle and skin (and other organs) have given estimates of the reflection coefficient for albumin (σ_{alb}) of the order of 0.98–0.995 (243, 258, 260, 261) and not of the order of 0.9–0.95 as obtained in lymph flux analyses or using, for example, the reversed osmotic transient or the integral mass balance techniques. In terms of the two-pore model, such high albumin reflection coefficients (> 0.98) indicate that α_L must be considerably less than 0.02. A σ_{alb} near unity implies that there is virtually no coupling between protein flux and fluid transfer across vascular walls. If so, there would also be no coupling of protein transfer to the increased capillary hydrostatic pressure in hypertension (226) or in volume expansion (227). Neither would there be any coupling between the apparent albumin permeability and the plasma colloid osmotic pressure as noted in quite a few studies (118, 145, 154, 155, 223, 261, 279, 358).

In lymphatic protein flux analyses using the washdown technique, large deviations from the steady state, i.e., high transcapillary volume flows, are needed for evaluating r_s , r_L , and α_L . This deviation from steady-state conditions may theoretically produce a false coupling between fluid volume and solute flux. If, for example, more lymph is drained than being formed at a given time, then the product of lymph flow and L/P will overestimate the transcapillary clearance. Also, if there is a marked hydration of the tissue gel (see below) during transcapillary ultrafiltration, lymph flow will be smaller than the transcapillary filtration rate, yielding higher L/P values at any given lymph flow than the C_i/C_p values of the capillary ultrafiltrate.

Another line of evidence against the validity of lymphatic protein flux studies relates to the heterogeneous nature of the interstitium (10, 17, 79, 162, 163). There is much evidence indicating that the gel-sol structure of the interstitium acts a gel filtration column (341, 342). In this model the tissue gel is penetrated by channels of free fluid, the protein concentration of which is rapidly exchanging with lymph. The free fluid channels thus have short turnover times, whereas the gel matrix appears to be rather impermeable to protein, hence being only slowly equilibrating with and partly excluding the lymph proteins (16, 239, 240, 341, 342). However, the gel may rather rapidly exchange (protein free) fluid by colloid osmosis. Actually, in skin and muscle, the time for complete equilibration of the gel compartment with lymph tracer macromolecules may be up to 2–3 days (317). In lymphatic protein flux studies, in which capillary pressures have been elevated to obtain steady-state L/P and J_v , it seems that a stabilization of L/P and J_v may occur already after 2–3 h of a sustained pressure elevation (259, 332a). However, during these conditions, relatively large amounts of protein-free fluid may have been taken up into the gel phase by local osmosis due to the drop in interstitial protein concentration in the free fluid phase, and proteins may still be washing out from the gel compartment. The excluded volume fraction for macromolecules may then have either decreased (220) or remained largely unchanged (14, 15). Thus a definite washdown of protein L/P to minimal values may take considerably longer than 2–3 h and require higher rates of fluid filtration (J_v) than employed in a majority of previous lymph studies (225) (cf. Fig. 7).

The mentioned phenomena thus seem to make lymph more concentrated than the capillary ultrafiltrate at elevated lymph flows. Moreover, if the two-compartment (gel filtration) interstitial model holds, the time for obtaining plasma-to-lymph equilibration at an increased J_v would be larger for a small macromolecule (cf. albumin) than for a larger one (cf. IgG or IgM), as demonstrated for paw tissue (16, 239, 342). Thus, for non-steady-state conditions following capillary pressure elevations, one would tend to overestimate clearances (or C_i/C_p) to smaller macromolecules relative to those of larger ones. The net effect would be an apparent increase in the ratio of clearances of small to large macromolecules at elevated J_v values as compared with control. In terms of the two-pore theory, the large-pore radius would then tend to decrease and the small-pore radius would tend to increase with increasing lymph flows. Such alterations are not evident from the analyses of the paw lymph data of Renkin and co-workers (259, 272, 274) but have been observed in other studies (cf. Figs. 14 and 15). Aside from the “latitudinal” heterogeneity of the interstitium discussed here, there may also be some “longitudinal” interstitial heterogeneity, implying transport restriction in the pathways conducting capillary ultrafiltrate through the interstitium to the initial lymphatics (250). The impact of interstitial transport resistances is to lower the L/P as compared

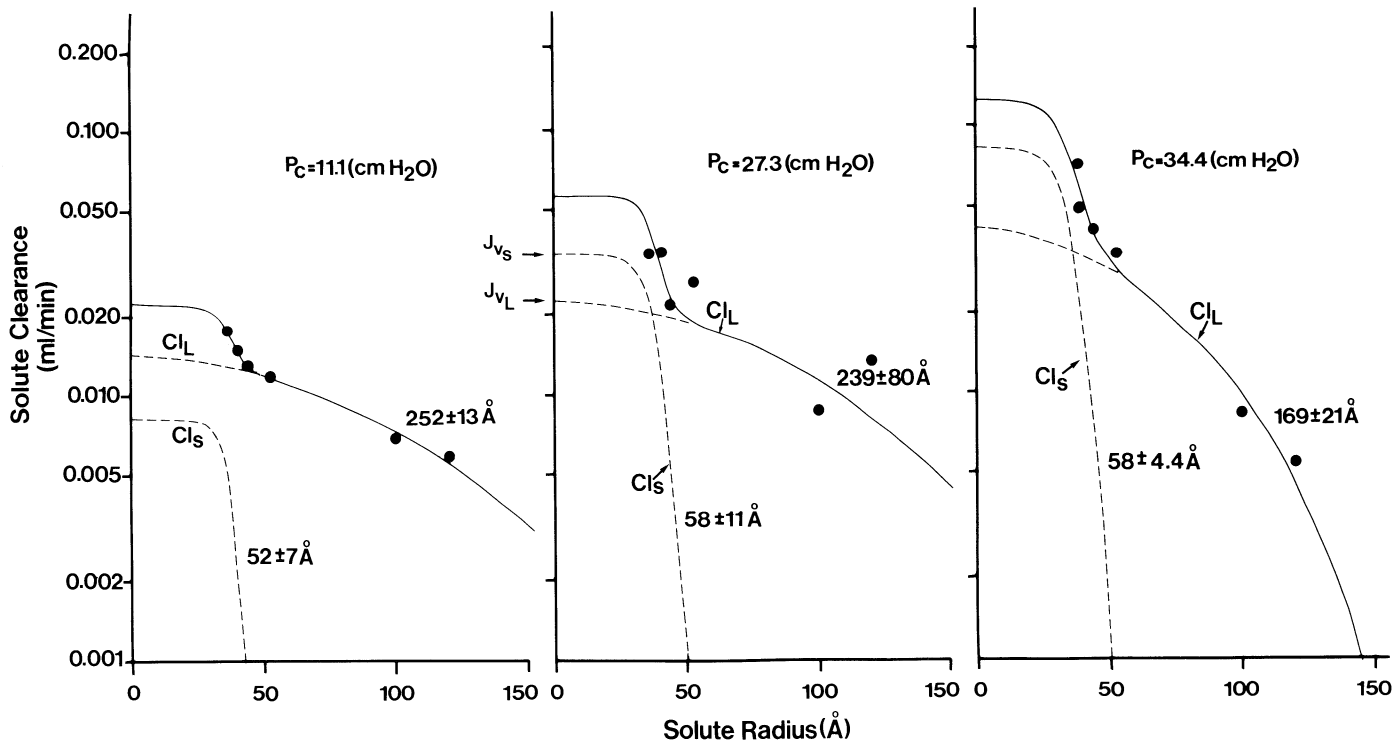


FIG. 14. Two-pore fit of steady-state plasma-to-lymph clearances (plotted on a semilogarithmic scale) in dog lung vs. molecular radius at 3 different lymph flows investigated. The $A_o/\Delta x$ values were calculated to be 84,979, 67,857, and 76,824 cm^2 , respectively, and J_{vL} was estimated to be 0.014, 0.022, and 0.041 ml/min for each of 3 calculated P_c levels, respectively. Note that average r_s for all 3 lymph flows was larger than any r_s value shown on figure. This is due to the fact that when fitting average r_L (215 Å) to data at $P_c = 34.4 \text{ cmH}_2\text{O}$, an r_s value as large as 67 Å was obtained. However, r_s remained largely unchanged when r_L was set to 215 Å for the 2 other P_c levels. [From Parker et al. (221).]

with C_i/C_p of the capillary ultrafiltrate, which is opposite to the impact of lateral interstitial heterogeneity.

A recent study on lung microvascular protein transport (130) points to the fact that actually both sampling of tissue and of lymph is needed to correctly evaluate transcapillary fluid and macromolecule fluxes, and that especially tissue sampling alone may lead to large errors. In the mentioned study, only a small fraction of the capillary ultrafiltrate and of protein tracer added to the vascular compartment remained in the lung interstitium during a period of 2 h. A major portion of macromolecular tracer had left the tissue in the lymph during the period of observation. This study may be criticized, however, since the lung interstitium is very small relative to the large pulmonary surface area available for exchange, leading to rapid equilibration (within 15–30 min) of the interstitium with the macromolecular tracers employed. However, the same general phenomena have also been observed in the cat ileum (332a), experiments less amenable to criticism. In general, it thus seems as if lymph flux analyses tend to overestimate protein fluxes, whereas tissue sampling may underestimate the overall blood-tissue fluxes of tracer. In other words, there appears to be a falsely high degree of coupling between protein fluxes and fluid flow using lymph collection techniques, whereas the reverse may be true using tissue sampling techniques.

C. Critique of Tissue Uptake Studies in Intact Animals

Tissue uptake studies in intact animals usually imply the assessment of the difference between two large quantities, i.e., the total amount of tracer present intra- and extravascularly in the tissue minus that present only in the intravascular compartment at the time of death. This is a statistically unfavorable situation, sometimes leading to even negative values (6, 113) for the portion of protein extravasated. Employing washout procedures to rid the vasculature of marker, on the other hand, tends to overestimate this quantity. Moreover, in intact animals, a significant portion of the tracer protein extravasated may leave the tissue via the lymphatics during the period of observation, when lymph drainage from the tissue is not hindered (130, 332a). In contrast, when lymph flow is blocked, as in perfused organs (76, 105, 279), these problems will be minor. Furthermore, vascular washout can be performed in a very controlled fashion *in vitro*. On the other hand, studies in isolated organs, such as perfused rat hindquarters, may suffer from problems associated with the artificial perfusion situation, even though plasma (containing orosomucoid) is used as perfusate. However, during cooling (or after isoprenaline), the sieving coefficient for albumin (C_i/C_p) in rat hindquarters was not significantly reduced as compared

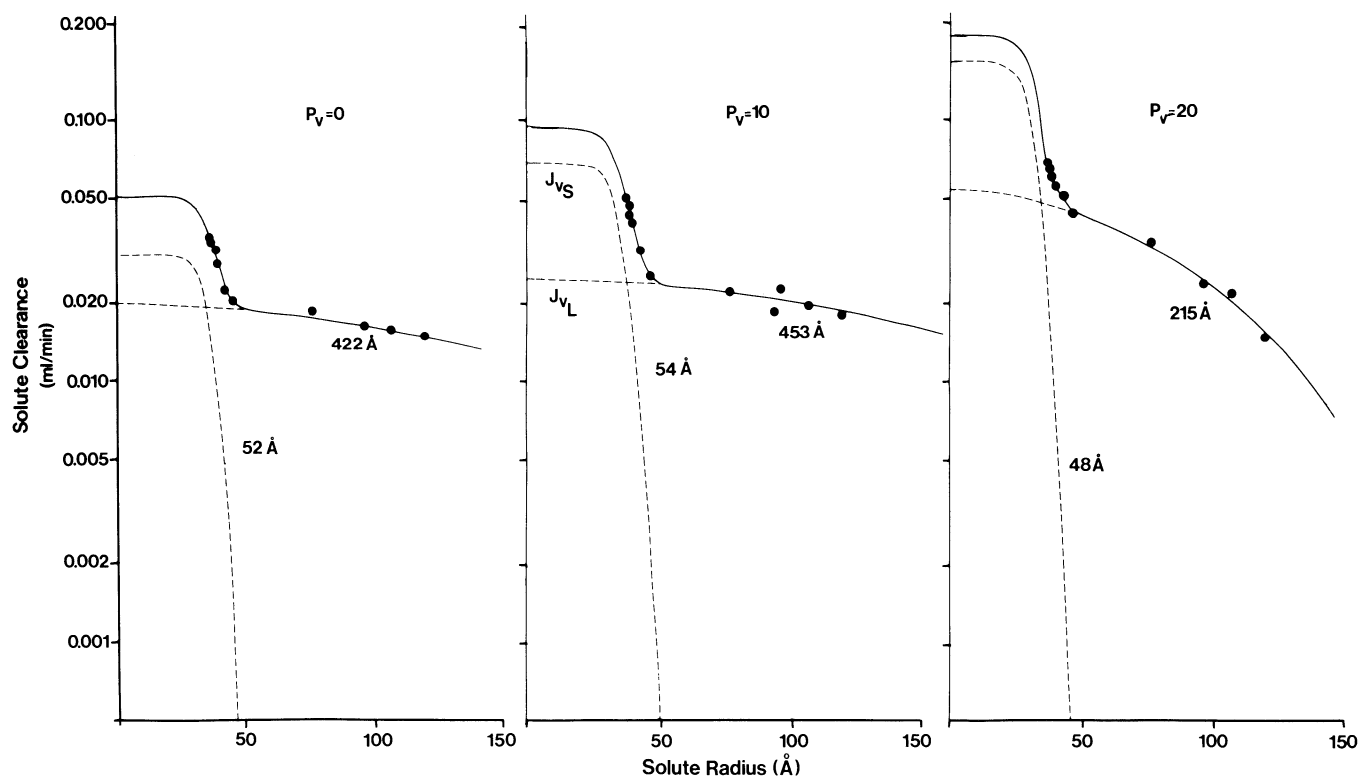


FIG. 15. Plasma-to-lymph solute clearances in cat ileum (97) plotted vs. molecular radius and shown as a function of 3 levels of venous pressure ($P_v = 0, 10$, and 20 mmHg). In this analysis α_L is set to 0.05. At highest level of venous pressure ($P_v = 30$ mmHg), not shown in figure, L_pS and $A_o/\Delta x$ decreased to $\sim 30\%$ of values prevailing at low P_v values (0–10 mmHg).

with control (279). This is contradictory to the notion that vascular permeability is increased due to the artificial perfusion, since both cooling and isoprenaline are known to counteract, at least, mediator-induced increases in microvascular permeability (269).

The present mode of two-pore analysis (cf. Tables 6 and 7) yields estimates of r_s , r_L , and α_L already in "steady-state" conditions, i.e., already at low lymph flows, that are closely similar to those obtained after manipulating the system by elevating the venous pressure (274). This also seems to contradict the notion of a falsely high coupling of protein flux to fluid flow obtained in lymphatic protein flux studies in the literature. As mentioned above, the rather high protein (albumin) clearances found in, for example, isolated perfused rat hindquarters may have other explanations than being due to an abnormally elevated vascular permeability. They may to a great extent be explained by differences in the degree of capillary recruitment between resting muscle and maximally vasodilated muscle, as recently discussed in detail (104, 109, 119). Finally, it has to be pointed out that data obtained in intact rats should be evaluated with great caution, since the experimental approach using whole animals does not allow for direct assessments of microvascular pressures, capillary surface area, or L_pS .

Haraldsson et al. (109) recently addressed the possibility that experimental errors other than those asso-

ciated with the tissue uptake technique per se may also have led to marked overestimations of σ for albumin in the rat studies referred to in References 243, 258, and 260. Venous congestion in one of the mentioned studies in the rat (258) was produced by unilateral femoral vein ligation, which was supposed to immediately raise venous pressure in the test hindlimb (P_v) by 10 mmHg, with the contralateral limb serving as a control. Haraldsson et al. (109), when they followed P_v via a T-tube inserted into the rat femoral vein, found that a similar maneuver increased P_v from 6 to 12.8 mmHg, but that there was a gradual return of P_v toward control during the following 60 min, the P_v leveling off at ~ 9.5 – 10 mmHg. It seems likely that the gradual return of P_v toward control is partly due to recruitment of collateral routes for venous return, reducing the effective capillary pressure elevation to just ~ 3 mmHg. Haraldsson et al. (109) argued that a large portion of fluid filtration occurring upon femoral vein ligation would not have been coupled to hydrostatic pressure, unless the capillary hydraulic conductance had very markedly increased from its resting value in this situation. However, L_pS should, if anything, have decreased during the period of increased venous pressure due to arteriolar constriction by myogenic mechanisms (189) or by the "venoarteriolar reflex" (124). Thus there is a possibility that some fluid may have entered the tissue driven by transcapillary crystalloid osmotic pressure gradients

[set up by tissue metabolites (18a)] via a transcellular route, thereby yielding a falsely low coupling of albumin flux to fluid flow (cf. Ref. 280).

There are, of course, several other possibilities for the disproportionality between the rather insignificant macromolecular efflux and the very large fluid transfer to the tissue observed in the study of Renkin et al. (258). 1) Some fluid may have accumulated intracellularly during the experiment. The procedure used by Reed (243) seems to have excluded this possibility, but it is notable that in his study σ_{alb} was lower than in that by Renkin et al. (258). 2) Some tracer albumin may have left via the lymph during the experiments, while fluid accumulated in the tissue. 3) The change in wet-to-dry weight ratio (assessed to calculate edema fluid accumulation) may have been overestimated in the test limb due to a reduction in wet weight of the control (contralateral) hindlimb secondary to a general sympathetic activation and peripheral vasoconstriction. Sympathetic activation would occur as a consequence of the reduced venous return following femoral vein ligation. Whereas capillary pressure was elevated in the test leg, it may thus have been reduced (by precapillary vasoconstriction) in the control leg. Whatever caused the marked fluid transfer from blood to tissue in the study by Renkin et al. (258), the high apparent L_pS value calculated for conditions of venous congestion in intact rats seems unrealistic and may not be compatible with increments in capillary filtration induced by capillary hydrostatic pressure elevations alone.

Although the mentioned whole animal studies are subject to great uncertainty, they are indeed interesting and point to the possibility that lymphatic protein flux studies, tissue uptake studies of macromolecular tracers in perfused organs, and studies on isolated vessels may all have underestimated the true reflection coefficient for albumin. When all data are taken together, however, it seems highly unlikely that the errors in these established techniques would have caused overestimations of C_i/C_p values by an order of magnitude or even more. Therefore, at present, it is too early to invalidate previous assessments of the blood-lymph or blood-tissue selectivity to large solutes simply based on the recent intact animal studies (109, 130).

VI. PROTEIN TRANSPORT IN VARIOUS VASCULAR BEDS AT LOW AND HIGH TRANSVASCULAR FILTRATION RATES: APPLICATION OF TWO-PORE EQUATIONS

A. General Considerations

There is a great variability in the rates of transvascular extravasation of macromolecules among different vascular beds, as demonstrated for albumin and IgG in previous studies (18, 58, 102, 113, 181, 325). The protein extravasation rate is particularly high in organs with discontinuous capillaries (liver, bone marrow, spleen,

and other organs of the reticuloendothelial system) but is also high in fenestrated or continuous capillary beds having a large vascular surface area per unit tissue weight, such as intestinal organs and the lung. The vascular surface area appears to be the major source of variation of protein clearances among continuous and fenestrated capillaries, since the calculated albumin extraction fraction (i.e., albumin clearance divided by plasma flow) seems to remain more or less invariant among tissues having these capillaries (18, 113). Implicit in this reasoning is that there is a rough correlation between plasma flow and vascular surface area per unit tissue weight.

Also, Taylor and Granger (325), in their review article in the *Handbook of Physiology*, demonstrated a remarkable uniformity of the vascular permeability properties among various capillary beds (cf. also Ref. 248). Actually, many fenestrated vascular beds seem to be, if anything, more size selective than continuous capillaries. Generally, the reflection coefficient to albumin is ~ 0.9 –0.95 in fenestrated as well as continuous vascular beds. In other words, with the possible exception of lung and kidney, the small- and large-pore radii as well as the fractional large-pore hydraulic conductances (α_L) do not seem to differ significantly among continuous and fenestrated endothelia.

In this section the two-pore theory described in section IV is applied to a few selected large-solute capillary clearance data from the literature. Modeling is performed using the concept of equivalent pores. Hence, electrical charge selectivity is not explicitly taken into account. A computerized least-squares regression analysis is applied to clearance data at defined steady-state transvascular filtration rates either at normal or elevated vascular pressures, and the four unknown parameters described above, i.e., r_S , r_L , $A_o/\Delta x$ (or L_pS), and J_{vL} (or α_L) are determined. Discontinuous capillaries and "tight junction" capillaries (representing the blood-brain barrier) are not included here.

Many of the lymphatic protein-sieving data analyzed here have been assessed previously according to the principles described by Taylor and Granger (324, 325), i.e., according to the wash-down principle. As discussed in section III B, realistic estimates of the small-pore and large-pore radius can be obtained with this technique at high filtration rates, whereas macromolecular PS values are greatly overestimated. When heteroporous concepts are used, it would, however, be possible to analyze lymphatic steady-state data at any level of transvascular filtration rate. This enables us to analyze capillary wall characteristics at normal lymph flows (cf. Refs. 272, 274). At least under these conditions, the blood-interstitial-lymphatic system should be in true steady state. With the classical wash-down technique, three unknowns were assessed (r_S , r_L , and α_L), but with the use of the present analysis, a fourth parameter is assessed, namely L_pS (or $A_o/\Delta x$), which reduces the degree of freedom of our analyses. However, by fully taking diffusive transport of small solutes into consider-

ation, the small-pore radius estimate will hopefully be more correct than that obtained in previous analyses. More realistic estimates of PS and of α_L will also be achieved. Furthermore, all parameters assessed, with the possible exception of $A_o/\Delta x$ (L_pS), should theoretically stay invariant as a function lymph flow (272, 274).

B. Continuous Capillaries

1. Subcutaneous tissue and muscle

In subcutaneous tissue, the clearance of albumin per 100 g of tissue is characteristically $6\text{--}25 \mu\text{l} \cdot \text{min}^{-1} \cdot 100 \text{ g}^{-1}$ (14, 18, 69, 239, 240, 243, 244, 258-260) as measured in whole organs, which is slightly higher than corresponding values for resting muscle ($2\text{--}8 \mu\text{l} \cdot \text{min}^{-1} \cdot 100 \text{ g}^{-1}$) (15, 18, 69, 242, 243, 317). Whilst the sieving characteristics of microvessels in subcutaneous tissue and paw are very well investigated, as illustrated here by the data of Renkin and co-workers (Tables 1, 5-7; Refs. 252, 272, 274), data on the selectivity properties of muscle capillaries are very scant. Measurements of osmotic reflection coefficients using the (reversed) osmotic transient technique as well as measurements of the restricted diffusion of small solutes (45), especially when corrected for the impact of flow heterogeneity (116, 120), however, strongly indicate that muscle capillaries are at least as selective or even more selective than skin capillaries. A compilation of selected data on reflection coefficients to albumin or total proteins for muscle is performed in Table 8.

As discussed in section VC, studies on intact animals (243, 258) indicate that lymphatic protein flux analyses or studies on, for example, perfused tissues (e.g., rat hindquarters or dog gracilis muscle) may have underes-

TABLE 8. Selected literature data on reflection coefficients for albumin and total proteins in muscle or hindlimb tissues

Tissue	σ_{alb}	$\sigma_{\text{tot prot}}$	Technique	Reference Number
Cat hindlimb	0.82	0.95	Isogravimetric	218
		0.83	IMB	355
		0.91	Isogravimetric	61
Dog hindlimb	0.91	Isogravimetric		60
		1.0	Isogravimetric	187
		0.94	ROT	149
Dog gracilis	0.95	ROT		151
		0.94	ROT	150
		0.89-0.90	IMB	34
Rat hindlimb	0.87		ROT	271
Rat hindlimb muscle	0.93 0.89 0.92-0.94 0.984-0.995 0.975		Tissue uptake	279
			Tissue uptake	104
			Tissue uptake	118
			Tissue uptake*	258
			Tissue uptake*	243

σ_{alb} , Reflection coefficient for albumin; $\sigma_{\text{tot prot}}$, reflection coefficient for total protein; IMB, integral mass balance technique; ROT, reversed osmotic transient technique. * Intact rats and isotope techniques.

timated the true selectivity of the microvascular walls in muscle. Even though the data by Firrell et al. (69) may be interpreted according to the present model as indicating the presence of an "uncharged" small-pore radius as large as 70 Å and an α_L of ~0.05 in muscle, there is, as previously mentioned, no clear evidence that the selectivity is really lower in skeletal muscle capillaries than in skin microvessels. When the present two-pore equations were applied to the tissue uptake muscle capillary data of Rippe et al. (279), and compared with the paw lymph flux data of Renkin et al. (259), we thus obtained almost nearly exactly the same values for equivalent small- and large-pore radii in skeletal muscle and skin capillaries, whereas α_L was slightly lower in muscle (0.056) than in skin (0.010) (cf. Ref. 233). Thus in both muscle and paw the σ_{alb} can be estimated to be on the order of ~0.9-0.95 from lymphatic flux studies and tissue uptake data in vitro, compatible with a fractional hydraulic conductance accounted for by the large pores on the order of 0.02-0.05 in these tissues (cf. membrane A in Table 5).

2. Peritoneal and mesenteric capillaries

The great advantage of the present two-pore model is that it allows for a quantitative evaluation of capillary membrane sieving characteristics (r_S , r_L , α_L , $A_o/\Delta x$) at any filtration rate. Venous congestion is not needed to produce high lymph flows and minimal estimates of C_i/C_p [$\sim(1 - \sigma)$]. Thus the present model has been successfully applied to transperitoneal transport data for small and large molecules collected in patients undergoing peritoneal dialysis at low and high rates of transmembrane fluid flow (280-282, 314). The two-pore analysis was here further refined and generalized according to Equation 18, due to the fact that, during peritoneal dialysis, there is a large glucose osmotic transient pulling fluid from the blood to the peritoneal cavity. Glucose (1.5-4.2%) is thus used as an osmotic agent in peritoneal dialysis to produce net fluid movement to the peritoneal cavity. Furthermore, there is an imbalance of a number of crystalloids other than glucose between the dialysis fluid and the blood.

At high glucose concentrations in the dialysis fluid, it can be shown that ~50% of the blood-peritoneal fluid flow must be occurring through a water-only (transcellular?) fluid conductive pathway, excluding the passage of small solutes (280). This pathway apparently accounts only for ~2% of the total hydraulic conductance (280). It is worth noting that during osmosis induced by large crystalloid osmotic pressure gradients, the coupling of albumin transport to volume flow is extremely low, the coupling coefficient being <0.01 for a σ_{alb} of 0.9 and a fluid flow of ~12 ml/min. Furthermore, sieving coefficients to small solutes are on the order of 0.5 instead of near unity, as would be predicted by the two-pore theory. Transperitoneal passage thus seems to be best described by a three-pore model of membrane selectivity in this situation. With respect to assessments of

TABLE 9. Peritoneal membrane characteristics simulated according to nonlinear least-squares regression analysis

Reference Number	$r_s, \text{Å}$	$r_L, \text{Å}$	$\frac{A_o}{\Delta x}, \text{cm}$	α_L	N_s/N_L
280, 281	47.4 ± 1.02	305 ± 41.3	$44,325 \pm 2,366$	0.051 ± 0.006	31,399
360	43.5 ± 3.9	228 ± 39.9	($15,331 \pm 21,111$)	0.070 ± 0.014	10,051
20	43.9 ± 3.9	202 ± 21.4	($35,231 \pm 39,152$)	0.091 ± 0.015	4,477

Values are means \pm SE. Because of lack of small-solute data in References 360 and 20, $A_o/\Delta x$ values in these studies cannot be accurately determined. Estimated $A_o/\Delta x$ values are therefore set within parentheses. N_s/N_L , ratio of small- to large-pore numbers. Other definitions are as in Table 6.

the small- and large-pore radii, however, the simple two-pore analysis is sufficiently accurate.

Some literature data on peritoneal transport in patients undergoing peritoneal dialysis, as analyzed according to the present two-pore theory, are summarized in Table 9. As seen from Table 9, the small-pore radius estimates range from 43 to 47 Å and the large-pore radius estimates from 200 to 300 Å. The large-pore fraction of total hydraulic conductance varied between 0.05 and 0.09. The data of Rippe et al. (281) comprise small-solute PS values (for urea, creatinine, and glucose) as well as large-solute clearances, which increases the precision in the $A_o/\Delta x$ value determined. Due to lack of similar data in the two other studies shown, the $A_o/\Delta x$ estimates show much lower precision in these cases. The permeability data obtained in patients on peritoneal dialysis are largely consistent with in vitro data obtained in single mesenteric capillaries (46, 48, 50, 191, 194). Note also the similarity in capillary selectivity among data from peritoneal continuous capillaries on the one hand and from skin and muscle capillaries on the other.

3. Lung capillaries

Lung vascular permeability to macromolecules has been covered in several recent reviews (65, 222, 266, 325, 327, 328). There is an ongoing controversy as to whether the permeability properties of the blood-interstitial barrier in lung are best reflected by the composition of postnodal lymph, as collected from lymphatics emerging from the caudal mediastinal lymph node in chronically instrumented sheep, or whether lymph has to be collected from fine prenodal lymphatic vessels (e.g., in acutely prepared dog lungs) to best reflect the interstitial fluid composition. Postnodal lymph may be modified due to the lymph nodal transit per se (1, 2, 63, 176, 250) or due to contamination of the lymph from nonpulmonary sources or from the bronchial mucosa (63). Prenodal lymphatic flux analyses are not subject to these problems. However, in acute models, lymph flux analyses may theoretically be affected by tissue trauma to a greater extent than data obtained using a chronic (postnodal) lymph fistula (313). Thus, when prenodal lymph is collected, the σ_{alb} is usually on the order of 0.5 using the wash-down technique, whereas in most studies in which postnodal lymph has been collected, values of ~ 0.7 are usually obtained (65, 266). Low values of σ_{alb}

have also been obtained using the osmotic transient technique (283) in isolated lungs.

In contrast to these data indicating a rather low selectivity of lung microvessels, Kern (140) calculated a σ_{alb} of 0.93 when evaluating the transcapillary albumin (tracer) flux over calculated volume flow in isolated perfused rabbit lungs. Furthermore, Ishibashi et al. (130) documented a ratio of labeled albumin clearance to capillary filtration rate of 0.19 for prenodal lymph and 0.20 for the sum of tissue and lymph in acute dog lungs. These values correspond to reflection coefficients for labeled albumin of 0.81 and 0.80, respectively. Simultaneously the filtration-independent minimal L/P for endogenous albumin in that study was 0.44, indicating a σ_{alb} of 0.56 according to the wash-down technique. It was suggested that previous assessments of the capillary permselectivity in lungs may not have been based on true steady-state data (see sect. VC).

If σ_{alb} in the lung is on the order of 0.75–0.8 and not close to 0.9–0.95 as in skin, muscle, and peritoneum, the selectivity of the blood-lymph barrier is indeed considerably lower in lung than in other continuous vascular beds, although there is little morphological evidence supporting this discrepancy. Rippe and Crone (266) recently argued that the lower selectivity in lung microvessels may be due to a relatively lower charge selectivity of lung microvessels as compared with other continuous microvessels. This is in keeping with ultrastructural findings of a relative paucity of anionic sites of the blood-alveolar barrier (304).

Although mathematical models have been constructed using a variety of pore sizes, the largest pore radius being 1,000 Å (19, 122, 188), the simplest model that adequately describes lymph sieving data depicts the capillary wall as having two dominant pore populations (24, 186, 221). McNamee (186) reported that dextrans with molecular radii greater than ~ 300 Å did not appear in sheep lung lymph at all. This molecular size cutoff is not compatible with the presence of an additional large-pore system of radius 1,000 Å predicted by Blake and Staub (19). Thus the pulmonary microvascular barrier seems to obey the general two-pore behavior amply demonstrated for a large number of other continuous microvascular beds.

We have applied the present two-pore model to two sets of data from the literature, and results based on nonlinear least-squares parameter estimation are tabu-

TABLE 10. Heteroporous analyses of prenodal and postnodal plasma-to-lymph clearances in two selected studies from the lung

Study	r_S , Å	r_L , Å	$\frac{A_o}{\Delta x}$, cm	α_L	N_S/N_L
Prenodal lymph	59.4 ± 6.37	215 ± 26.5	$81,227 \pm 42,787$	0.068 ± 0.050	2,661
Postnodal lymph	48.0 ± 2.02	218 ± 19.6	$184,206 \pm 66,335$	0.074 ± 0.024	5,299

Values are means \pm SE. Definitions are as in Tables 6 and 9. [Prenodal data from Parker et al. (221); postnodal data from Smith et al. (313).]

lated in Table 10. The data collected by Parker et al. (221) from prenodal dog lung lymph at three levels of estimated capillary pressure (P_c) are shown in Figure 14. Note that previous analyses of these data have yielded much larger values of the small-pore radius and of α_L for the pulmonary microvasculature (325). Moreover, from Figure 14 it seems evident that the wash-down data may not have been in true steady state, because the large-pore radius seems to decrease with increasing lymph flows. However, we do not know the actual hydraulic conductance of the portion of lung drained in the study, and our estimates of hydraulic conductance are larger than obtained from the simple relationship between the estimated increase in capillary pressure and lymph flow (0.035 vs. 0.005 – 0.009 ml·min $^{-1}$ ·mmHg $^{-1}$). This imparts uncertainty to the small-pore estimation. However, including diffusive transport into the analysis should represent a step toward a more correct data evaluation. Furthermore, the advantage of the present procedure is that the small-pore estimate remains reasonably invariant as a function of lymph flow.

C. Fenestrated Capillaries

Fenestrated capillaries are characterized by having a large exchange surface area available for fluid and small-solute transport, yet showing a high selectivity. Actually, the glomerular filter, if the blood-brain barrier is excluded, is the most protein-selective microvascular barrier in the body. Furthermore, the intestinal capillaries due to their large exchange surface area show very high absolute clearances for proteins, although the clearances per surface area (permeability) are about the same as for skin and muscle (113, 248, 249, 325). Mann et al. (173) discussed the fenestrations as functionally behaving as a "high concentration of small pores," and similar conclusions have been reached by other authors (112, 157). The functional correlate to this finding is discussed in section VII B. An equally tenable explanation is that the "molecular sieve" in fenestrated capillaries be represented by the microvascular basement membrane in accordance with the fiber matrix theory (51). The high selectivity of fenestrated capillaries is illustrated by data from the intestine (97, 231a, 263) and by data on glomerular permselectivity (21).

1. Gastrointestinal capillaries

Lymphatic protein flux data obtained in cat ileum (97) analyzed using the present two-pore model are shown in Figure 15. One problem in modeling these data is that, although clearances increase with increasing vascular pressures up to the venous pressure level of 20 mmHg for all proteins, there is a sharp decline in clearances for all proteins investigated at the highest P_v (30 mmHg) studied. Thus it seems as if the capillary surface area ($A_o/\Delta x$) varies as a function of hydrostatic pressure. A parameter estimation with "floating" in parameters for the whole set of data could therefore not be done as for lung (221) or skin (259). Instead, we set α_L equal to 0.05 as obtained for the highest pressure level, and subsequently, the best estimates of r_S , r_L , and $A_o/\Delta x$ (L_pS) for each level of vascular pressure were determined. As can be seen from Figure 15 and Table 11, the calculations of the small-pore radius seem to decrease somewhat with increasing pressures. The large-pore radius decreased from ~ 422 to 185 Å, which is statistically significant. Again this may indicate that data obtained at the highest lymph flow states may not have been collected at a true steady state. Note that the inclusion of diffusive transport across small pores has markedly reduced the small-pore radius as compared with the original analysis done from these data, where the estimates of r_S for the two lowest pressure levels were 59 and 70 Å, respectively. Large-pore estimates are approximately the same as in the original analysis (Fig. 9, p. 476 in Ref. 325).

Data from intact rats (260) indicate slightly lower reflection coefficients for intestinal vessels than for skin and muscle, where σ_{alb} was found to be >0.99 . In intact animal studies (260), the apparent PS for albumin seems to increase in the direction of cecum to ileum to jejunum, in a pattern compatible with that obtained by Haraldsson et al. (113). In lymphatic flux analyses, however, there appears to be no great difference in microvascular selectivity between different segments of the intestine. Applying the present two-pore equations for dog colon (261a) and dog stomach (231a), the small-pore radius was estimated to be 48.1 ± 4.38 and 44.1 ± 9.24 (SE) Å and the large-pore radius was estimated to be 173 ± 6.8 and 248 ± 32 Å, respectively; the α_L was determined to be 0.025 ± 0.035 and 0.01 ± 0.034 for these organs, respectively. Finally, it is of considerable interest to note that the intestinal capillary permeability may

TABLE 11. Two-pore analysis of data from cat ileum

P_v , mmHg	J_v , ml/min	$\Delta\pi$, mmHg	J_{vS}/J_v	J_{vL}/J_v	$\frac{A_o}{\Delta x}$, cm/100 g	$L_p S$, ml · min ⁻¹ · mmHg ⁻¹	r_s , Å	r_L , Å
0	0.051	7.64	0.606	0.394	144,399 ± 6,150	0.0587 ± 0.0025	51.8 ± 0.98	422.5 ± 43.0
10	0.093	9.99	0.734	0.266	120,205 ± 7,771	0.0523 ± 0.0034	53.7 ± 0.90	452.8 ± 71.1
20	0.221	12.61	0.760	0.240	232,589 ± 9,658	0.0800 ± 0.0032	47.7 ± 0.70	214.9 ± 4.66
30	0.447	15.09	0.933	0.067	40,456 ± 31,499	0.0121 ± 0.0094	44.5 ± 2.22	185.4 ± 15.7

Values are means ± SE. Here, α_L is set to 0.05, and overall σ for albumin was 0.861. When venous pressure (P_v) is elevated from 0 or 10 to 20 mmHg, $A_o/\Delta x$ seems to increase 2-fold, but when P_v is further increased (to 30 mmHg), $A_o/\Delta x$ falls to approximately one-third of the original value. Note that r_s remains reasonably invariant as a function of J_v . [Data from Granger and Taylor (97).]

vary physiologically and increase after a fat-rich meal (96).

2. Glomerular capillaries

The major sieving barrier in the glomerular capillaries is nowadays assumed to be morphologically represented by the glomerular basement membrane (GBM) (25), with its rather regular meshwork arrangement of collagen IV molecules together with entactin, laminin, and heparan sulfate molecules (330). Few authors today believe that the slit structure of glomerular epithelium of Bowman's capsule is the dominant barrier to transglomerular macromolecule transport, such as proposed by Rodewald and Karnovsky (287). Thus, from a strict morphological point of view, a model describing transport across a matrix of fibers would be the most adequate one for conceptualizing glomerular permselectivity. Traditionally, the size selectivity of the glomerular filter is, however, described in terms of equivalent pores bearing a net negative charge (25, 36, 37). Since the beginning of the 1980s, the two-pore concept has been introduced also into renal capillary physiology (56, 203). Large pores are usually envisioned as being totally non-size selective, representing a so-called "shunt pathway," accounting for only a very small fraction of the total hydraulic conductivity (0.002 or less). Small pores are thought to be small enough to totally restrict the transport of albumin, i.e., the equivalent small-pore radius is assumed to be on the order of 30–35 Å. This corresponds to an uncharged pore radius of 45–48 Å according to the double-layer model outlined in section III D3 (202).

The glomerular barrier transport properties are characterized by the large surface area available for fluid flow and especially for diffusive transport. Yet, the glomerular barrier is probably the most size-selective capillary barrier in the body. Furthermore, due to the large diffusion surface area, it is not possible to employ the wash-down concept to assess glomerular permselectivity. Diffusive (small-pore) transport must be taken into account in the modeling, and because of that, the present model and that previously employed by Brenner and co-workers (25, 36, 37) are applicable. As discussed previously, the large diffusive component of transport across the glomerular barrier makes the sieving coeffi-

cient for small solutes [ranging in size from urea (mol radius 2.6 Å) to inulin (mol radius ~15 Å)] to become ~1, but for solutes >15 Å in radius, there is a sharp drop in the relationship between sieving coefficient and molecular radius (cf. Figs. 13B and 16).

In Figure 16 the fractional clearance of neutral and negatively charged dextrans in primary urine of Munich-Wistar rats (21) are plotted versus solute molecular radius together with simulated predictions using the present two-pore model (cf. Ref. 25). The equivalent pore

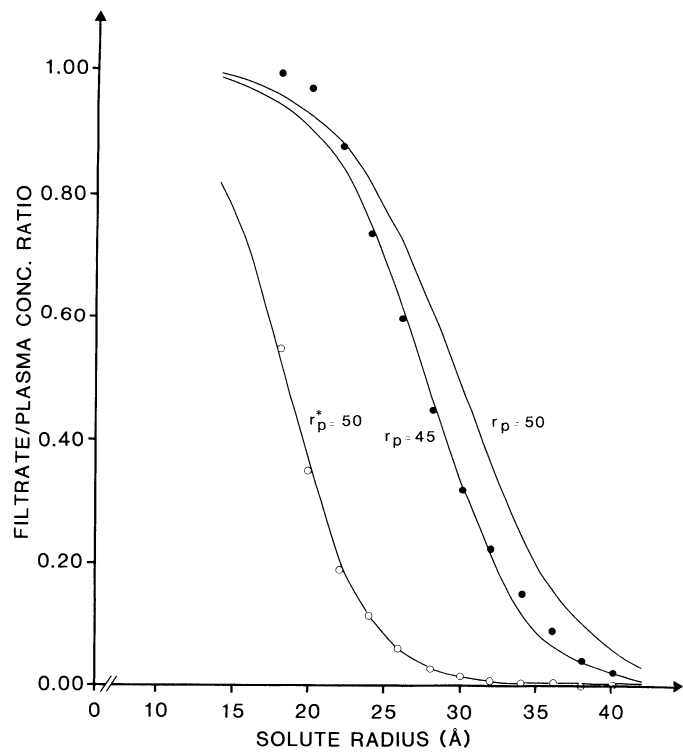


FIG. 16. Fractional clearances (ϕ) of (negatively) charged dextran sulfate and neutral dextran molecules (21, 25) plotted vs. molecular radius (a_e), together with simulated predictions according to 2-pore theory (top and middle curves), and this theory was modified according to double-layer hypothesis (209) to model charge effects (bottom curve). To model ϕ vs. a_e for charged species according to double-layer hypothesis, uncharged small-pore radius (r_p) had to be set at 50 Å. Thus bottom curve is modeled setting small-pore radius equal to 42 Å, $r_p^* = r_p - 8$, and radius of negatively charged solutes equal to $(a_e + 8)$. Uncharged pore radius fitting to these data is 45 Å. The α_L value was set at 0.002 (56).

radius is set to 50 Å (45 Å yielding the best fit, however) and 42 Å (50–8 Å) for neutral and negatively charged solutes, respectively, assuming the presence of charged solute-charged membrane interactions according to the simple Munch model (*Eq. 45*). Model inputs are essentially the same as those employed by Bohrer et al. (21), i.e., L_pS was set to $4.8 \text{ nl} \cdot \text{min}^{-1} \cdot \text{mmHg}^{-1}$ per nephron and the glomerular filtration rate (GFR) to 22 ml/min. The $A_e/\Delta x$ value was calculated from L_pS to be 16.72 cm/nephron, which is approximately two orders of magnitude higher per unit weight of tissue than in skeletal muscle.

Note that according to the present model the albumin molecule does not pass through the small-pore equivalent at all under normal conditions but is for its blood to urine passage exclusively confined to the large-pore pathway. In rat primary urine, the albumin sieving coefficient (ϕ) is $\sim 1 \times 10^{-3}$ or slightly higher (110), but in humans, it is assumed to be $\sim 1 \times 10^{-4}$, implying a glomerular reflection coefficient of at least 0.9999. Normally, >90% of the filtered load of albumin is thought to be “reabsorbed” to the blood (315) by being processed by the proximal tubular epithelium. Thus the apparent sieving coefficient of albumin (clearance of albumin from plasma to final urine divided by the glomerular filtration rate) is usually $<10^{-5}$. Note that an increased GFR would normally lead to a drop in ϕ and that a reduced GFR will normally produce increases in ϕ .

The two-pore theory (including the impact of negative charges in the small-pore equivalent) has been employed extensively to describe the normal and pathologically altered glomerular filter (e.g., Refs. 56, 203, 331, 349). Pathological changes in the blood-urine barrier may either affect the charge-selective properties (effective small-pore radius), such as in minimal changes nephropathy (27) or early diabetic nephropathy (55, 331), or the size selectivity toward the largest of the macromolecules, i.e., affecting the large-pore pathway. The large-pore pathway is recruited in, for example, diabetic nephropathy (203, 331) or in membranous nephropathy (300, 359). When charge selectivity is affected, the curve of ϕ versus a_e shown in Figure 16 is shifted to the right (i.e., from charged to uncharged solutes). However, when the large-pore number is increased, the “flat” portion of the curve, i.e., that for $a_e > 40 \text{ \AA}$, is shifted upward. Actually, a decreased size selectivity, implying increases in clearances for solutes larger than albumin, usually occurs in conjunction with a reduced surface area. In that situation, glomerular filtration is usually increased through a membrane affected by the reduced surface area. Then, the Pe number for transport is increased, and therefore, the curves depicting ϕ versus a_e will usually become less steep in, for example, membranous nephropathy than as shown in Figure 16 (see also Fig. 13B).

It should be noted that the presently available information about glomerular sieving properties in humans is obtained using (uncharged) dextran clearances from blood to urine and that the uncharged small-pore radius, in these experiments, is usually larger than dis-

cussed above ($\sim 55 \text{ \AA}$). This may be an artifact, since dextrans are elongated flexible molecules that can move along their long axes across structures smaller than their own Stokes-Einstein radius (202). It is therefore safe to conclude, based on the present knowledge, that albumin (mol radius $\sim 35.5 \text{ \AA}$) is not to a significant extent able to pass through the small-pore equivalent in the GBM, i.e., that the effective small-pore radius of the GBM can be assumed to be $<36 \text{ \AA}$ (33–35 Å). The fractional hydraulic conductance accounted for by large pores (α_L) would be on the order of 0.001–0.002 based on dextran clearances, but may be even lower when assessed using endogenous proteins or other spherical macromolecules for probing the glomerular filtration barrier (214).

VII. STRUCTURE-FUNCTION CORRELATIONS: TRANSPORT PATHWAYS

A. Continuous Capillaries

1. Slit concept

The spaces between endothelial cells, i.e., the interendothelial clefts (slits), are the likely and logical candidates for the small pores in continuous microvessels. The three-dimensional ultrastructure of the interendothelial cleft in muscle capillaries started to be revealed in detail in the 1970s by the use of freeze-fracture techniques (351). Using these techniques, one can split the plasmalemma membrane bilayer into two halves at the level of an interendothelial cleft, and the junctional complexes within the cleft can be demonstrated en face in replicas of the inner and outer leaflets. Intramembrane junctional complexes are now seen to form branching irregular strands (or mirror image grooves) on either leaflet, and these strands appear to be occasionally interrupted by discontinuities.

Bundgaard (31), using ultrathin ($\sim 140 \text{ \AA}$) serial sectioning of cardiac muscle endothelium, provided strong evidence that these intramembrane strands really correspond to extramembrane junctional complexes and that there must be paracellular tortuous pathways between the strands and through their discontinuities that permit passage of small solutes and fluid between blood and tissue. The cleft width was found to average $\sim 200 \text{ \AA}$ except at the discontinuities of the junctional strands, where it was $\sim 40\text{--}70 \text{ \AA}$. In all continuous capillaries, the slit structure appears to be basically the same. However, the degree of “tightness” of the junctional strand complexes may vary considerably among various capillary types. Thus the extent to which the slit is open appears to be variable, similar to a zipper mechanism (42, 44, 45). In brain capillaries, for example, intercellular junctions are almost tight, i.e., the mentioned discontinuities are extremely infrequent, whereas in mesenteric microvessels, discontinuities of the junctional complexes are abundant, rendering the

slit effectively open by $\sim 90\%$ of its length (45, 48). Muscle endothelium is intermediate in this respect, since only $\sim 10\%$ of the slit appears to be effectively open (42, 44, 45). The fractional slit area in relation to total endothelial surface area can be calculated to be $\sim 2 \times 10^{-4}$ in skeletal muscle (45) and $\sim 3-5 \times 10^{-3}$ in mesentery (40a, 48). The order of magnitude of this fractional slit area can be inferred from the definition of permeability (Fick's first law of diffusion). If the endothelial thickness is 10^{-4} cm while small-solute diffusion coefficients are of the order of 10^{-5} $\text{cm}^2 \cdot \text{s}^{-1}$, and the degree of diffusional restriction to small solutes is negligible, then the fractional endothelial surface area available for solute permeation would be 10^{-4} . This value is calculated for measured small-solute permeabilities of the order of 10^{-5} cm/s , as found in, for example, muscle and lung (45).

The large-pore equivalent has not yet been clearly identified, and the morphology of the continuous capillary wall offers several possibilities for the structural counterpart for this pathway. In this review we have tested the hypothesis that macromolecules are transported across vascular walls in aqueous channels due to passive mechanisms, and we conclude that this is a reasonably good hypothesis. We cannot, of course, exclude that "nonporous" mechanisms are also involved to some extent, especially for transport of specific substances such as hormones or lipoproteins (124a, 146, 310, 335), but these mechanisms should quantitatively only marginally contribute to the overall transport of the major plasma proteins for reasons outlined in section II. We therefore have to postulate that the large-pore equivalent actually corresponds to fluid-filled pathways represented by either 1) interendothelial clefts, where the junctional discontinuities are wider than in ordinary clefts ($\sim 200-300$ Å), or 2) transcellular channels, 300–700 Å wide, formed by chains of fused endothelial vesicles (invaginations). Despite intensive efforts to demonstrate transcellular channels, however, their frequency appears to be too low to account for the large pores. According to Bundgaard et al. (32) and Frøkjær-Jensen (83), they may be even absent from the true capillary portion of the endothelium in frog mesenteric microvessels, but present in the venular portion. We therefore believe that "wide" interendothelial clefts represent the most plausible morphological candidate for the large pores.

The endothelial cell membrane proper, like all other cell membranes, has a conductivity to fluid that cannot be neglected. From studies on single mesenteric vessels, the contribution of a water-only (transcellular) pathway (α_c) seems to be $<10\%$ of the total L_pS (50), which agrees with a majority of whole organ studies (325). In rat hindlimb tissues, Rippe and Haraldsson (271) estimated the fractional hydraulic conductance accounted for by the water-only pathway to range between ~ 4 and 7% , but for the human peritoneal membrane, Rippe and Stelin (280) calculated α_c to be as low as $\sim 2\%$. Although the data of some authors (355) indicate a much higher α_c in continuous vessels, the bulk of the

literature data indicate that no more than 7–10% of hydraulic conductivity (L_p) can be accounted for by channels available to water but excluding small hydrophilic solutes.

In view of the morphological appearance of the slits of continuous capillaries bearing a net negative wall charge, the simple cylindrical pore model is indeed an oversimplification. Still, it may presently be the simplest model that with reasonable accuracy can predict solute transport across microvascular membranes. It is not surprising, however, to note that it is usually difficult to reconcile data on microvascular selectivity based on measurements of reflection coefficients with data on transvascular diffusion of small solutes according to the equivalent cylindrical pore theory. In perfused rat hindquarters, for example, Rippe and Haraldsson (271) measured an equivalent small-pore radius of 41 Å (slit width of 53 Å) based on measurements of reflection coefficients to small solutes. In this preparation there was hardly any degree of diffusional restriction to Cr-EDTA and cyanocobalamin (116). With correction for tissue and flow heterogeneity according to the theory of Bass and Robinson (12), however, the equivalent small-pore radius was estimated to be 53 Å (slit width 54 Å) at an $A_o/\Delta x$ of 4.6×10^4 $\text{cm}/100 \text{ g}$. It is worth noting that without any correction for heterogeneity, the calculated small-pore radius (slit width) became 70 Å. Furthermore, combining the L_pS value obtained in these studies with $A_o/\Delta x$ for water (calculated by backward extrapolation of $A_o/\Delta x$ vs. molecular radius to that corresponding to the a_e of water), as done in the pioneering studies of muscle vascular permeability by Pappenheimer et al. (217), resulted in a small-pore radius of 80 Å. Thus combining convective and diffusive data in the same model yielded a relatively large equivalent pore radius. Previous attempts to interpret such data have led either to postulations of wide pores (slits) containing constricted portions along the pore length (42, 44, 45) or to postulations of a network of fibrous macromolecules filling up the pores and constituting the major molecular sieve between blood and tissue (48, 51, 256) or both.

The model conceptualizing a wide pore (slit) (of width ~ 17 nm) with a constricted portion along a portion of its length (45) has recently been evaluated in detail by Curry (48). In such a model, the diffusion of small solutes (a_e radius <10 Å) is affected mainly by the wide portion of the pore, and the equivalent small-pore radius will be quite large when assessed from small solute permeabilities alone (~ 90 Å). The transcapillary clearances of large solutes will be mainly determined by the narrow portion of the slit (pore). If, for example, a cylindrical pore of radius 100 Å and length of 7,000 Å is constricted down to a radius of 50 Å over a distance (length) of 700 Å, then the diffusional restriction of albumin will mimic that of a uniform equivalent pore of radius ~ 62 Å, whereas Cr-EDTA and cyanocobalamin (vitamin B₁₂) will exhibit a degree of diffusional restriction compatible with that occurring in an equivalent pore of radius $\sim 85-90$ Å. If, in addition, such a cylindrical pore is negatively charged, the equivalent pore ra-

dius for albumin will be of the order of 45 Å. The functional behavior of a such restricted pore (or slit) with a negative wall charge will thus be similar to that currently assessed for "equivalent pores" in a majority of permeability studies on continuous vascular beds in whole organ studies. The constricted pore (slit) thus seems to be a plausible structural candidate for the small-pore equivalent in a majority of continuous capillaries.

2. Fiber matrix concept

One striking feature of studies on single capillaries, and also noted in whole organ studies, is that there is usually a great variability in hydraulic conductance among capillaries (or capillary beds), despite the capillary size selectivity (σ_{alb}) remaining rather invariant from capillary to capillary (or among various capillary beds). Furthermore, there seems to be a good correlation between the capillary hydraulic conductance and the small-solute PS among various continuous and fenestrated capillary beds (47, 48, 193, 194). In terms of the slit theory, this may reflect a variable degree of openness of the slit pathway from capillary to capillary. Thus the number of openings of the slit structure (small pores) restricting macromolecules may be variable, but not their size. Furthermore, the relative frequency of large pores to that of small ones seems to be rather invariant among various types of capillary.

Another way of interpreting this phenomenon is to impart functional properties to the endothelial glycocalyx (166, 167). If a matrix of fibrous macromolecules fills out all aqueous spaces within the endothelial membrane including the transcapillary pathways discussed above, the selectivity properties of the membrane would be mainly determined by this "fiber matrix" and not primarily by the pathway structure itself (51). The hydraulic conductance and sieving properties of such a matrix will be determined by the (average) fiber radius (r_f) and the fractional void volume of the matrix (ϵ). Such a homogeneous sieve would display an equal hydraulic conductivity whether fluid filtration occurs from blood to tissue or vice versa, whereas a slit would show "rectification" of flow. However, there is no evidence for the existence of this phenomenon in the endothelium of single frog mesenteric capillaries (for review, see Refs. 48, 194) which would favor the concept of the fiber matrix theory. Furthermore, the fiber matrix theory can readily account for the decreased selectivity of the microvascular walls occurring upon removal of proteins from the solution bathing the capillary endothelium, the so-called "protein effect." Thus one argument in favor of the fiber matrix theory is based on the assumption that in the presence of albumin, this molecule would adsorb mainly to the walls within the wide portions of the slit. For an intermediate-size solute such as myoglobin ($\sigma \sim 0.4-0.5$), approximately one-half (~40%) of its diffusion resistance should reside in the wide portion and approximately one-half (~60%) in the

tight region. Removal of albumin from the wide region would increase σ to myoglobin due to a reduction in the diffusion restriction in the wide but not in the narrow slit portion, because a relatively greater fraction of the osmotic gradient would then be exerted over the portion showing the highest σ . However, in recent experiments, Curry et al. (52) clearly found a decrease in σ for myoglobin after albumin removal from the perfusate, not an increase.

Although the arguments cited above may support the fiber matrix theory, one must bear in mind that we do not precisely understand the morphological nature of the capillary barrier and that alternative explanations for the protein effect can also be invoked. Albumin may as well restrict entrance of macromolecules also into the narrow regions of the pore, as discussed in section VIIIB. Furthermore, the large amount of physiological data compatible with the capillary barrier as a dual sieve requires the presence of a nonuniform fiber matrix, essentially showing a functional two-pore behavior. This would only be possible if there were occasional dislocations in an otherwise uniform lattice of fibers. While this is indeed conceivable, we are then, in essence, back to a situation not very different from the classical small-pore, large-pore concept of transvascular exchange.

B. Fenestrated Capillaries

The highly selective fenestrated capillaries, having fenestrations of radius ~300 Å in most organs, display a high fluid conductivity and solute exchange capacity for small solutes. The fenestrations, whether covered by a diaphragm (as in the intestinal circulation) or not (cf. glomerular capillaries), have been considered to act at regions showing a high frequency of small pores (173). Levick and Smaje (165) have convincingly argued that the major resistance to small solute and water transport in fenestrations covered by a (porous) membrane does not reside in the fenestra itself, but in the basement membrane, and possibly also in the endothelial glycocalyx. The high selectivity of the basement membrane in fenestrated vessels may also be inferred from ultrastructural studies demonstrating that large macromolecules, such as ferritin, are impeded in their passage across the membrane (38, 306). Actually, ferritin seems to "pile up" against the basement membrane also in nonfenestrated capillaries (132, 133). Concerning the interendothelial junctions in fenestrated microvessels, these pathways are of much less importance for the overall water and small-solute transfer than the fenestrations. Aside from being shorter, they have, however, a similar architecture as the small-pore pathway in continuous capillaries (306).

In general, microvascular basement membranes consist of type IV collagen fibers (radius 7.5 Å) (330), laminin (radius 10–35 Å) (68), heparan sulfate (radius 6 Å), and rather coarse fibers (radius 20–30 Å; Ref. 139). The thick GBM is specialized to withstand very high

vascular pressures, while maintaining an extremely high permselectivity. The core structure of the GBM is a chicken wire-like network of type IV collagen molecules sandwiched between layers consisting of entactin, laminin, and heparan sulfate molecules (330). Entactin and laminin are usually regarded as molecules providing adhesion of the endothelium to the GBM. From a structural viewpoint, however, the predominating fiber radius in the GBM would be that of type IV collagen, i.e., 7–8 Å, and the relative fiber volume in this network has been estimated to be 0.12 (286). Such a membrane would show rather uniform selectivity properties, implying that an equivalent small-pore pathway would be the major determinant of glomerular permselectivity. The minimum σ for this membrane is of the order of 0.999. This high selectivity is obtained for a fiber matrix having a mean fiber radius (r_f) of 7.5 Å (collagen type IV) and a fractional void volume (ϵ) of 0.76. To obtain a σ value of 0.9999, a fractional void volume of 0.68 is required in such a membrane according to the partition expression employed by Curry and Michel (51) for a fiber matrix. Such a membrane would show a hydraulic conductance of 1.53×10^{-8} and $3.21 \times 10^{-8} \text{ cm}^3 \cdot \text{s}^{-1} \cdot \text{dyn}^{-1}$, respectively, according to the so-called "drag model" (Carman-Kozeny equation; cf. Ref. 51). This hydraulic conductance is actually in line with the in vitro measurements of glomerular membrane conductivity (286). However, ϵ is much too low as compared with measured values. For ϵ equal to 0.88 (286) and r_f equal to 7.5 Å, σ becomes 0.957, which is far from the normal selectivity of the glomerular basement membrane ($\sigma = 0.999\text{--}0.9999$). Either these inconsistencies may be due to the presence of negative charges in the basement membrane, enhancing its selectivity to macromolecules, or the fiber matrix theory cannot adequately describe the selectivity properties of the normal glomerular barrier. Alternatively, both the epithelial slit structures and the GBM fiber matrix have to functionally interact to produce the high selectivity of the glomerular filter.

Although, conceptually, the fiber matrix theory would be superior to pore theory for describing transglomerular transport and glomerular basement membrane selectivity, the theory of equivalent pores is in this context, with some exceptions (135a), still the predominant model in the literature. Furthermore, because there seems to be a parallel pathway in the GBM that is very little protein restrictive (shunt pathway) (56), the two-pore theory has until now been the model of choice also in renal physiology. Models taking into account more complex fiber matrix arrangements than that outlined above, with serial resistances offered by matrices of varying fiber radii and fractional void volumes and being negatively charged, may be the proper, yet very complex, way of describing glomerular permselectivity. Hence, a sophisticated, yet highly controversial, gel model of the glomerular barrier was recently introduced by Wolgast and Öjteg (357). The two-pore theory is, however, presently the simplest one that can relatively accurately describe transglomerular protein transport.

VIII. MODULATION OF VASCULAR LARGE-SOLUTE PERMEABILITY

A. Effects of Some Autacoids

In acute inflammation or following injections of autacoids such as histamine, bradykinin, and 5-hydroxytryptamine (5-HT), vascular permeability increases in postcapillary venules of diameter 8–15 μm through the formation of gaps of diameter ~0.05–0.1 μm between endothelial cells, which apparently contract upon activation, as demonstrated already by Majno and co-workers (169, 170) and subsequently by a large number of authors (for review, see Refs. 9, 43, 98, 234, 321, 325). This formation of gaps seems to be due to an active temperature-dependent (269), transient and reversible (112, 121, 152, 153, 213, 269, 318, 319, 354) contractile endothelial or pericytic process, dependent on the level of the external calcium concentration (43, 121, 183, 212, 299) and most likely involving contraction of intracellular actin-myosin filaments. In whole organ studies, a full-fledged response to, for example, histamine is seen within 2 min (e.g., Refs. 11, 269, 318). However, this response usually fades away upon continued autacoid exposure within ~20 min (121, 152, 153, 318, 319, 354). In nonvasodilated tissues, elevations of microvascular pressure and most likely capillary recruitment (147) also contribute to the marked extravasation of proteins produced by, for example, histamine. Note, however, that 5-HT exerts vasoconstricting effects in rat muscle and skin microvessels in addition to being an autacoid (268).

It was shown early that the formation of "leaky sites" in postcapillary venules in the hamster cheek-pouch preparation is (linearly) correlated to the (log) dose of the autacoid administered (318). Furthermore, upon repeated stimulation, there is usually a marked reduction in the response when the interval between successive stimulations is shortened down to 15 min (319). The permeability increases induced by, for example, bradykinin and histamine can be markedly attenuated by β_2 -receptor stimulants such as terbutaline (62, 318, 320), catecholamines (174), or isoprenaline (269). Thus rat hindquarters simultaneously exposed to infusions of histamine and isoprenaline for 10 min are refractory to another dose of histamine for ~60 min (269). The formation of gaps in postcapillary venules has also been demonstrated to be sensitive to inhibition by glucocorticoids (for review, see Refs. 234, 321) or inhibitors of prostaglandin synthesis (5, 321), and with regard to histamine-induced responses, by histamine antagonists (H_2 blockers) (123, 201).

Note that in the pulmonary circulation histamine does not appear to affect vascular permeability. However, here histamine is a potent postcapillary vasoconstrictor (64, 175, 265) causing increases in fluid filtration due to elevations of the pulmonary capillary pressure. Note also that in systemic vascular beds lymphatic flux analyses generally indicate that there may be a sustained phase of increased microvascular permeabil-

ity to macromolecules following autacoid administration and succeeding the initial large permeability increase (35, 134, 240, 255). Whether this sustained increase in the plasma-to-lymph clearance of large solutes represents a phenomenon of delayed interstitial washout of proteins extravasated during an early permeability transient or represents a real capillary wall phenomenon is controversial (240, 278).

Very high doses of calcium antagonists such as verapamil (183, 199, 321) appear to markedly inhibit the endothelial contraction induced by autacoids. When pharmacological doses of verapamil or felodipine (another calcium antagonist) were tested in perfused rat hindquarters, however, these agents were not able to inhibit histamine-induced increases in the capillary filtration coefficient (121). Still it was demonstrated that such an inhibition occurred upon removal of calcium from the outer medium. Hence, Haraldsson et al. (121) concluded that voltage-gated calcium channels are not operative in the calcium-dependent response to histamine in normal endothelium *in vivo*. Since then, large amounts of evidence for the lack of function of voltage-gated calcium channels (i.e., channels that can be blocked by calcium antagonists) have been gathered for cultured endothelial cells (3) as also shown for single capillaries (122a).

The cellular mechanisms of the events leading to endothelial (or pericytic) cell contraction induced by autacoids include (receptor) activation of ion channels and chemical second messengers (inositol 1,4,5-trisphosphate) to elevate cytosolic calcium released from intracellular stores, usually followed by a sustained intracellular Ca plateau, which is dependent on the presence of calcium outside the cell and on the membrane potential. Actually, membrane depolarization, induced by raising the potassium concentration in the outer medium, leads to a lowered intracellular calcium concentration, which again contradicts voltage-dependent mechanisms initiating endothelial contraction (122a). The details of the calcium-dependent cellular events leading to contraction of intracellular proteins have been reviewed extensively elsewhere and are not, however, further discussed here (3, 85, 241).

In summary, several autacoids induce in skin and muscle capillaries an augmentation of vascular permeability by an active transient and reversible contraction of endothelial cells (or pericytes), preferentially in postcapillary venules, producing large gaps between the cells. This process is calcium dependent and is probably initiated via receptor-operated calcium channels. It can be inhibited by β_2 -adrenoceptor stimulation or by glucocorticoids and also, specifically, by histamine antagonists (H_2 blockers) or inhibitors of prostaglandin synthesis. The coupling between agonist stimulation and cell contraction is a complex process involving the activation of ion channels and chemical second messengers to elevate cytosolic calcium in endothelial (or pericytic) cells in a manner similar to that observed in other non-excitable cells.

Vascular permeability can be modulated by a large number of other stimuli, including changes in the chemi-

cal environment of the endothelial cell. In this review, we focus on just a few of these. Permeability changes due to ischemia or ischemia/reperfusion (e.g., Refs. 60, 95, 149, 150), inhibition of nitric oxide (156a), hyperosmolality (77, 78), pH variations (87, 316), or reductions in plasma calcium or magnesium concentrations (121, 144, 204, 205, 212, 316) are not discussed here. However, we focus on the impact of alterations in the composition of plasma proteins on vascular permeability, especially with respect to its contents of albumin and orosomucoid. The effects of high concentrations of neutral dextran and of high vascular pressures are also briefly reviewed.

B. Protein Effect and Albumin Effect

It was noted already (156) that nonprotein colloids are less effective in preventing edema in perfused frog tissues than protein-containing colloids. In addition to the effect that colloids exert on the capillary Starling balance, proteins *per se* seem to increase the effectiveness whereby colloids in general exert their osmotic pressure (66). Danielli (54) suggested that this protein effect is exerted by a thin molecular layer of albumin molecules adsorbing to the walls of the permeable pathways. Later, Kinter and Pappenheimer (see Ref. 159) demonstrated a doubling of the capillary hydraulic conductance in cat hindlimb after shifting the organ's perfusate from blood or plasma to dextran in a Ringer solution. In a series of elegant studies on isolated frog mesenteric vessels, Michel and co-workers (163, 180) and a number of subsequent authors (52, 126–128, 197, 198, 333) have provided massive documentation for the protein effect in single frog mesenteric microvessels. In such studies, the capillary hydraulic conductance was found to increase by a factor of 3–5 and σ to Ficoll 70 (196) and σ to hemoglobin and myoglobin (235) was found to fall when albumin in the perfusate was reduced to low values. Actually, Huxley and Curry (126) found these albumin levels to be as low as 0.1 g/l. Recently, the albumin effect was also demonstrated for isolated glomeruli from the dog kidney, where reductions of the albumin concentration to 0.1 g/l produced a 12-fold increase in the glomerular L_pS (75).

In whole organ studies, Areekul (7) and Rippe and Folkow (267) found only slight increases in the capillary filtration coefficient in skin and muscle, respectively, when proteins were totally removed from the perfusate. Also, studies of Gamble (86, 87) demonstrated rather moderate increases in the capillary filtration coefficient in the perfused rat mesentery after albumin removal from the perfusate. Similarly, Mann (172) demonstrated only slight alterations in the capillary diffusion capacities for ^{51}Cr -EDTA and cyanocobalamin in hearts perfused with Ringer solution containing no albumin. Furthermore, it should be noted that the observed changes in the capillary diffusion and filtration coefficients were time dependent and appeared first after 15–20 min of protein-free perfusion.

The rather insignificant protein effects on L_pS in

whole organ studies actually led Weselcouch et al. (347) to seriously question the protein effect. However, much larger changes in measured hydraulic conductance in response to nonprotein colloids have been measured by Diana et al. (59) in isolated dog hindlimbs and by Watson (339) in the cat hindlimb. Furthermore, Watson (340) also demonstrated that blood addition to albumin-crystalloid solutions can further reduce the hydraulic conductance, denoted the "blood effect." In the latter studies (59, 340), however, the microvascular beds appear not to have been maximally recruited. It is then possible that the capillary surface area did not remain completely constant during the perfusate shifts. Thus the control L_pS values in these papaverine-treated vascular beds were low, usually only ~40% of the values characterizing maximally recruited skeletal muscle vascular beds (41, 67, 70, 147). A major effect of shifts from blood to cell-free perfusates may then have been relaxation of precapillary sphincter regions, and hence, capillary recruitment due to reduced oxygen delivery to the tissues (41). The study by McDonagh (184), also suggesting a blood effect, may also suffer from disturbances due to an uncontrolled capillary surface area.

Although the protein effect has been demonstrated beyond doubt in single frog mesenteric vessels, the effect thus seems to be more variable in whole organ experiments. Nicolaysen (206) found that bovine albumin in a balanced and buffered crystalloid solution caused edema to form in rabbit lungs, unlike rabbit plasma or whole blood. Albumin may thus not be the only plasma factor that is required for the maintenance of lung capillary permeability (168, 295). Moreover, according to some authors, platelets or platelet-derived factor(s) need to interact with the endothelium to preserve its barrier function (54, 301). Rippe et al. (284) found that when either whole blood or plasma was diluted, the hydraulic conductance of a perfused canine lung lobe increased abruptly at a plasma protein concentration between 4 and 5 g/l, an effect which was not dependent on the erythrocyte mass. A preparation containing 6 g/l of albumin in Tyrode solution was, however, unable to fully reduce the hydraulic conductance to control values, once it had increased due to plasma-free perfusion (284).

The apparent discrepancy between the protein effect in frog vessels and in mammalian vessels is obscure. It is possible that in whole organ studies, plasma proteins are not completely washed out of the preparation and that very low concentrations of extravascular albumin can actually maintain capillary permeability at a normal level (127). Furthermore, albumin is not the only serum protein that is important in maintaining normal vascular permeability in mammals as discussed in section VIII C. Indeed, the precise nature of the processes responsible for the protein effect is presently not known. It has been shown in frog microvessels that cationic proteins and also cationic groups of the albumin molecule (guanidino groups of the arginine residues) can bind to the capillary wall structures, that is, probably components of the endothelial glycocalyx (198). Indeed, specific binding sites for albumin (glycoproteins

60, 30, and 18) have been demonstrated on the surface of endothelial cells (293, 294).

In terms of the fiber matrix theory, it has been suggested that albumin may affect the barrier to fluid and macromolecules by simply occupying space in the glycocalyx at the endothelial cell surface. Still, this effect would be insufficient to account for the rather large permeability changes occurring after removing proteins from the perfusate. Michel (192) therefore suggested that albumin (and also cationic ferritin) may reduce capillary permeability by ordering the lattice of fibrous macromolecules at the endothelial cell surface from an irregular array to a regular array. At present, this hypothesis needs, however, further experimental confirmation. Thus there may be several other possibilities to explain the protein effect as related to simple slit theory. It is, for example, not likely that albumin is non-specifically adsorbed to the walls of the wide portion of the interendothelial slits in a regular fashion. It is more likely that albumin can specifically bind to strategic areas in the irregular labyrinth cleft structures (293, 294). Therefore, it may, for example, increase the impact of the most restrictive portions of the slit.

C. Orosomucoid Effect

In experiments on perfused rat hindquarters, Haraldsson and Rippe (114, 115) noted that while albumin can maintain the hydraulic conductance, other plasma proteins are also necessary to prevent the permeability to (negatively charged) macromolecules (cf. albumin) from increasing. Thus, in the presence of albumin in the perfusate, removal of all other nondialyzable serum factors produced a near threefold increase in transvascular albumin clearance, whereas L_pS and PS for Cr-EDTA and cyanocobalamin stayed at control (115). Later, Haraldsson and Rippe (117) reported that the serum α_1 -acid glycoprotein orosomucoid apparently adds negative charge to the vessel wall, thereby reducing its permeability to anionic macromolecules. This effect occurs already at orosomucoid levels of 0.1 g/l. Further evidence supporting this view was recently provided by Curry et al. (53) in studies on single frog mesenteric capillaries. Addition of low concentrations of orosomucoid to a serum-free albumin-Ringer perfusate increased the ratio of capillary permeability of ribonuclease (positively charged) to that of the equally sized and negatively charged α -lactalbumin (radius ~20 Å), from ~2.5 to 5.8. This is in line with the present two-pore theory. Thus, theoretically, the presence of a negative pore charge will increase the restriction of a negatively charged solute, compared with that of a neutral solute (mol radius ~20 Å), fourfold in pores of radius 65 Å. It is also of great interest to note that the orosomucoid effect has recently been established for the (rat) glomerular capillaries (110), which may be of pathophysiological significance for the understanding of certain clinical disorders such as the nephrotic syndrome. This syndrome is characterized by massive urinary losses of albumin, hypoprotein-

emia, and the presence of peripheral edema. Can part of the suggested loss of negativity of the blood-urine barrier, as characterizing some of the glomerular disorders leading to the nephrotic syndrome such as the "minimal changes" nephropathy, be due to alterations also in the plasma protein composition?

It was recently shown that (bovine) orosomucoid is able to bind to (bovine) microvascular endothelial cells in culture in a quantity that may be consistent with its effect on capillary charge selectivity (294a). Maximum binding of orosomucoid was calculated to increase the negativity of the endothelial cell surface by 16.7 meq/l. This agrees almost exactly with the estimation of Curry et al. (53) of the effect of the presence of orosomucoid on the charge selectivity of the walls of individually perfused frog mesenteric capillaries. In the study of Schnitzer and Pinney (294a), orosomucoid binding showed specificity, saturability, reversibility, selective compatibility, and dependence on time and ligand concentration, but it was not calcium dependent.

The orosomucoid effect may simply be due to binding of negatively charged glycoprotein molecules to the glycocalyx or to the cell membrane surface, thereby enhancing the functional negativity of the capillary wall. Another possibility is that serum acidic glycoproteins induce conformational changes in the endothelial glycocalyx so that its negative charges become "exposed" after being more or less "hidden" during serum free perfusion. Indeed, conformational changes in fibrous molecular networks have been reported to occur as a result of interactions of orosomucoid with collagen in vitro. Thus, in the presence of orosomucoid, randomly oriented collagen fibers have been reported to arrange themselves into a regular pattern (fibrous long spacing formation) (74). The interaction of albumin and acidic glycoproteins with the capillary endothelium and its glycocalyx, however, needs further investigation to identify the mechanism(s) that are responsible for the protein effect and the orosomucoid effect.

D. Effects of Neutral Dextran on Microvascular Permselectivity

Even in the presence of serum in the perfusate, neutral dextrans appear to decrease the selectivity of capillary walls to proteins. Similar to the orosomucoid effect, these changes seem to occur without any large changes in L_pS or in small-solute diffusion capacity (115, 264, 267). Areekul (8) noted that the blood-tissue leakage of albumin increased markedly in the perfused rabbit ear when dextran solutions were used as perfusates. Rippe and Folkow (267) measured sieving coefficients for radiolabeled albumin in perfused rat hindquarters at high filtration rates and were thus able to estimate σ_{alb} according to the wash-down principle. When a mixture of 5–6 g/l (10 vol%) horse serum and 4% dextran in Tyrode solution made up the perfusate, they measured a σ_{alb} of 0.55. Increases in the concentration of serum relative to that of neutral dextran seemed to increase the selectiv-

ity of the microvascular walls, as evidenced by the increase in σ_{alb} measured. The σ_{alb} was not normalized (~0.94), however, until the concentration of neutral dextran in the serum perfusate was practically zero.

The mechanisms by which neutral dextran decreases the microvascular permselectivity in skin and muscle capillaries even in presence of orosomucoid are not known. Because neutral dextran seems to affect capillary selectivity without markedly altering L_pS and small-solute diffusion capacities (115, 267), it is tempting to speculate that also the dextran effects involve interactions with the charge-selective properties of microvascular walls (264). It has been suggested that dextrans may form a filter cake or a "plug" in the capillary structures responsible for water and solute permeation, thereby decreasing L_pS and also restricting transport of proteins from blood to tissue (59, 196, 343). Although high dextran concentrations may reduce L_pS , presumably by affecting fluid filtration through unselective large pores (59, 284), dextran effects on capillary walls imply reduction, not enhancement of capillary permselectivity (7, 267). The "filter cake" theory thus seems highly unlikely. Anyway, it seems possible that high concentrations of neutral dextran somehow can mask anionic sites in the microvascular membrane, thereby enhancing the transvascular flux of small anionic macromolecules, such as albumin, across small pores, without markedly affecting capillary filtration properties.

E. Effect of High Vascular Pressures on Vascular Permeability

Already Landis et al. (158) noted that large elevations of vascular pressures (>60 mmHg) apparently produced a fall in capillary wall selectivity in the human forearm. Also, Renkin et al. (259) and Rippe et al. (279) found that prolonged venous pressure elevations above the level of ~45–50 mmHg seemed to increase the vascular permeability to macromolecules. The exact mechanisms behind these permeability changes are, however, not known. Wasserman et al. (338) and Shirley et al. (302) suggested that pressure elevations may cause "stretching" of the microvascular membrane pores, thereby increasing their diameter and hence also increasing microvascular permeability, denoted "the stretched pore phenomenon." Shirley et al. (302) suggested that such a pore stretching could occur already at low venous pressure elevations. However, Rippe et al. (277) demonstrated in maximally vasodilated perfused rat hindquarters that short (3 min) periods of marked pressure elevations caused increased in L_pS and PS for Cr-EDTA only at P_v values ≥ 55 mmHg. While the L_pS elevations were then always pronounced (up to 5-fold), the concomitant increases in PS for Cr-EDTA were small (at most ~30%). This pattern was quantitatively similar to that observed after infusion of histamine-type mediators into this maximal vasodilated tissue (268, 269). Furthermore, similar to histamine-mediated responses, the high pressure insult was largely revers-

ible. They concluded that the reversible increases in capillary hydraulic conductivity occurring after brief pressure elevations were mainly due to a forceful opening of ordinarily closed large pores in the microvascular membrane, rather than being caused by "lesional rifts" in the endothelium. Furthermore, cooling did not eliminate the pressure-induced changes in vascular permeability, indicating that this may be a passive phenomenon.

Further support for the contention that high vascular pressures cause increases in the number of large pores was recently given by Wolf et al. (353). In their study on the perfused isolated cat hindlimb, σ_f was measured using the integral-mass balance method. In their study (353), σ_f decreased linearly from 0.81 when P_v was raised above 50 mmHg to ~ 0.2 at P_v equal to 120 mmHg. The capillary hydraulic conductance increased about four- to fivefold over the same pressure range. Like Rippe et al. (277), they concluded that the data could be best described by a reversible creation of additional large pores in the microvascular membrane at high vascular pressures.

Evidence that the capillary hydraulic conductance can increase upon just moderate elevations of microvascular pressure has been obtained for the pulmonary microcirculation. Pietra et al. (237) demonstrated an increased microvascular leakage of hemoglobin following pressure elevations in the pulmonary circulation. Later Nicolaysen et al. (207) found that the slope of the relationship between the rate of filtration and left arterial pressure increased markedly, when the latter was increased above 33 cmH₂O. The data suggest that the capillary wall L_pS may have been increased two- to threefold. They also found that these signs of an increased hydraulic conductance were partly reversible. This was later confirmed by Rippe et al. (285), who assessed L_pS in isolated perfused dog lungs. Vascular pressures exceeding 55 cmH₂O caused L_pS to increase reversibly in the majority of lungs, although the reversibility was not complete in about one-fifth of the organs investigated.

Contrary to the situation in hindlimb tissue, there is no obvious parallel between changes in L_pS and σ to macromolecules following high vascular pressures in the lung. Maron (177) found that σ_f decreased, shortly after exposure of lungs to high vascular pressure, but only after pressures exceeding 90 cmH₂O. This is in disparity with morphological assessments of the stretched pore phenomenon. West et al. (348) thus noted in a morphometric analysis that "stretch failure" of the rabbit pulmonary capillary walls usually occurred already at transmural pressures above 40 mmHg. The stress-failure damage actually implied lesional rifts in the endothelial membrane. In contrast, Townsley et al. (332), assessing vascular selectivity using the integral-mass balance technique in canine lungs, noted an increased σ_f at high vascular pressures, although L_pS increased. They concluded that high vascular pressures may not radially stretch pores, but rather produce tension of the entire vascular wall, including thinning of the endothelial and extraendothelial layers and elongation of existing inter-

endothelial pores. It is not clear what accounts for these differences between morphology and physiological assessments of σ_f . However, some endothelial disruptions that are observable morphologically may have little effect on functional measurements. Methodological differences concerning whether permeability characteristics are evaluated during conditions of constantly elevated pressures or after recovery from an imposed pressure transient may also be involved. However, it seems safe to conclude that following barotrauma in lungs, increases in L_pS and morphological lesions seem to occur concomitantly (284, 348), whereas the effects on σ_f may have to be further investigated.

IX. SUMMARY

In this review we summarized the evidence favoring the concept that the major plasma proteins are passively transported across vascular walls through water-filled pathways by means of convection and diffusion. With regard to solute transport, a majority of microvascular walls seems to show a bimodal size selectivity. This implies the presence of a high frequency of functional small pores, restricting proteins, and an extremely low number of non-size-selective pathways, permitting the passage of macromolecules from blood to tissue, here denoted large pores. We discussed the general behavior of such a heteroporous system.

A major consequence of two-pore heteroporosity is that large-solute transport must mainly occur due to convection through large pores at low filtration rates, that is, at normal or even zero lymph flows. Indeed, convection must be the predominating transport mode for most solutes across large pores when the net filtration rate is zero. Under these (transient) conditions, the convective leak of macromolecules across large pores will be counterbalanced by absorption of essentially protein-free fluid through protein-restrictive pores. In a heteroporous membrane, proteins can thus be transported by solvent drag across vascular walls in the absence of a net convection. Normally the steady-state transcapillary fluid flow (lymph flow) is about equally partitioned among small and large pores, which makes lymph essentially a "half and half" mixture of protein-free ultrafiltrate and plasma. With increasing fluid flows, however, the plasma filtrate will be progressively diluted, eventually reaching a protein concentration largely in proportion to the fractional hydraulic conductance accounted for by the large pores (α_L). Under these high lymph flow conditions, not only the large-pore transport but also the small-pore transport (of smaller macromolecules) will become convective. At low lymph flows, however, the small-pore transport of smaller macromolecules is usually mostly diffusive.

An important implication of capillary heteroporosity is that single-pore formalism is inadequate for correctly evaluating the capillary sieving characteristics. With the use of homoporous transport formalism, the "lumped" macromolecular PS and σ will therefore

vary as a function of transcapillary fluid flow (J_v). However, it is approximately correct to use single-pore formalism for conditions when J_v is very high during steady state. Thus, if minimal sieving coefficients can be measured for macromolecules, then these values will accurately reflect $(1 - \sigma)$. Furthermore, the slope of the linear portion of a plot of steady-state macromolecular clearances Cl versus steady-state J_v values for a heteroporous membrane has been demonstrated here to very closely reflect $(1 - \sigma)$. However, the "offset" of the linear portion of the Cl versus J_v relationship from the abscissa (and origin) only to a very minor degree reflects diffusive transport. A major portion of this offset is due to heteroporosity effects and, most likely, does not mirror dissipative transport. The heteroporosity effects are dependent on the level of the hydrostatic vascular pressure and on the net transvascular colloid osmotic pressure gradient prevailing when net lymph flow is zero ($\Delta\pi$). However, there is presently no accurate *in vivo* technique for separating heteroporosity effects from dissipative transport mechanisms. In contrast, in *in vitro* systems, such determinations have been possible by manipulating $\Delta\pi$ experimentally (118, 145, 274, 279). The results of these analyses yield diffusive transport components of the same order of magnitude, or only slightly larger, than those theoretically calculated using two-pore capillary models. It is therefore reasonable to conclude that components representing nonporous transport (cf. transecytosis) (cf. 252) may be rather small (274, 279) at least in *in vitro*-perfused organs.

Recent *in vivo* studies have indicated that the small-pore radius may be small enough to almost completely restrict the transport of albumin from blood to tissue in muscle and skin, and that the fractional hydraulic conductance accounted for by large pores may here be <2%. Whether the high apparent selectivity of microvascular membranes obtained in intact animal studies resists further testing remains to be seen. Furthermore, capillary walls generally seem to carry a net negative charge, probably residing in the glycocalyx. Because the negatively charged albumin molecule (radius 35.5 Å) is the major molecular probe for assessing the small-pore radius, an equivalent pore radius of 43–45 Å may actually correspond to a "structural" pore radius of 63–65 Å, allowing, for example, the IgG molecule (radius 54–56 Å) to normally pass to some extent through the small-pore system (by diffusion) as well as through the large pores.

During the last two decades it has become evident that the capillary wall exchange characteristics are highly dependent on the chemical composition of the medium bathing the endothelial cells. While albumin is required to maintain the capillary hydraulic conductance (and protein selectivity) normal, plasma orosomucoid evidently must be present to maintain the negative vascular wall charge at a physiological level. Lack of orosomucoid in plasma apparently leads to critical reductions in capillary wall charge, hence implying increases in the equivalent small-pore radius. Thus loss of negativity of the glomerular barrier can lead to very

marked (hundredfold) increases in the urinary protein excretion in certain glomerular disorders. During inflammation, however, protein extravasation is enhanced due to the formation of gaps in postcapillary venules through active Ca-dependent cellular mechanisms and, partly, due to increases in microvascular pressures and, most likely, also as a consequence of vascular recruitment.

The classical wash-down technique (325) for evaluating minimal sieving coefficients for macromolecules at high lymph flows, to assess capillary membrane selectivity in terms of reflection coefficients, is elegant in its simplicity. By necessity, heteroporous models are considerably more complex. Thus, to separate fluid flows among small and large pores as well as to correctly assess the (diffusive) small-pore transport, the hydraulic conductance (or surface area) of the blood-tissue barrier and $\Delta\pi$ have to be known at steady state. These requirements restrict the present two-pore analysis and limit its applicability. Furthermore, combined data from lymph collection and tissue sampling, performed during prolonged periods of blood-tissue equilibration of macromolecules, may be needed to accurately assess the nature of the microvascular barrier in its details. Hence, future approaches to measure transcapillary macromolecular transport will have to not only include heteroporosity effects and charge effects exerted by the microvascular membrane, but also to deal with the effects of heterogeneity of the interstitium. This will be a major challenge to future studies, but also impart additional complexity to the modeling of transvascular exchange. Hopefully, however, the present review has demonstrated that including the effects of microvascular membrane heteroporosity into the calculations represents a necessary step toward a better understanding of the mechanisms that account for the normal passage of macromolecules from blood to tissue.

Margita Andersson is gratefully acknowledged for skillful typing of the manuscript.

This work was supported by Swedish Medical Research Council Grant 8285 and the Medical Faculty, University of Lund.

REFERENCES

- ADAIR, T. H., D. S. MOFFAT, A. W. PAULSEN, AND A. C. GUYTON. Quantitation of changes in lymph protein concentration during lymph node transit. *Am. J. Physiol.* 243 (Heart Circ. Physiol. 12): H351–H359, 1982.
- ADAIR, T. H., J.-P. MONTANI, AND A. C. GUYTON. Modification of lymph by sheep caudal mediastinal node: effect of intranodal endotoxin. *J. Appl. Physiol.* 57: 1597–1601, 1984.
- ADAMS, D. J., J. BARAKEH, R. LASKEY, AND C. VAN BREEMEN. Ion channels and regulation of intracellular calcium in vascular endothelial cells. *FASEB J.* 3: 2389–2400, 1989.
- ADAMSON, R. H., V. H. HUXLEY, AND F. E. CURRY. Single capillary permeability to proteins having similar size but different charge. *Am. J. Physiol.* 254 (Heart Circ. Physiol. 23): H304–H312, 1988.
- ANDERSON, G. L., F. N. MILLER, AND R.-J. XIU. Inhibition of histamine-induced protein leakage in rat skeletal muscle by blockade of prostaglandin synthesis. *Microvasc. Res.* 28: 51–61, 1984.

6. APPELGREN, L., S. JACOBSSON, AND I. KJELLMER. Estimation of the protein concentration of the capillary filtrate by an isotope technique. *Acta Physiol Scand.* 66: 353-361, 1966.
7. AREEKUL, S. Reflection coefficients of neutral and sulphate-substituted dextran molecules in the isolated perfused rabbit ear. *Acta Soc. Med. Ups.* 74: 129-138, 1969.
8. AREEKUL, S. Effect of dextran 40 on the accumulation of ^{131}I -labelled human serum albumin in the isolated perfused rabbit ear. *Acta Soc. Med. Ups.* 74: 139-142, 1969.
9. ARFORSS, K. E., G. RUTILI, AND E. SVENNSJÖ. Microvascular transport of macromolecules in normal and inflammatory conditions. *Acta Physiol. Scand. Suppl.* 463: 93-103, 1979.
10. AUKLAND, K., AND G. NICOLAYSEN. Interstitial fluid volume: local regulatory mechanisms. *Physiol. Rev.* 61: 556-643, 1981.
11. BAKER, C. H. Nonhemodynamic effects of histamine on gracilis muscle capillary permeability. *J. Pharmacol. Exp. Ther.* 211: 672-677, 1979.
12. BASS, L., AND P. J. ROBINSON. Capillary permeability of heterogeneous organs: a parsimonious interpretation of indicator diffusion data. *Clin. Exp. Pharmacol. Physiol.* 9: 363-388, 1982.
13. BASSINGTHWAIGHTE, J. B. A concurrent flow model for extraction during transcapillary passage. *Circ. Res.* 35: 483-503, 1974.
14. BELL, R. D., AND R. J. MULLINS. Effects of increased venous pressure on albumin- and IgG-excluded volumes in skin. *Am. J. Physiol.* 242 (Heart Circ. Physiol. 11): H1038-H1043, 1982.
15. BELL, D. R., AND R. J. MULLINS. Effects of increased venous pressure on albumin- and IgG-excluded volumes in muscle. *Am. J. Physiol.* 242 (Heart Circ. Physiol. 11): H1044-H1049, 1982.
16. BELL, D. R., P. D. WATSON, AND E. M. RENKIN. Exclusion of plasma proteins in interstitium of tissues from the dog hindpaw. *Am. J. Physiol.* 239 (Heart Circ. Physiol. 8): H532-H538, 1980.
- 16a. BENT-HANSEN, L. Initial plasma disappearance and tissue uptake of ^{131}I -albumin in normal rabbits. *Microvasc. Res.* 41: 345-356, 1991.
17. BERT, J. L., AND R. H. PEARCE. The interstitium and microvascular exchange. In: *Handbook of Physiology. The Cardiovascular System. Microcirculation*. Bethesda, MD: Am. Physiol. Soc., 1984, sect. 2, vol. IV, pt. 1, chapt. 12, p. 521.
18. BILL, A. Plasma protein dynamics: albumin and IgG capillary permeability, extravascular movement and regional blood flow in unanesthetized rabbits. *Acta Physiol. Scand.* 101: 28-42, 1977.
- 18a. BJÖRNBERG, J. Forces involved in transcapillary fluid movement in exercising cat skeletal muscle. *Acta Physiol. Scand.* 140: 221-236, 1990.
19. BLAKE, L. H., AND N. C. STAUB. Pulmonary vascular transport in sheep: a mathematical model. *Microvasc. Res.* 12: 197-220, 1976.
20. BLUMENKRANTZ, M. J., G. M. GAHL, J. D. KOPPLE, A. V. KADMAR, M. R. JONES, M. KESSEL, AND J. W. DOBURN. Protein losses during peritoneal dialysis. *Kidney Int.* 19: 593-602, 1981.
21. BOHRER, M. P., C. BAYLIS, H. D. HUMES, R. J. GLASSOCK, C. R. ROBERTSON, AND B. M. BRENNER. Permselectivity of the glomerular capillary wall. Facilitated filtration of circulating polycations. *J. Clin. Invest.* 61: 72-78, 1978.
22. BRACE, R. A., D. N. GRANGER, AND A. E. TAYLOR. Analysis of lymphatic protein flux data. II. Effect of capillary heteroporosity on estimates of reflection coefficients and PS products. *Microvasc. Res.* 14: 215-226, 1977.
23. BRACE, R. A., D. N. GRANGER, AND A. E. TAYLOR. Analysis of lymphatic protein flux data. III. Use of the non-linear flux equation to estimate σ and PS. *Microvasc. Res.* 16: 297-303, 1978.
24. BRADLEY, J. D., R. J. ROSELLI, R. E. PARKER, AND T. R. HARRIS. Effects of endotoxemia on the sheep lung microvascular membrane: a two-pore theory. *J. Appl. Physiol.* 64: 2675-2683, 1988.
25. BRENNER, B. M., T. H. HOSTETTER, AND H. D. HUMES. Glomerular permselectivity: barrier function based on discrimination of molecular size and charge. *Am. J. Physiol.* 234 (Renal Fluid Electrolyte Physiol. 3): F455-F460, 1978.
26. BRESLER, E. H., AND L. J. GROOME. On equations for combined convective and diffusive transport of neutral solute across porous membranes. *Am. J. Physiol.* 241 (Renal Fluid Electrolyte Physiol. 10): F469-F476, 1981.
27. BRIDGES, C. R., B. D. MYERS, B. M. BRENNER, AND W. M. DEEN. Glomerular charge alterations in human minimal change nephropathy. *Kidney Int.* 22: 677-684, 1982.
28. BRUNS, R. R., AND G. E. PALADE. Studies on blood capillaries. II. Transport of ferritin molecules across the wall of muscle capillaries. *J. Cell Biol.* 37: 277-299, 1968.
29. BUNDGAARD, M. Transport pathways in capillaries—in search of pores. *Annu. Rev. Physiol.* 42: 325-336, 1980.
30. BUNDGAARD, M. Vesicular transport in capillary endothelium: does it occur? *Federation Proc.* 42: 2425-2430, 1983.
31. BUNDGAARD, M. The three-dimensional organization of tight junctions in a capillary endothelium revealed by serial-section electron microscopy. *J. Ultrastruct. Res.* 88: 1-17, 1984.
32. BUNDGAARD, M., J. FROKJAER-JENSEN, AND C. CRONE. Endothelial plasmalemmal vesicles as elements in a system of branching invaginations from the cell surface. *Proc. Natl. Acad. Sci. USA* 76: 6439-6442, 1979.
33. BUNDGAARD, M., P. HAGMAN, AND C. CRONE. The three-dimensional organization of plasmalemmal vesicular profiles in the endothelium of rat heart capillaries. *Microvasc. Res.* 25: 358-368, 1983.
34. CARDEN, D. L., J. K. SMITH, AND R. J. KORTHUIS. Oxidant-mediated, CD_{18} -dependent microvascular dysfunction induced by complement-activated granulocytes. *Am. J. Physiol.* 260 (Heart Circ. Physiol. 29): H1144-H1152, 1991.
35. CARTER, R. D., W. L. JOYNER, AND E. M. RENKIN. Effects of histamine and some other substances on molecular selectivity of the capillary wall to plasma proteins and dextran. *Microvasc. Res.* 7: 31-48, 1975.
36. CHANG, R. L. S., W. M. DEEN, C. R. ROBERTSON, AND B. M. BRENNER. Permselectivity of the glomerular capillary wall. III. Restricted transport of polyanions. *Kidney Int.* 8: 212-218, 1975.
37. CHANG, R. L. S., I. F. UEKI, W. M. DEEN, J. L. TROY, C. R. ROBERTSON, AND B. M. BRENNER. Permselectivity of the glomerular capillary wall to macromolecules. I. Theoretical considerations. *Biophys. J.* 15: 877-895, 1975.
38. CLEMENTI, F., AND G. E. PALADE. Intestinal capillaries. I. Permeability to peroxidase and ferritin. *J. Cell Biol.* 41: 33-58, 1969.
39. CLOUGH, G. The steady-state transport of cationized ferritin by endothelial cell vesicles. *J. Physiol. Lond.* 328: 389-401, 1982.
40. CLOUGH, G., AND C. C. MICHEL. The role of vesicles in the transport of ferritin through frog endothelium. *J. Physiol. Lond.* 315: 127-142, 1981.
- 40a. CLOUGH, G., AND C. C. MICHEL. Quantitative comparisons of hydraulic permeability and endothelial intercellular cleft dimensions in single frog capillaries. *J. Physiol. Lond.* 405: 563-576, 1988.
41. COBBOLD, A., B. FOLKOW, I. KJELLMER, AND S. MELLANDER. Nervous and local chemical control of precapillary sphincters in skeletal muscle as measured by changes in capillary filtration coefficient. *Acta Physiol. Scand.* 57: 180-192, 1963.
42. CRONE, C. The function of capillaries. In: *Recent Advances in Physiology*, edited by P. F. Baker. London: Churchill Livingstone, 1984, p. 125.
43. CRONE, C. Modulation of solute permeability in microvascular endothelium. *Federation Proc.* 45: 77-83, 1986.
44. CRONE, C. The Malpighi lecture. From "Porosites carnis" to cellular microcirculation. *Int. J. Microcirc. Clin. Exp.* 6: 101-122, 1987.
45. CRONE, C., AND D. G. LEVITT. Capillary permeability to small solutes. In: *Handbook of Physiology. The Cardiovascular System. Microcirculation*. Bethesda, MD: Am. Physiol. Soc., 1984, sect. 2, vol. IV, pt. 1, chapt. 10, p. 411.
46. CURRY, F. E. Permeability coefficients of the capillary wall to low molecular weight hydrophilic solutes measured in single perfused capillaries of frog mesentery. *Microvasc. Res.* 17: 290-308, 1979.
47. CURRY, F. E. Mechanics and thermodynamics of transcapillary exchange. In: *Handbook of Physiology. The Cardiovascular Sys-*

- tem. *Microcirculation*. Bethesda, MD: Am. Physiol. Soc., 1984, sect. 2, vol. IV, pt. 1, chapt. 8, p. 309.
48. CURRY, F. E. Determinants of capillary permeability: a review of mechanisms based on single capillary studies in the frog. *Circ. Res.* 59: 367-380, 1986.
 49. CURRY, F. E., V. H. HUXLEY, AND R. H. ADAMSON. Permeability of single capillaries to intermediate-sized colored solutes. *Am. J. Physiol.* 245 (*Heart Circ. Physiol.* 14): H495-H505, 1983.
 50. CURRY, F. E., J. C. MASON, AND C. C. MICHEL. Osmotic reflection coefficients of capillary walls to low molecular weight hydrophilic solutes measured in single perfused capillaries of the frog mesentery. *J. Physiol. Lond.* 261: 319-336, 1976.
 51. CURRY, F. E., AND C. C. MICHEL. A fibre matrix model of capillary permeability. *Microvasc. Res.* 20: 96-99, 1980.
 52. CURRY, F. E., C. C. MICHEL, AND M. E. PHILLIPS. Effect of albumin on the osmotic pressure exerted by myoglobin across capillary walls in frog mesentery. *J. Physiol. Lond.* 387: 69-82, 1987.
 53. CURRY, F. E., J. C. RUTLEDGE, AND J. F. LENZ. Modulation of microvessel wall charge by plasma glycoprotein orosomucoid. *Am. J. Physiol.* 257 (*Heart Circ. Physiol.* 26): H1354-H1359, 1989.
 54. DANIELLI, J. F. Capillary permeability and oedema in the perfused frog. *J. Physiol. Lond.* 98: 109-129, 1940.
 55. DECKERT, T., B. FELDT-RASMUSSEN, R. DJURUP, AND M. DECKERT. Glomerular size and charge selectivity in insulin-dependent diabetes mellitus. *Kidney Int.* 33: 100-106, 1988.
 56. DEEN, W. M., C. R. BRIDGES, B. M. BRENNER, AND B. D. MYERS. Heteroporous model of glomerular size selectivity: application to normal and nephrotic humans. *Am. J. Physiol.* 249 (*Renal Fluid Electrolyte Physiol.* 18): F374-F389, 1985.
 57. DEEN, W. M., B. SATVAT, AND J. M. JAMIESON. Theoretical model for glomerular filtration of charged solutes. *Am. J. Physiol.* 238 (*Renal Fluid Electrolyte Physiol.* 7): F126-F139, 1980.
 58. DEWEY, W. C. Vascular-extravascular exchange of ^{131}I -plasma proteins in the rat. *Am. J. Physiol.* 197: 428-431, 1959.
 59. DIANA, J. N., J. KEITH, AND B. P. FLEMING. Influence of macromolecules on capillary filtration coefficients in isolated dog hindlimbs. *Microvasc. Res.* 20: 106-107, 1977.
 60. DIANA, J. N., AND M. H. LAUGHLIN. Effect of ischemia on capillary pressure and equivalent pore radius in capillaries of the isolated dog hindlimb. *Circ. Res.* 35: 77-101, 1974.
 61. DIANA, J. N., S. C. LONG, AND H. YAO. Effect of histamine on equivalent pore radius in capillaries of isolated dog hindlimb. *Microvasc. Res.* 4: 413-437, 1972.
 62. DOBBINS, D. E., C. Y. SOIKA, A. J. PREMEN, G. J. GREGA, AND J. M. DABNEY. Blockade of histamine and bradykinin-induced increases in lymph flow, protein concentration and protein transport by terbutaline in vivo. *Microcirculation* 2: 127-150, 1982.
 63. DRAKE, R., T. ADAIR, D. TRABER, AND J. GABEL. Contamination of caudal mediastinal node efferent lymph in sheep. *Am. J. Physiol.* 241 (*Heart Circ. Physiol.* 10): H354-H357, 1981.
 64. DRAKE, R. E., AND J. C. GABLE. Effect of histamine and alloxan on canine pulmonary vascular permeability. *Am. J. Physiol.* 239 (*Heart Circ. Physiol.* 8): H96-H100, 1980.
 65. DRAKE, R. E., AND G. A. LAINE. Pulmonary microvascular permeability to fluid and macromolecules. *J. Appl. Physiol.* 64: 487-501, 1988.
 66. DRINKER, C. K. The permeability and diameter of the capillaries in the web of the brown frog (*R. temporaria*) when perfused with solutions containing pituitary extract and horse serum. *J. Physiol. Lond.* 63: 249-269, 1927.
 67. ELIASSEN, E., B. FOLKOW, S. M. HILTON, B. ÖBERG, AND B. RIPPE. Pressure-volume characteristics of the interstitial fluid space in the skeletal muscle of the cat. *Acta Physiol. Scand.* 90: 583-593, 1974.
 68. ENGEL, J., E. ODERMATT, A. ENGEL, J. MADRI, H. FURTHMAYR, H. RHODE, AND R. TIMPLE. Shapes, domain organization and flexibility of laminin and fibronectin, two multifractional proteins of the extracellular matrix. *J. Mol. Biol.* 150: 97-120, 1981.
 69. FIRRELL, J. C., G. P. LEWIS, AND L. J. F. YOULTEN. Vascular permeability to macromolecules in rabbit paw and skeletal muscle: a lymphatic study with a mathematical interpretation of transport processes. *Microvasc. Res.* 23: 294-310, 1982.
 70. FLEMING, B. P., AND J. N. DIANA. Effects of papaverine administration on pre- and postcapillary resistance and filtration coefficient in isolated dog hindlimbs (Abstract). *Federation Proc.* 36: 470, 1977.
 71. FLESSNER, M. F. Peritoneal transport physiology: insights from basic research. *J. Am. Soc. Nephrol.* 2: 122-135, 1991.
 72. FLESSNER, M. F., R. L. DEDRICK, AND J. S. SCHULTZ. A distributed model of peritoneal plasma transport: analysis of experimental data in the rat. *Am. J. Physiol.* 248 (*Renal Fluid Electrolyte Physiol.* 17): F413-F424, 1985.
 73. FLESSNER, M. F., R. L. DEDRICK, AND J. S. SCHULTZ. Exchange of macromolecules between peritoneal cavity and plasma. *Am. J. Physiol.* 248 (*Heart Circ. Physiol.* 17): H15-H25, 1985.
 74. FRANZBLAU, C., K. SCHMID, B. FARIS, J. BELDEKAS, P. GARVIN, H. M. KAGAN, AND B. J. BAUM. The interaction of collagen with α -acid glycoprotein. *Biochim. Biophys. Acta* 427: 302-314, 1976.
 75. FRIED, T. A., R. N. MCCOY, R. W. OSGOOD, AND J. H. STEIN. Effect of albumin on glomerular ultrafiltration coefficient in isolated perfused dog glomerulus. *Am. J. Physiol.* 250 (*Renal Fluid Electrolyte Physiol.* 19): F901-F906, 1986.
 76. FRIEDMAN, J. J. Transcapillary protein leakage and fluid movement. Effect of venous pressure. *Microvasc. Res.* 13: 275-290, 1976.
 77. FRIEDMAN, J. J. Hyperosmolality and transcapillary fluid and protein movement in skeletal muscle. *Microvasc. Res.* 29: 340-349, 1985.
 78. FRIEDMAN, J. J., AND N. E. DE ROSE. The effects of flow and hyperosmolar superfusion on the K^+ permeability of single capillaries. *Microvasc. Res.* 24: 68-76, 1982.
 79. FRIEDMAN, J. J., AND S. WITTE. The radial protein concentration profile in the interstitial space of the rat ileal mesentery. *Microvasc. Res.* 31: 277-287, 1986.
 80. FRØKJAER-JENSEN, J. Three-dimensional organization of plasmalemmal vesicles in endothelial cells. *J. Ultrastruct. Res.* 73: 9-20, 1980.
 81. FRØKJAER-JENSEN, J. The plasmalemmal vesicular system in capillary endothelium. Conventional electron microscopic (EM) thin sections compared with the picture arising from ultrathin ($\sim 140 \text{ \AA}$) serial sectioning. *Prog. Appl. Microcirc.* 1: 17-34, 1983.
 82. FRØKJAER-JENSEN, J. The plasmalemmal vesicular system in striated muscle capillaries and in pericytes. *Tissue Cell* 16: 31-42, 1984.
 83. FRØKJAER-JENSEN, J. The vesicle controversy. *Prog. Appl. Microcirc.* 9: 21-42, 1985.
 84. FRØKJAER-JENSEN, J., R. C. WAGNER, S. B. ANDREWS, P. HAGMAN, AND T. S. A. REESE. Three-dimensional organization of the plasmalemmal vesicular system in directly frozen capillaries of the rete mirabile in the swim bladder of the eel. *Cell Tissue Res.* 254: 17-24, 1988.
 85. GALLACHER, D. V. Control of calcium influx in cells without action potentials. *News Physiol. Sci.* 3: 244-249, 1988.
 86. GAMBLE, J. The effect of low concentrations of bovine albumin on the vascular transduction coefficient of the isolated perfused rat mesentery (Abstract). *J. Physiol. Lond.* 289: 63P-64P, 1979.
 87. GAMBLE, J. Influence of pH on capillary filtration coefficient of rat mesenteries perfused with solutions containing albumin. *J. Physiol. Lond.* 339: 505-518, 1983.
 88. GARBY, L., AND S. AREEKUL. Reflection coefficients of neutral and sulphate-substituted dextran molecules in the capillaries of the isolated rabbit ear. In: *Capillary Permeability*, edited by C. Crone and N. A. Lassen. Copenhagen: Munksgaard, 1970, p. 560. (Alfred Benzon Symp. II)
 89. GARBY, L., AND J. GRONLUND. A note on the single injection residue function method to determine capillary permeability. *Acta Physiol. Scand.* 104: 360-363, 1978.
 90. GARLICK, D. G., AND E. M. RENKIN. Transport of large molecules from plasma to interstitial fluid and lymph in dogs. *Am. J. Physiol.* 219: 1595-1605, 1970.
 91. GHINEA, N., M. ESKENASY, M. SIMIONESCU, AND N. SIMIONESCU. Endothelial albumin binding proteins are mem-

- brane-associated components exposed on the cell surface. *J. Biol. Chem.* 264: 4755-4758, 1989.
92. GHITESCU, L., A. FIXMAN, M. SIMIONESCU, AND N. SIMIONESCU. Specific binding sites for albumin restricted to plasma-lemmal vesicles of continuous capillary endothelium: receptor-mediated transcytosis. *J. Cell Biol.* 102: 1304-1311, 1986.
 93. GILCHRIST, S. A., AND J. C. PARKER. Exclusion of charged macromolecules in the pulmonary interstitium. *Microvasc. Res.* 30: 88-98, 1985.
 94. GLAUSER, F. L., R. P. FAIRMAN, AND J. E. MILLEN. Facilitated transport of anionic dextrans in the pulmonary microvasculature of normal sheep. *Int. J. Microcirc. Clin. Exp.* 2: 1-10, 1982.
 95. GRANGER, D. N., M. E. HOLLWARTH, AND D. A. PARKS. Ischemia-reperfusion injury: role of oxygen-derived free radicals. *Acta Physiol. Scand.* 126, Suppl. 548: 47-63, 1986.
 96. GRANGER, D. N., M. A. PERRY, P. R. KVIETYS, AND A. E. TAYLOR. Permeability of intestinal capillaries: effects of fat absorption and gastrointestinal hormones. *Am. J. Physiol.* 242 (Gastrointest. Liver Physiol. 5): G194-G201, 1982.
 97. GRANGER, D. N., AND A. E. TAYLOR. Permeability of intestinal capillaries to endogenous macromolecules. *Am. J. Physiol.* 238 (Heart Circ. Physiol. 7): H457-H464, 1980.
 98. GREGA, G. J., AND E. SVENSSJÖ. Pharmacology of water and macromolecular permeability in the forelimb of the dog. In: *Edema*, edited by N. C. Staub and A. E. Taylor. New York: Raven, 1986, p. 405.
 99. GROOME, L. J., AND G. T. KINASEWITZ. A simple method for determining the homoporous solute-membrane permeability from plasma-to-lymph measurements. *Microvasc. Res.* 30: 235-241, 1985.
 100. GROOME, L. J., AND G. T. KINASEWITZ. Dependence of permeability on solute concentration: effects due to membrane heteroporosity. *Microvasc. Res.* 32: 248-254, 1986.
 101. GROOME, L. J., G. T. KINASEWITZ, AND J. N. DIANA. Diffusion and convection across heteroporous membranes: a simple macroscopic equation. *Microvasc. Res.* 26: 307-322, 1983.
 102. GROTTE, G. Passage of dextran molecules across the blood-lymph barrier. *Acta Chir. Scand. Suppl.* 211: 1-84, 1956.
 103. HADDY, F. J., J. B. SCOTT, AND G. J. GREGA. Effects of histamine on lymph protein concentration and flow in the dog forelimb. *Am. J. Physiol.* 223: 1172-1177, 1972.
 104. HARALDSSON, B. Effects of noradrenaline on the transcapillary passage of albumin, fluid and CrEDTA in the perfused rat hindlimb. *Acta Physiol. Scand.* 125: 561-571, 1985.
 105. HARALDSSON, B. *Physiological Studies of Macromolecular Transport Across Capillary Walls. Studies on Continuous Capillaries in Rat Skeletal Muscle* (PhD thesis). Göteborg, Sweden: Univ. of Göteborg, 1986.
 106. HARALDSSON, B. Diffusional transport of albumin from interstitium to blood across small pores in the capillary walls of rat skeletal muscle. *Acta Physiol. Scand.* 133: 63-71, 1988.
 107. HARALDSSON, B., C. EKHOLM, AND B. RIPPE. Importance of molecular charge for the passage of endogenous macromolecules across continuous capillary walls, studied by serum clearance of lactate dehydrogenase (LDH) isoenzymes. *Acta Physiol. Scand.* 117: 123-130, 1983.
 108. HARALDSSON, B., AND B. R. JOHANSSON. Changes in transcapillary exchange induced by perfusion fixation with glutaraldehyde, followed by simultaneous measurements of capillary filtration coefficient, diffusion capacity and albumin clearance. *Acta Physiol. Scand.* 124: 99-106, 1985.
 109. HARALDSSON, B., E. JOHNSSON, AND B. RIPPE. A note on the errors of using venous congestion in intact rats for determinations of microvascular permeability. *Acta Physiol. Scand.* 143: 233-238, 1991.
 110. HARALDSSON, B., E. JOHNSSON, AND B. RIPPE. Glomerular permselectivity is dependent on adequate serum concentrations of orosomucoid. *Kidney Int.* 41: 310-316, 1992.
 111. HARALDSSON, B., B. J. MOXHAM, AND B. RIPPE. Capillary permeability to sulphate-substituted and neutral dextran fractions in the rat hindquarter vascular bed. *Acta Physiol. Scand.* 115: 397-404, 1982.
 112. HARALDSSON, B., B. J. MOXHAM, B. RIPPE, AND B. FOLKOW. Permeability of fenestrated capillaries in the isolated pig pancreas, with effects of bradykinin and histamine, as studied by simultaneous registration of filtration and diffusion capacities. *Acta Physiol. Scand.* 114: 67-74, 1982.
 113. HARALDSSON, B., L. REGNÉR, R. HULTBORN, L. WEISS, AND B. RIPPE. Transcapillary passage of albumin in mammary tumours and in normal lactating mammary glands of the rat. *Acta Physiol. Scand.* 122: 497-505, 1984.
 114. HARALDSSON, B., AND B. RIPPE. Higher albumin clearance in rat hindquarters perfused with pure albumin solutions than with serum as perfusate. *Acta Physiol. Scand.* 122: 93-95, 1984.
 115. HARALDSSON, B., AND B. RIPPE. Serum factors other than albumin are needed for the maintenance of normal capillary permeability in rat hindlimb muscle. *Acta Physiol. Scand.* 123: 427-436, 1985.
 116. HARALDSSON, B., AND B. RIPPE. Restricted diffusion of CrEDTA and cyanocobalamin in rat hindquarters. *Acta Physiol. Scand.* 127: 359-372, 1986.
 117. HARALDSSON, B., AND B. RIPPE. Orosomucoid as one of the serum components contributing to normal capillary permselectivity in rat skeletal muscle. *Acta Physiol. Scand.* 129: 127-135, 1987.
 118. HARALDSSON, B., AND B. RIPPE. Influence of perfusate oncotic pressure on the transcapillary clearance of albumin in maximally vasodilated rat skeletal muscle. *Acta Physiol. Scand.* 130: 219-228, 1987.
 119. HARALDSSON, B., AND B. RIPPE. Transcapillary clearance of albumin in rat skeletal muscle monitored by external detection. Effects of alterations in capillary surface area. *Acta Physiol. Scand.* 132: 495-504, 1988.
 120. HARALDSSON, B., AND B. RIPPE. Upper and lower bounds on capillary permeability ratios of Cr-EDTA to cyanocobalamin in rat hindquarters. *Acta Physiol. Scand.* 143: 239-244, 1991.
 121. HARALDSSON, B., U. ZACKRISSON, AND B. RIPPE. Calcium dependence of histamine-induced increases in capillary permeability, studied in isolated rat hindlimbs. *Acta Physiol. Scand.* 128: 247-258, 1986.
 122. HARRIS, T. R., AND R. J. ROSELLI. A theoretical model of protein, fluid, and small molecule transport in the lung. *J. Appl. Physiol.* 50: 1-14, 1981.
 - 122a. HE, P., AND F. E. CURRY. Depolarization modulated endothelial cell calcium influx and microvessel permeability. *Am. J. Physiol.* 261 (Heart Circ. Physiol. 30): H1246-H1254, 1991.
 123. HELTIANU, C., M. SIMIONESCU, AND N. SIMIONESCU. Histamine receptors of the microvascular endothelium revealed in situ with a histamine-fourteen conjugate: characteristic high-affinity binding sites in venules. *J. Cell Biol.* 93: 357-364, 1982.
 - 123a. HENRIKSEN, J. H. Plasma disappearance of tracer albumin and lymph flow. *Microvasc. Res.* 27: 223-225, 1984.
 124. HENRIKSEN, O. Local sympathetic reflex mechanism in regulation of blood flow in human subcutaneous adipose tissue. *Acta Physiol. Scand. Suppl.* 450, 1-48, 1977.
 - 124a. HOLMÄNG, A., P. BJÖRNTORP, AND B. RIPPE. Tissue uptake of insulin and inulin in red and white skeletal muscle in vivo. *Am. J. Physiol.* 263 (Heart Circ. Physiol. 32): H1170-H1176, 1992.
 125. HOUSE, C. R. *Water Transport in Cells and Tissues*. London: Arnold, 1974.
 126. HUXLEY, V. H., AND F. E. CURRY. Albumin modulation of capillary permeability: test of an adsorption mechanism. *Am. J. Physiol.* 248 (Heart Circ. Physiol. 17): H264-H273, 1985.
 127. HUXLEY, V. H., AND F. E. CURRY. The effect of superfusate albumin on single capillary hydraulic conductivity. *Am. J. Physiol.* 252 (Heart Circ. Physiol. 21): H395-H401, 1987.
 128. HUXLEY, V. H., AND F. E. CURRY. Differential actions of albumin and plasma on capillary solute permeability. *Am. J. Physiol.* 260 (Heart Circ. Physiol. 29): H1645-H1654, 1991.
 129. HUXLEY, V. H., F. E. CURRY, AND R. H. ADAMSON. Quantitative fluorescence microscopy on single capillaries: α -lactalbumin transport. *Am. J. Physiol.* 252 (Heart Circ. Physiol. 21): H188-H197, 1987.
 130. ISHIBASHI, M., R. K. REED, M. I. TOWNSLEY, J. C. PARKER, AND A. E. TAYLOR. Albumin transport across pulmonary capil-

- lary-interstitial barrier in anesthetized dogs. *J. Appl. Physiol.* 70: 2104-2110, 1991.
131. JENNINGS, M. A., AND H. FLOREY. An investigation of some properties of endothelium related to capillary permeability. *Proc. R. Soc. Lond. B Biol. Sci.* 167: 39-63, 1967.
 132. JOHANSSON, B. R. *The Microvasculature in Skeletal Muscle. An Electron-Microscopic Study With Special Reference to the Endothelial Permeability to Macromolecules* (PhD thesis). Göteborg, Sweden: Univ. of Göteborg, 1977.
 133. JOHANSSON, B. R. Permeability of muscle capillaries to interstitially microinjected ferritin. *Microvasc. Res.* 16: 362-368, 1978.
 134. JOYNER, W. L., R. D. CARTER, G. RAIZES, AND E. M. RENKIN. Influence of histamine and some other substances on blood-lymph transport of plasma protein and dextran in the dog paw. *Microvasc. Res.* 7: 19-30, 1974.
 135. KATZ, M. A. Comparison of crosspoint and least-squares regression methods in computation of membrane protein flux parameters from lymph flux analysis. *Microvasc. Res.* 30: 207-221, 1985.
 - 135a. KATZ, M. A. Structural change in fiber matrix allows for enhanced permeability and reduced hydraulic conductivity. *Microvasc. Res.* 43: 1-6, 1992.
 136. KEDEM, O., AND A. KATCHALSKY. Thermodynamic analysis of the permeability of biological membranes to nonelectrolytes. *Biochim. Biophys. Acta* 27: 229-246, 1958.
 137. KEDEM, O., AND A. KATCHALSKY. A physical interpretation of the phenomenological coefficients of membrane permeability. *J. Gen. Physiol.* 45: 143-179, 1961.
 138. KEDEM, O., AND A. KATCHALSKY. Permeability of composite membranes. Parts 1, 2, and 3. *Trans. Faraday Soc.* 59: 1918-1954, 1963.
 139. KEFALIDES, N. A. Chemistry of basement membranes: structure and biosynthesis. In: *Vascular Endothelium and Basement Membranes*, edited by B. M. Altura. Basel: Karger, 1980, p. 295.
 140. KERN, D. F. *Pulmonary Capillary Permeabilities and Reflection Coefficients* (PhD thesis). Minneapolis: Univ. of Minnesota, 1981.
 141. KERN, D. F., D. R. BELL, AND F. A. BLUMENSTOCK. The effect of charge on albumin permeability and uptake in the lung. *Microvasc. Res.* 23: 241, 1983.
 142. KERN, D. F., C. KIVLEN, AND A. G. MALIK. Pulmonary capillary filtration coefficient (K_f): blood vs. Albumin-Ringer's. *Microvasc. Res.* 27: 248, 1984.
 143. KERN, D. F., D. LEVITT, AND D. WANGENSTEEN. Endothelial albumin permeability measured with a new technique in perfused rabbit lung. *Am. J. Physiol.* 245 (Heart Circ. Physiol. 14): H229-H236, 1983.
 144. KERN, D. F., AND A. B. MALIK. Microvascular albumin permeability in isolated perfused lung: effects of EDTA. *J. Appl. Physiol.* 58: 372-375, 1985.
 145. KINASEWITZ, G. T., L. J. GROOME, D. K. PAYNE, AND J. N. DIANA. Concentration dependence of protein permeability across the canine visceral pleura. *Microvasc. Res.* 33: 35-49, 1987.
 146. KING, G. L., AND S. JOHNSON. Receptor-mediated transport of insulin across the endothelial cells. *Science Wash. DC* 227: 1583-1586, 1985.
 147. KJELLMER, I., AND H. ODELRAM. The effect of some physiological vasodilators on the vascular bed of skeletal muscle. *Acta Physiol. Scand.* 63: 94-102, 1965.
 148. KOBAYASHI, S. Ferritin labelling in the fixed muscle capillary. A doubt on the tracer experiments as the basis for the vesicular transport theory. *Arch. Histol. Jpn.* 32: 81-86, 1970.
 149. KORTHUIS, R. J., D. N. GRANGER, M. I. TOWNSLEY, AND A. E. TAYLOR. The role of oxygen-derived free radicals in ischemia-induced increases in canine skeletal muscle vascular permeability. *Circ. Res.* 57: 599-609, 1985.
 150. KORTHUIS, R. J., M. B. GRISHAM, B. J. ZIMMERMAN, D. N. GRANGER, AND A. E. TAYLOR. Vascular injury in dogs during ischemia-reperfusion: improvement with ATP-MgCl₂ pretreatment. *Am. J. Physiol.* 254 (Heart Circ. Physiol. 23): H702-H708, 1988.
 151. KORTHUIS, R. J., C. R. KERR, M. I. TOWNSLEY, AND A. E. TAYLOR. Microvascular pressure, surface area, and permeability in the hindquarters of spontaneously hypertensive rats. *Am. J. Physiol.* 249 (Heart Circ. Physiol. 18): H498-H504, 1985.
 152. KORTHUIS, R. J., C. Y. WANG, AND J. B. SCOTT. Transient effects of histamine on microvascular fluid movements. *Microvasc. Res.* 23: 316-328, 1982.
 153. KORTHUIS, R. J., C. Y. WANG, AND W. S. SPIELMAN. Transient effects of histamine on capillary filtration coefficient. *Microvasc. Res.* 28: 322-344, 1984.
 154. KRAMER, G. C., B. A. HARMS, B. I. BODAI, R. H. DEMLING, AND E. M. RENKIN. Mechanisms for redistribution of plasma protein following a protein depletion. *Am. J. Physiol.* 243 (Heart Circ. Physiol. 12): H803-H809, 1982.
 155. KRAMER, G. C., B. A. HARMS, R. A. GUNTHER, E. M. RENKIN, AND R. H. DEMLING. The effects of hypoproteinemia on blood-to-lymph fluid transport in sheep lung. *Circ. Res.* 49: 1173-1180, 1981.
 156. KROGH, A., AND G. A. HARROP. Some observations on stasis and oedema. *J. Physiol. Lond.* 54: 125-126, 1921.
 - 156a. KUBES, P., AND D. N. GRANGER. Nitric oxide modulates microvascular permeability. *Am. J. Physiol.* 262 (Heart Circ. Physiol. 31): H611-H615, 1992.
 157. KVIETYS, P. R., M. A. PERRY, AND D. N. GRANGER. Permeability of pancreatic capillaries to small molecules. *Am. J. Physiol.* 245 (Gastrointest. Liver Physiol. 8): G519-G524, 1983.
 158. LANDIS, E. M., L. JONAS, M. ANGEVINE, AND W. ERB. The passage of fluid and protein through the human capillary wall during venous congestion. *J. Clin. Invest.* 11: 717-734, 1932.
 159. LANDIS, E. M., AND J. R. PAPPENHEIMER. Exchange of substances through the capillary walls. In: *Handbook of Physiology. Circulation*. Washington, DC: Am. Physiol. Soc, 1963, sect. 2, vol. II, chapt. 29, p. 961-1034.
 160. LANKEN, P. N., J. H. HANSEN-FLASCHEN, P. M. SAMPSON, G. G. PIETRA, F. R. HASELTON, AND A. P. FISHMAN. Passage of uncharged dextrans from blood to lung lymph in awake sheep. *J. Appl. Physiol.* 59: 580-591, 1985.
 161. LASSEN, N. A., H.-H. PARVING, AND N. ROSSING. Filtration as the main mechanism of overall transcapillary protein escape from the plasma. *Microvasc. Res.* 7: 1-4, 1974.
 162. LAURENT, T. C. The structure and function of the intercellular polysaccharides in connective tissue. In: *Capillary Permeability*, edited by C. Crone and N. A. Lassen. Copenhagen: Munksgaard, 1970, p. 261.
 163. LEVICK, J. R. Blood flow and mass transport in synovial joints. In: *Handbook of Physiology. The Cardiovascular System. Microcirculation*. Bethesda, MD: Am. Physiol. Soc., 1984, sect. 2, vol. IV, pt. 2, chapt. 19, p. 917-948.
 164. LEVICK, J. R., AND C. C. MICHEL. The effect of bovine albumin on the permeability of frog mesenteric capillaries. *Q. J. Exp. Physiol.* 58: 87-97, 1973.
 165. LEVICK, J. R., AND L. H. SMAJE. An analysis of the permeability of a fenestra. *Microvasc. Res.* 33: 233-256, 1987.
 166. LUFT, J. H. Fine structure of capillary and endocapillary layer as revealed by ruthenium red. *Federation Proc.* 25: 1773-1783, 1966.
 167. LUFT, J. H. The structure and properties of the cell surface coat. *Int. Rev. Cytol.* 45: 291-382, 1976.
 168. LUNDE, P. K. M. *The Influence of Perfusate Composition on Edema Development in Isolated Perfused Rabbit Lungs* (PhD thesis). Oslo, Norway: Universitetsforlaget, 1967.
 169. MAJNO, G., V. GILMORE, AND M. LEVENTHAL. On the mechanism of vascular leakage caused by histamine-type mediators. *Circ. Res.* 21: 833-847, 1967.
 170. MAJNO, G., AND G. E. PALADE. Studies on inflammation I. Effect of histamine and serotonin on vascular permeability. An electron microscopic study. *J. Biophys. Biochem. Cytol.* 11: 571-606, 1961.
 171. MANEGOLD, E., AND K. SOLF. Über kapillarsysteme XIV. 1. Die dynamik osmotischer zellen. *Kolloid Z.* 59: 179-195, 1932.
 172. MANN, G. E. Alterations of myocardial permeability by albumin in the isolated, perfused rabbit heart. *J. Physiol. Lond.* 319: 311-323, 1981.
 173. MANN, G. E., L. H. SMAJE, AND D. L. YUDILEVICH. Permeability of the fenestrated capillaries in the cat submandibular gland to lipid-insoluble molecules. *J. Physiol. Lond.* 297: 335-354, 1979.
 174. MARCINIAK, D. L., D. E. DOBBINS, J. J. MACIEJKO, J. B.

- SCOTT, F. J. HADDY, AND G. GREGA. Effects of systematically infused histamine on transvascular fluid and protein transfer. *Am. J. Physiol.* 233 (*Heart Circ. Physiol.* 2): H148-H153, 1977.
175. MARON, M. B. Differential effects of histamine on protein permeability in dog lung and forelimb. *Am. J. Physiol.* 242 (*Heart Circ. Physiol.* 11): H565-H572, 1982.
 176. MARON, M. B. Modification of lymph during passage through the lymph node: effect of histamine. *Am. J. Physiol.* 245 (*Heart Circ. Physiol.* 14): H553-H559, 1983.
 177. MARON, M. B. Effect of elevated vascular pressure transient on protein permeability in the lung. *J. Appl. Physiol.* 67: 305-310, 1989.
 178. MARON, M. B., C. G. PILATI, AND K. C. MAENDER. Effect of hemolysis on reflection coefficient determined by endogenous blood indicators. *J. Appl. Physiol.* 62: 2252-2257, 1987.
 179. MASON, E. A., R. P. WENDT, AND E. H. BRESLER. Similarity relations (dimensional analysis) for membrane transport. *J. Membr. Sci.* 6: 283-298, 1980.
 180. MASON, J. C., F. E. CURRY, AND C. C. MICHEL. The effects of proteins upon the filtration coefficient of individually perfused frog mesenteric capillaries. *Microvasc. Res.* 13: 185-202, 1977.
 181. MAYERSON, H. S. The physiological importance of lymph. In: *Handbook of Physiology. Circulation*. Washington, DC: Am. Physiol. Soc., 1963, sect. 2, vol. II, chapt. 30, p. 1035-1074.
 182. MAYERSON, H. S., C. G. WOLFRAM, H. H. SHIRLEY, AND K. WASSERMAN. Regional differences in capillary permeability. *Am. J. Physiol.* 198: 155-160, 1960.
 183. MAYHAN, W. G., AND W. L. JOYNER. The effects of altering the external calcium concentration and a calcium channel blocker, verapamil, on microvascular leaky sites and dextran clearance in the hamster cheek pouch. *Microvasc. Res.* 28: 159-179, 1984.
 184. McDONAGH, P. F. Both protein and blood cells reduce coronary microvascular permeability to macromolecules. *Am. J. Physiol.* 245 (*Heart Circ. Physiol.* 14): H698-H706, 1983.
 185. McELEARNEY, P. M., AND D. N. GRANGER. Intestinal capillary wall as a charge-selective filter. *Physiologist* 22: 85, 1979.
 186. McNAMEE, J. E. Restricted dextran transport in the sheep lung lymph preparation. *J. Appl. Physiol.* 52: 585-590, 1982.
 187. McNAMEE, J. E., AND F. S. GRODINS. Effects of histamine on microvasculature of isolated dog gracilis muscle. *Am. J. Physiol.* 229: 119-125, 1975.
 188. McNAMEE, J. E., AND N. C. STAUB. Pore models of sheep lung microvascular barrier using new data on protein tracers. *Microvasc. Res.* 18: 229-244, 1979.
 189. MELLANDER, S., B. ÖBERG, AND H. ODELRAM. Vascular adjustments to increased transmural pressure in cat and man with special reference to shifts in capillary fluid transfer. *Acta Physiol. Scand.* 61: 34-48, 1964.
 190. MICHEL, C. C. Flows across the capillary wall. In: *Cardiovascular Fluid Dynamics*, edited by D. H. Bergel. London: Academic, 1972, vol. II, p. 241.
 191. MICHEL, C. C. Filtration coefficients and osmotic reflection coefficients of the walls of single frog mesenteric capillaries. *J. Physiol. Lond.* 309: 341-355, 1980.
 192. MICHEL, C. C. The effects of certain proteins on capillary permeability to fluid and macromolecules. In: *Pathogenicity of Cationic Proteins*, edited by P. P. Lambert, P. Bergmann, and R. Beauwens. New York: Raven, 1983, p. 125.
 193. MICHEL, C. C. Fluid movements through capillary walls. In: *Handbook of Physiology. The Cardiovascular System. Microcirculation*. Bethesda, MD: Am. Physiol. Soc., 1984, sect. 2, vol. IV, pt. 1, chapt. 9, p. 375.
 194. MICHEL, C. C. Review lecture. Capillary permeability and how it may change. *J. Physiol. Lond.* 404: 1-29, 1988.
 195. MICHEL, C. C., AND J. R. LEVICK. Variations in permeability along individually perfused capillaries of the frog mesentery. *Q. J. Exp. Physiol.* 62: 1-10, 1977.
 196. MICHEL, C. C., AND M. E. PHILLIPS. The effect of Ficoll 70 and bovine serum albumin on the permeability properties of individually perfused frog mesenteric capillaries (Abstract). *J. Physiol. Lond.* 291: 39P, 1979.
 197. MICHEL, C. C., AND M. E. PHILLIPS. The effects of bovine serum albumin and a form of cationised ferritin upon the molecular selectivity of the walls of single frog capillaries. *Microvasc. Res.* 29: 190-203, 1985.
 198. MICHEL, C. C., AND M. E. PHILLIPS. Steady-state fluid filtration at different capillary pressures in perfused frog mesenteric capillaries. *J. Physiol. Lond.* 388: 421-435, 1987.
 199. MILLER, F. N., I. G. JOSHUA, J. T. FLEMING, AND N. PARERKH. Histamine-induced protein leakage in hypertensive rats: inhibition by verapamil. *Am. J. Physiol.* 250 (*Heart Circ. Physiol.* 19): H284-H290, 1986.
 200. MOORE, D. H., AND H. RUSKA. The fine structure of capillaries and small arteries. *Proc. Soc. Exp. Biol. Med.* 3: 457-462, 1957.
 201. MORTILLARO, N. A., D. N. GRANGER, P. R. KVIETYS, G. RUTILI, AND A. E. TAYLOR. Effects of histamine and histamine antagonists on intestinal capillary permeability. *Am. J. Physiol.* 240 (*Gastrointest. Liver Physiol.* 3): G381-G386, 1981.
 202. MUNCH, W. D., L. P. ZESTAR, AND J. L. ANDERSON. Rejection of polyelectrolytes from microporous membranes. *J. Membr. Sci.* 5: 77-102, 1979.
 203. MYERS, B. D., J. A. WINETZ, F. CHUI, AND A. S. MICHAELS. Mechanisms of proteinuria in diabetic nephropathy: a study of glomerular barrier function. *Kidney Int.* 21: 633-641, 1982.
 204. NICOLAYSEN, G. Intravascular concentrations of calcium and magnesium ions and edema formation in isolated lungs. *Acta Physiol. Scand.* 81: 325-339, 1971.
 205. NICOLAYSEN, G. Increase in capillary filtration rate resulting from reduction in the intravascular calcium ion concentration. *Acta Physiol. Scand.* 81: 517-527, 1971.
 206. NICOLAYSEN, G. Perfusate qualities and spontaneous edema formation in an isolated perfused lung preparation. *Acta Physiol. Scand.* 83: 563-570, 1971.
 207. NICOLAYSEN, G., B. A. WAALER, AND P. AARSETH. On the existence of stretchable pores in the exchange vessels of the isolated rabbit lung preparation. *Lymphology* 12: 201-207, 1979.
 208. NOER, I., AND N. A. LASSEN. Evidence of active transport (filtration?) of plasma proteins across the capillary walls in muscle and subcutis. *Acta Physiol. Scand. Suppl.* 463: 105-110, 1978.
 209. ÖJTEG, G. *Permeability of Renal Capillaries* (PhD thesis). Uppsala, Sweden: Univ. of Uppsala, 1986.
 210. ÖJTEG, G., K. NYGREN, AND M. WOLGAST. Permeability of renal capillaries. I. Preparation of neutral and charged protein probes. *Acta Physiol. Scand.* 129: 277-286, 1987.
 211. ÖJTEG, G., K. NYGREN, AND M. WOLGAST. Permeability of renal capillaries. II. Transport of neutral and charged protein probes. *Acta Physiol. Scand.* 129: 287-294, 1987.
 212. OLESEN, S.-P. A calcium-dependent reversible permeability increase in microvessels in frog brain, induced by serotonin. *J. Physiol. Lond.* 361: 103-113, 1985.
 213. OLESEN, S.-P., AND C. CRONE. Substances that rapidly augment ionic conductance of endothelium in cerebral venules. *Acta Physiol. Scand.* 127: 233-241, 1986.
 214. OLIVER, D. J., S. ANDERSON, J. L. TROY, B. M. BRENNER, AND W. M. DEEN. Normal glomerular filtration barrier is more size-restrictive than previously determined (Abstract). *J. Am. Soc. Nephrol.* 2: 525, 1991.
 215. PALADE, G. E. Fine structure of blood capillaries (Abstract). *J. Appl. Physiol.* 24: 1424, 1953.
 216. PALADE, G. E. Role of plasmalemmal vesicles. In: *The Lung: Scientific Foundations*, edited by R. G. Cyrstal, J. B. West, P. J. Barnes, N. S. Cherniack, and E. R. Weibel. New York: Raven, 1991, p. 359.
 217. PAPPENHEIMER, J. R., E. M. RENKIN, AND L. M. BORRERO. Filtration, diffusion and molecular sieving through peripheral capillary membranes. A contribution to the pore theory of capillary permeability. *Am. J. Physiol.* 167: 13-46, 1951.
 218. PAPPENHEIMER, J. R., AND A. SOTO-RIVERA. Effective osmotic pressure of the plasma proteins and other quantities associated with the capillary circulation in the hindlimbs of dogs and cats. *Am. J. Physiol.* 152: 471-491, 1948.
 219. PARKER, J. C., S. GILCHRIST, AND J. T. CARTLEDGE.

- Plasma-lymph exchange and interstitial distribution volumes of charged macromolecules in the lung. *J. Appl. Physiol.* 59: 1128-1136, 1985.
220. PARKER, J. C., R. E. PARKER, D. N. GRANGER, AND A. E. TAYLOR. The effect of fluid volume loading on exclusion of albumin and lymph flow in the dog lung. *Circ. Res.* 45: 440-450, 1979.
 221. PARKER, J. C., R. E. PARKER, D. N. GRANGER, AND A. E. TAYLOR. Vascular permeability and transvascular fluid and protein transport in the dog lung. *Circ. Res.* 48: 545-561, 1981.
 222. PARKER, J. C., M. A. PERRY, AND A. E. TAYLOR. Permeability of the microvascular barrier. In: *Edema*, edited by N. C. Staub and A. E. Taylor. New York: Raven, 1984, p. 143.
 223. PARKER, J. C., B. RIPPE, AND A. E. TAYLOR. Fluid filtration and protein clearances through large and small populations in dog lung capillaries. *Microvasc. Res.* 31: 1-17, 1986.
 224. PARKER, J. C., M. I. TOWNSLEY, B. RIPPE, A. E. TAYLOR, AND J. THIGPEN. Increased microvascular permeability in dog lungs due to high peak airway pressures. *J. Appl. Physiol.* 57: 1809-1816, 1984.
 225. PARKER, R. E., R. J. ROSELLI, AND K. L. BRIGHAM. Effects of prolonged elevated microvascular pressure on lung fluid balance in sheep. *J. Appl. Physiol.* 58: 869-874, 1985.
 226. PARVING, H.-H., S. L. NIELSEN, AND N. A. LASSEN. Increased transcapillary escape rate of albumin, IgG and IgM during angiotensin II-induced hypertension in man. *Scand. J. Clin. Lab. Invest.* 34: 111-118, 1974.
 227. PARVING, H.-H., N. ROSSING, S. L. NIELSEN, AND N. A. LASSEN. Increased transcapillary escape rate of albumin, IgG, and IgM after plasma volume expansion. *Am. J. Physiol.* 227: 245-250, 1974.
 228. PATLAK, C. S., D. A. GOLDSTEIN, AND J. F. HOFFMAN. The flow of solute and solvent across two-membrane system. *J. Theor. Biol.* 5: 425-442, 1963.
 229. PATLAK, C. S., AND S. I. RAPOPORT. Theoretical analysis of net tracer flux due to volume circulation in a membrane with pores of different sizes. Relation to solute drag model. *J. Gen. Physiol.* 57: 113-124, 1971.
 230. PERL, W. Convection and permeation of albumin between plasma and interstitium. *Microvasc. Res.* 10: 83-94, 1975.
 231. PERRY, M. A., J. N. BENOIT, P. R. KVIETYS, AND D. N. GRANGER. Restricted transport of cationic macromolecules across the intestinal capillaries. *Am. J. Physiol.* 245 (*Gastrointest. Liver Physiol.* 8): G568-G572, 1983.
 - 231a. PERRY, M. A., W. J. CROOK, AND D. N. GRANGER. Permeability of gastric capillaries to small and large molecules. *Am. J. Physiol.* 241 (*Gastrointest. Liver Physiol.* 4): G478-G486, 1981.
 232. PERRY, M., AND D. GARLICK. Transcapillary efflux of gamma globulin in rabbit skeletal muscle. *Microvasc. Res.* 9: 119-126, 1975.
 233. PERRY, M. A., C. A. NAVIA, D. N. GRANGER, J. C. PARKER, AND A. E. TAYLOR. Calculation of equivalent pore radii in dog hindpaw capillaries using endogenous lymph and plasma proteins. *Microvasc. Res.* 26: 250-253, 1983.
 234. PERSSON, C. G. A., AND E. SVENJSÖ. Vascular responses and their suppression: drugs interfering with venular permeability. In: *Handbook of Inflammation. The Pharmacology of Inflammation*, edited by I. L. Bonta, M. A. Bray, and M. J. Parnham. Amsterdam: Elsevier, 1985, vol. 5, p. 61.
 235. PHILLIPS, M. E., AND M. R. TURNER. The effects of haemoglobin and myoglobin on the filtration coefficient of single frog mesenteric capillaries (Abstract). *J. Physiol. Lond.* 329: 39P, 1981.
 236. PIETRA, G. G., A. P. FISHMAN, P. N. LANKEEN, P. SAMPSON, AND J. HANSEN-FLASCHEN. Permeability of pulmonary endothelium to neutral and charged macromolecules. *Ann. NY Acad. Sci.* 401: 241-247, 1982.
 237. PIETRA, G. G., J. P. SZIDON, M. M. LEVENTHAL, AND A. P. FISHMAN. Hemoglobin as a tracer in hemodynamic pulmonary edema. *Science Wash. DC* 166: 1643-1646, 1969.
 238. PILATI, C. F., AND M. B. MARON. A technique to measure the reflection coefficient using endogenous vascular indicators. *Microvasc. Res.* 32: 255-260, 1986.
 239. POWERS, M. R., AND D. R. BELL. Initial equilibration of albumin and IgG in rabbit hind paw skin and lymph. *Microvasc. Res.* 40: 230-245, 1990.
 240. POWERS, M. R., J. R. WALLACE, AND D. R. BELL. Initial equilibration of albumin in rabbit hindpaw skin and lymph. *Am. J. Physiol.* 254 (*Heart Circ. Physiol.* 23): H89-H101, 1988.
 241. PUTNEY, J. W., JR., H. TAKEMURA, A. R. HUGHES, D. A. HORSTMAN, AND O. THASTRUP. How do inositol phosphates regulate calcium signalling? *FASEB J.* 3: 1899-1905, 1989.
 242. REED, R. K. Transcapillary extravasation rate of albumin in rat skeletal muscle. Effect of motor activity. *Acta Physiol. Scand.* 125: 719-725, 1985.
 243. REED, R. K. Transcapillary albumin extravasation in rat skin and skeletal muscle: effect of increased venous pressure. *Acta Physiol. Scand.* 134: 375-382, 1988.
 244. REED, R. K., S. JOHANSEN, AND H. NODDELAND. Turnover rate of interstitial albumin in rat skin and skeletal muscle. Effects of limb movements and motor activity. *Acta Physiol. Scand.* 125: 711-718, 1985.
 245. REED, R. K., M. I. TOWNSLEY, AND A. E. TAYLOR. Estimation of capillary reflection coefficients and unique PS products in the dog paw. *Am. J. Physiol.* 257 (*Heart Circ. Physiol.* 26): H1037-H1041, 1989.
 246. REED, R. K., M. I. TOWNSLEY, R. J. KORTHUIS, AND A. E. TAYLOR. Analysis of lymphatic protein flux data. V. Unique PS products and σ_{ds} at low lymph flows. *Am. J. Physiol.* 261 (*Heart Circ. Physiol.* 30): H1728-H1749, 1991.
 247. RENKIN, E. M. Transport of large molecules across capillary walls. *Physiologist* 7: 13-28, 1964.
 248. RENKIN, E. M. Multiple pathways of capillary permeability. *Circ. Res.* 41: 735-743, 1977.
 249. RENKIN, E. M. Relation of capillary morphology to transport of fluid and large molecules: a review. *Acta Physiol. Scand. Suppl.* 463: 81-91, 1979.
 250. RENKIN, E. M. Lymph as a measure of the composition of interstitial fluid. In: *Pulmonary Edema*, edited by A. P. Fishman and E. M. Renkin. Bethesda, MD: Am. Physiol. Soc., 1979, p. 145.
 251. RENKIN, E. M. Ambiguities and errors in evaluation of capillary pore sizes. Letter to the editor. *Am. J. Physiol.* 240 (*Heart Circ. Physiol.* 9): H145-H147, 1980.
 252. RENKIN, E. M. Capillary transport of macromolecules: pores and other endothelial pathways. *J. Appl. Physiol.* 58: 315-325, 1985.
 253. RENKIN, E. M. Some consequences of capillary permeability to macromolecules: Starling's hypothesis reconsidered. *Am. J. Physiol.* 250 (*Heart Circ. Physiol.* 19): H706-H710, 1986.
 254. RENKIN, E. M. Transport pathways and processes. In: *Endothelial Cell Biology*, edited by N. Simionescu and M. Simionescu. New York: Plenum, 1988, p. 51.
 255. RENKIN, E. M., R. D. CARTER, AND W. L. JOYNER. Mechanism of the sustained action of histamine and bradykinin on transport of large molecules across capillary walls in the dog paw. *Microvasc. Res.* 7: 49-60, 1974.
 256. RENKIN, E. M., AND F. E. CURRY. Transport of water and solutes across capillary endothelium. In: *Membrane Transport in Biology*, edited by G. Giebisch, D. C. Tosteson, and H. H. Ussing. Berlin: Springer-Verlag, 1978, vol. IV, chapt. 1, p. 1.
 257. RENKIN, E. M., AND D. G. GARLICK. Blood-lymph transport of macromolecules. *Microvasc. Res.* 2: 392-398, 1970.
 258. RENKIN, E. M., M. GUSTAFSON-SGRO, AND L. SIBLEY. Coupling of albumin flux to volume flow in skin and muscles of anesthetized rats. *Am. J. Physiol.* 255 (*Heart Circ. Physiol.* 24): H458-H466, 1988.
 259. RENKIN, E. M., W. L. JOYNER, C. H. SLOOP, AND P. D. WATSON. Influence of venous pressure on plasma-lymph transport in the dog's paw: convective and dissipative mechanisms. *Microvasc. Res.* 14: 191-204, 1977.
 260. RENKIN, E. M., K. REW, M. WONG, D. O'LOUGHLIN, AND L. SIBLEY. Influence of saline infusion on blood-tissue albumin transport. *Am. J. Physiol.* 257 (*Heart Circ. Physiol.* 26): H525-H533, 1989.
 261. RENKIN, E. M., V. L. TUCKER, K. REW, D. O'LOUGHLIN, M. WONG, AND L. SIBLEY. Volume expansion with colloids in-

- creases blood-tissue albumin transport. *Am. J. Physiol.* 262 (Heart Circ. Physiol. 31): H1054-H1067, 1992.
262. RENKIN, E. M., P. D. WATSON, W. M. SLOOP, AND F. E. CURRY. Transport pathways for fluid and large molecules in microvascular endothelium of the dog's paw. *Microvasc. Res.* 14: 205-214, 1977.
 263. RICHARDSON, P. D. I., D. N. GRANGER, D. MAILMAN, AND P. R. KVIETYS. Permeability characteristics of colonic capillaries. *Am. J. Physiol.* 239 (Gastrointest. Liver Physiol. 2): G300-G305, 1980.
 264. RIPPE, B. *Relationships Between Diffusion and Convection Across Capillary Walls* (PhD thesis). Göteborg, Sweden: Univ. of Göteborg, 1978, p. 1-75.
 265. RIPPE, B., R. C. ALLISON, J. C. PARKER, AND A. E. TAYLOR. Effects of histamine, serotonin, and norepinephrine on circulation of dog lungs. *J. Appl. Physiol.* 57: 223-232, 1984.
 266. RIPPE, B., AND C. CRONE. Pores and intercellular junctions. In: *The Lung: Scientific Foundations*, edited by R. G. Crystal, J. B. West, P. J. Barnes, N. S. Cherniack, and E. R. Weibel. New York: Raven, 1991, p. 349.
 267. RIPPE, B., AND B. FOLKOW. Capillary permeability to albumin in normotensive and spontaneously hypertensive rats. *Acta Physiol. Scand.* 101: 72-83, 1977.
 268. RIPPE, B., AND B. FOLKOW. Simultaneous measurements of capillary filtration and diffusion capacities during infusions of noradrenaline (NA) and 5-hydroxytryptamine (5-HT) into the rat hindquarter vascular bed. *Acta Physiol. Scand.* 109: 265-273, 1980.
 269. RIPPE, B., AND G. J. GREGA. Effects of isoprenaline and cooling on histamine induced changes of capillary permeability in the rat hindquarter vascular bed. *Acta Physiol. Scand.* 103: 252-262, 1978.
 270. RIPPE, B., AND B. HARALDSSON. Underestimation of capillary convection of albumin by homoporous treatment of protein transport across the microvascular membrane. *Microvasc. Res.* 30: 246-248, 1985.
 271. RIPPE, B., AND B. HARALDSSON. Capillary permeability in rat hindquarters as determined by estimations of capillary reflection coefficients. *Acta Physiol. Scand.* 127: 289-303, 1986.
 272. RIPPE, B., AND B. HARALDSSON. A technique for assessing capillary permeability from transvascular protein flux data obtained at low filtration rates. *Acta Physiol. Scand.* 127: 263-265, 1986.
 273. RIPPE, B., AND B. HARALDSSON. On the steady-state relationship between the microvascular hydrostatic pressure and the transvascular filtration rate. Effects of heteroporosity. *Acta Physiol. Scand.* 129: 441-442, 1987.
 274. RIPPE, B., AND B. HARALDSSON. Fluid and protein fluxes across the microvasculature. Application of two-pore equations. *Acta Physiol. Scand.* 131: 411-428, 1987.
 275. RIPPE, B., AND B. HARALDSSON. Mechanisms associated with charged macromolecule transport across capillary endothelium. In: *Microcirculation—An Update*, edited by M. Tsuchiya, M. Asano, Y. Mishima, and M. Oda. Amsterdam: Elsevier, 1987, vol. 1, p. 145.
 276. RIPPE, B., AND B. HARALDSSON. How are macromolecules transported across the capillary wall? *News Physiol. Sci.* 2: 135-138, 1987.
 277. RIPPE, B., B. HARALDSSON, AND B. FOLKOW. Evaluation of the "stretched pore phenomenon" in isolated perfused rat hindquarters. *Acta Physiol. Scand.* 125: 453-459, 1985.
 278. RIPPE, B., A. KAMIYA, AND B. FOLKOW. Simultaneous measurements of capillary diffusion and filtration exchange during shifts in filtration/absorption and at graded alterations in the capillary permeability surface area product (PS). *Acta Physiol. Scand.* 105: 171-187, 1978.
 279. RIPPE, B., A. KAMIYA, AND B. FOLKOW. Transcapillary passage of albumin, effects of tissue cooling and of increases in filtration and plasma colloid osmotic pressure. *Acta Physiol. Scand.* 105: 171-187, 1979.
 280. RIPPE, B., AND G. STELIN. Simulations of peritoneal solute transport during CAPD. Application of two-pore formalism. *Kidney Int.* 35: 1234-1244, 1989.
 281. RIPPE, B., G. STELIN, AND I. AHLMÉN. Basal permeability of the peritoneal membrane during continuous ambulatory peritoneal dialysis (CAPD). In: *Advances in Peritoneal Dialysis; Proceedings of the Second International Symposium on Peritoneal Dialysis 1981*. Amsterdam: Excerpta Med., 1981, p. 5-9. (Int. Congr. Ser. 567)
 282. RIPPE, B., G. STELIN, AND B. HARALDSSON. Computer simulations of peritoneal fluid transport in CAPD. *Kidney Int.* 40: 315-325, 1991.
 283. RIPPE, B., M. I. TOWNSLEY, J. C. PARKER, AND A. E. TAYLOR. Osmotic reflection coefficient for total plasma protein in lung microvessels. *J. Appl. Physiol.* 58: 436-442, 1985.
 284. RIPPE, B., M. I. TOWNSLEY, AND A. E. TAYLOR. Effects of plasma- and cell-free perfusates on filtration coefficient of perfused canine lungs. *J. Appl. Physiol.* 58: 1521-1527, 1985.
 285. RIPPE, B., M. I. TOWNSLEY, J. THIGPEN, J. C. PARKER, R. J. KORTHUIS, AND A. E. TAYLOR. Effects of vascular pressure on the pulmonary microvasculature in isolated dog lungs. *J. Appl. Physiol.* 57: 233-239, 1984.
 286. ROBINSON, G. B., J. BRAY, J. BYRNE, AND D. A. HUME. Studies of ultrafiltration of macromolecules across glomerular basement membranes. In: *Glomerular Basement Membrane*, edited by G. Lubec and B. G. Hudson. London: Libby, 1985, p. 7.
 287. RODEWALD, R., AND M. J. KARNOVSKY. Porous substructure of the glomerular slit diaphragm in the rat and mouse. *J. Cell Biol.* 60: 423-433, 1974.
 288. ROSELL, S. Microcirculation in adipose tissue. In: *Handbook of Physiology. The Cardiovascular System. Microcirculation*. Bethesda, MD: Am. Physiol. Soc., 1984, sect. 2, vol. IV, pt. 2, chapt. 20, p. 949-968.
 289. RUTILI, G. *Transport of Macromolecules in Subcutaneous Tissue Studied by FITC-Dextran* (PhD thesis). Uppsala, Sweden: Univ. of Uppsala, 1978.
 290. RUTILI, G., AND K.-E. ARFORSS. Fluorescein labelled dextran measurement in interstitial fluid in studies of macromolecular permeability. *Microvasc. Res.* 12: 221-230, 1976.
 291. RUTILI, G., AND K.-E. ARFORSS. Protein concentration in interstitial and lymphatic fluids from the subcutaneous tissue. *Acta Physiol. Scand.* 99: 1-8, 1977.
 292. RUTILI, G., D. N. GRANGER, A. E. TAYLOR, J. C. PARKER, AND N. A. MORTILLARO. Analysis of lymphatic protein data IV. Comparison of the different methods used to estimate reflection coefficients and permeability-surface area products. *Microvasc. Res.* 23: 347-360, 1982.
 293. SCHNITZER, J. E., P. O. J. BRAVO, AND E. PINNEY. High affinity albumin binding to pulmonary microvascular endothelium is inhibited by the interaction of anti-sparc antibodies with GP60 (Abstract). In: *Proc. World Congr. Microcirc. 5th Louisville KY 1991*, p. 98.
 294. SCHNITZER, J. E., W. W. CARLEY, AND G. E. PALADE. Albumin interacts specifically with a 60-kDa microvascular endothelial glycoprotein. *Proc. Natl. Acad. Sci. USA* 85: 6773-6777, 1988.
 - 294a. SCHNITZER, J. E., AND E. PINNEY. Quantitation of specific binding of orosomucoid to cultured microvascular endothelium: role in capillary permeability. *Am. J. Physiol.* 263 (Heart Circ. Physiol. 32): H48-H55, 1992.
 295. SEEGER, W., D. WALMRATH, N. HEIMBURGER, AND H. NEUHOF. Fibronectin decreases pulmonary vascular permeability under baseline conditions and after administration of arachidonic acid in rabbit lungs. *Thromb. Res.* 44: 135-146, 1986.
 296. SEJRSEN, P. Capillary permeability measured by bolus injection, residue and venous detection. *Acta Physiol. Scand.* 105: 73-92, 1979.
 297. SEJRSEN, P., W. P. PAASKE, AND O. HENRIKSEN. Capillary permeability of 131-I-albumin in skeletal muscle. *Microvasc. Res.* 29: 265-281, 1985.
 298. SHASBY, D. M., AND S. S. SHASBY. Active transendothelial transport of albumin. Interstitium to lumen. *Circ. Res.* 57: 903-908, 1985.
 299. SHASBY, D. M., AND S. S. SHASBY. Effects of calcium on transendothelial albumin transfer and electrical resistance. *J. Appl. Physiol.* 60: 71-79, 1986.
 300. SHEMESH, O., J. C. ROSS, W. M. DEEN, G. W. GRANT, AND B. D. MYERS. Nature of the glomerular capillary injury in hu-

- man membranous glomerulopathy. *J. Clin. Invest.* 77: 868-877, 1986.
301. SHEPARD, J. M., D. G. MOON, P. F. SHERMAN, L. K. WESTON, P. J. DEL VECCHIO, F. L. MINNEAR, A. B. MALIK, AND J. E. KAPLAN. Platelets decrease albumin permeability of pulmonary artery endothelial cell monolayers. *Microvasc. Res.* 37: 256-266, 1989.
 302. SHIRLEY, H. H., G. G. WOLFRAM, K. WASSERMAN, AND H. S. MAYERSON. Capillary permeability to macromolecules: stretched pore phenomenon. *Am. J. Physiol.* 190: 189-193, 1957.
 303. SIFLINGER-BIRNBOIM, A., P. J. DEL VECCHIO, J. A. COOPER, AND A. B. MALIK. Transendothelial albumin flux: evidence against asymmetric transport. *J. Appl. Physiol.* 61: 2035-2039, 1986.
 304. SIMIONESCU, D., AND M. SIMIONESCU. Differentiated distribution of the cell surface charge on the alveolar-capillary unit. *Microvasc. Res.* 25: 85-100, 1983.
 305. SIMIONESCU, M., L. GHITESCU, A. FIXMAN, AND N. SIMIONESCU. How plasma macromolecules cross the endothelium. *News Physiol. Sci.* 2: 97-100, 1987.
 306. SIMIONESCU, M., AND N. SIMIONESCU. Ultrastructure of the microvascular wall: functional correlations. In: *Handbook of Physiology. The Cardiovascular System. Microcirculation*. Bethesda, MD: Am. Physiol. Soc., 1984, sect. 2, vol. IV, pt. 1, p. 41.
 307. SIMIONESCU, M., AND N. SIMIONESCU. Functions of the endothelial cell surface. *Annu. Rev. Physiol.* 48: 279-293, 1986.
 308. SIMIONESCU, M., N. SIMIONESCU, AND G. E. PALADE. Preferential distribution of anionic sites on the basement membrane and the abluminal aspect of the endothelium in fenestrated capillaries. *J. Cell Biol.* 95: 425-434, 1982.
 309. SIMIONESCU, N. Cellular aspects of transcapillary exchange. *Physiol. Rev.* 63: 1536-1579, 1983.
 310. SIMIONESCU, N., AND M. SIMIONESCU. Interactions of endogenous lipoproteins with capillary endothelium in spontaneously hyperlipoproteinemic rats. *Microvasc. Res.* 30: 314-332, 1985.
 311. SIMIONESCU, N., M. SIMIONESCU, AND G. E. PALADE. Permeability of muscle capillaries to small heme peptides. Evidence for the existence of patent transendothelial channels. *J. Cell Biol.* 64: 586-607, 1975.
 312. SMITH, F. G., AND W. M. DEEN. Electrostatic double-layer interactions for spherical colloids in cylindrical pores. *J. Colloid Interface Sci.* 78: 444-465, 1980.
 313. SMITH, L., S. ANDREASSON, K. THORÉN-TOLLING, B. RIPPE, AND B. RISBERG. Estimations of equivalent small and large pore radii in the pulmonary microvasculature following lung lymph fistula preparation in sheep. *J. Appl. Physiol.* 62: 2300-2307, 1987.
 314. STELIN, G., AND B. RIPPE. A phenomenological interpretation of the variation in dialysate volume with dwell time in CAPD. *Kidney Int.* 38: 465-472, 1990.
 315. STOLTE, H., H.-J. SCHUREK, AND J. M. ALT. Glomerular albumin filtration: a comparison of micropuncture studies in the isolated perfused rat kidney with in vivo experimental conditions. *Kidney Int.* 16: 377-384, 1979.
 316. STRAY-PEDERSEN, S. The effect of Ca^{2+} , Mg^{2+} and H^+ on the capillary permeability of the rete mirabile of the eel, *Anguilla vulgaris* L. *Acta Physiol. Scand.* 94: 423-441, 1975.
 317. STUDER, R., AND J. POTCHEN. The radioisotopic assessment of regional microvascular permeability to macromolecules. *Microvasc. Res.* 3: 35-48, 1971.
 318. SVEN SJÖ, E. *Characterization of Leakage of Macromolecules in Postcapillary Venules* (PhD thesis). Uppsala, Sweden: Univ. of Uppsala, 1978.
 319. SVEN SJÖ, E., AND W. L. JOYNER. The effects of intermittent and continuous stimulation of microvessels in the cheek pouch of hamsters with histamine and bradykinin on the development of venular leaky sites. *Microcirc. Endothelium Lymphatics* 1: 381-396, 1984.
 320. SVEN SJÖ, E., C. G. A. PERSSON, AND G. RUTILI. Inhibition of bradykinin induced macromolecular leakage from postcapillary venules by a β_2 -adrenoceptors stimulant, terbutaline. *Acta Physiol. Scand.* 101: 504-506, 1977.
 321. SVEN SJÖ, E., AND K. ROEMPKE. Microvascular aspects of edema formation and its inhibition by β_2 -receptor stimulants and some other anti-inflammatory drugs. In: *Progress in Microcirculation Research II*, edited by F. C. Courtice, D. G. Garlick, and M. A. Perry. Australia: Univ. of New South Wales, 1984, vol. 1, p. 449.
 322. TAY, M., W. D. COMPER, AND A. K. SINGH. Charge selectivity in kidney ultrafiltration is associated with glomerular uptake of transport probes. *Am. J. Physiol.* 260 (Renal Fluid Electrolyte Physiol. 29): F549-F554, 1991.
 323. TAYLOR, A. E. Capillary fluid filtration: Starling forces and lymph flow. *Circ. Res.* 49: 557-575, 1981.
 324. TAYLOR, A. E., AND D. N. GRANGER. Equivalent pore modeling: vesicles and channels. *Federation Proc.* 42: 2440-2445, 1983.
 325. TAYLOR, A. E., AND D. N. GRANGER. Exchange of macromolecules across the microcirculation. In: *Handbook of Physiology. The Cardiovascular System. Microcirculation*. Bethesda, MD: Am. Physiol. Soc., 1984, sect. 2, vol. IV, chapt. 11, p. 467.
 326. TAYLOR, A. E., D. N. GRANGER, AND R. A. BRACE. Analysis of lymphatic protein flux data. I. Estimation of the reflection coefficient and permeability surface area product for total protein. *Microvasc. Res.* 13: 297-313, 1977.
 327. TAYLOR, A. E., AND J. C. PARKER. The pulmonary interstitial spaces and lymphatics. In: *Handbook of Physiology. Circulation and Nonrespiratory Functions. The Respiratory System*. Bethesda, MD: Am. Physiol. Soc., 1985, sect. 3, vol. I, chapt. 4, p. 167.
 328. TAYLOR, A. E., AND B. RIPPE. Pulmonary edema. In: *Physiology of Membrane Disorders* (2nd ed.), edited by T. E. Andreoli, D. D. Fanestil, J. F. Hoffman, and S. G. Schultz. New York: Plenum, 1986, p. 1025-1039.
 329. THOMAS, S. R., AND D. C. MIKULECKY. Transepithelial solute exchange. A comparison of the Kedem-Katchalsky convection-diffusion equations with the rigorous non-linear equations for this special case. *Microvasc. Res.* 15: 207-220, 1978.
 330. TIMPLE, R., H. WIEDEMAN, V. VAN DELDEN, H. FURTH-MAYR, AND K. KUHN. Network model for the organization of type IV collagen molecules in basement membranes. *Eur. J. Biochem.* 120: 203-211, 1981.
 331. TOMLANOVICH, S., W. M. DEEN, H. W. JONES III, H. C. SCHWARTZ, AND B. D. MYERS. Functional nature of glomerular injury in progressive diabetic glomerulopathy. *Diabetes* 36: 556-565, 1987.
 332. TOWNSLEY, M. I., E. H. LIM, T. M. SAHAWNEH, AND W. SONG. Interaction of chemical and high vascular pressure injury in isolated canine lung. *J. Appl. Physiol.* 69: 1657-1664, 1990.
 - 332a. TOWNSLEY, M. I., S. M. SMITH, R. K. REED, V. H. PITTS, AND A. E. TAYLOR. Ileal microvascular permeability: a comparison of PS and σ_d using lymphatic and isotopic protein clearances. *Am. J. Physiol.* 262 (Gastrointest. Liver Physiol. 25): G572-G580, 1992.
 333. TURNER, M. R., G. CLOUGH, AND C. C. MICHEL. The effects of cationised ferritin and native ferritin upon the filtration coefficient of single frog capillaries. Evidence that proteins in the endothelial cell coat influence permeability. *Microvasc. Res.* 25: 205-222, 1983.
 334. VARGAS, F., AND J. A. JOHNSON. An estimate of reflection coefficients for rabbit heart capillaries. *J. Gen. Physiol.* 47: 667-677, 1964.
 335. VASILE, E., M. SIMIONESCU, AND N. SIMIONESCU. Visualization of the binding, endocytosis, and transcytosis of low density lipoprotein in the arterial endothelium in situ. *J. Cell Biol.* 96: 1677-1689, 1983.
 336. WAGNER, R. C., AND J. R. CASLEY-SMITH. Review: endothelial vesicles. *Microvasc. Res.* 21: 267-298, 1981.
 337. WAGNER, R. C., AND S.-C. CHEN. Transepithelial transport of solute by the endothelial vesicular system: evidence from thin serial section analysis. *Microvasc. Res.* 42: 139-150, 1991.
 338. WASSERMAN, K., L. LOEB, AND H. S. MAYERSON. Capillary permeability to macromolecules. *Circ. Res.* 3: 594-603, 1955.
 339. WATSON, P. D. Effects of blood-free and protein-free perfusion on CFC in the isolated cat hindlimb. *Am. J. Physiol.* 245 (Heart Circ. Physiol. 14): H911-H919, 1983.
 340. WATSON, P. D. Effect of plasma and red blood cells on water

- permeability in cat hindlimb. *Am. J. Physiol.* 246 (Heart Circ. Physiol. 15): H818-H823, 1984.
341. WATSON, P. D., D. R. BELL, AND E. M. RENKIN. Early kinetics of large molecule transport between plasma and lymph in dogs. *Am. J. Physiol.* 239 (Heart Circ. Physiol. 8): H525-H531, 1980.
 342. WATSON, P. D., AND F. S. GRODINS. An analysis of the effects of the interstitial matrix on plasma-lymph transport. *Microvasc. Res.* 16: 19-41, 1978.
 343. WATSON, P. D., AND M. B. WOLF. Dextran and capillary filtration coefficient in cat hindlimb. *Am. J. Physiol.* 248 (Heart Circ. Physiol. 17): H452-H456, 1985.
 344. WATSON, P. D., AND M. B. WOLF. Filtration coefficient in cat hindlimb using protein concentration changes. *Am. J. Physiol.* 256 (Heart Circ. Physiol. 25): H186-H194, 1989.
 345. WEISER, P. C., AND F. GRANDE. Estimation of fluid shifts and protein permeability during pulmonary edemagenesis. *Am. J. Physiol.* 226: 1028-1034, 1974.
 346. WENDT, R. P., E. A. MASON, AND E. H. BRESLER. Effect of heteroporousity on flux equations for membranes. *Biophys. Chem.* 4: 237-247, 1976.
 347. WESELCOUCH, E. O., C. J. LUNEAU, K. J. WILLIAMS, AND R. E. GOSELIN. The failure of serum albumin to affect capillary permeability in the isolated rabbit heart. *Microvasc. Res.* 28: 373-386, 1984.
 348. WEST, J. B., K. TSUKIMOTO, O. MATHIEU-COSTELLO, AND R. PREDILETTO. Stress failure in pulmonary capillaries. *J. Appl. Physiol.* 70: 1731-1742, 1991.
 349. WINETZ, J. A., H. V. GOLBETZ, R. J. SPENCER, J. A. LEE, AND B. D. MYERS. Glomerular function in advanced human diabetic nephropathy. *Kidney Int.* 21: 750-756, 1982.
 350. WINNE, D. Die Capillarpermeabilität hochmolekularen Substanzen. *Pfluegers Arch.* 283: 119-136, 1965.
 351. WISSIG, S. L. Identification of the small pore in skeletal muscle. *Acta Physiol. Scand. Suppl.* 463: 33-44, 1979.
 352. WISSIG, S. L., AND M. C. WILLIAMS. Permeability of muscle capillaries to microperoxidase. *J. Cell Biol.* 76: 341-359, 1978.
 353. WOLF, M. B., L. P. PORTER, AND P. D. WATSON. Effects of elevated venous pressure on capillary permeability in cat hindlimbs. *Am. J. Physiol.* 257 (Heart Circ. Physiol. 26): H2025-H2032, 1989.
 354. WOLF, M. B., D. R. SCOTT II, AND P. D. WATSON. Microvascular permeability transient due to histamine in cat limb. *Am. J. Physiol.* 261 (Heart Circ. Physiol. 30): H220-H228, 1991.
 355. WOLF, M. B., AND P. D. WATSON. Measurement of osmotic reflection coefficient for small molecules in cat hindlimbs. *Am. J. Physiol.* 256 (Heart Circ. Physiol. 25): H282-H290, 1989.
 356. WOLF, M. B., P. D. WATSON, AND D. R. SCOTT II. Integral-mass balance method for determination of solvent-drag reflection coefficient. *Am. J. Physiol.* 253 (Heart Circ. Physiol. 22): H194-H204, 1987.
 357. WOLGAST, M., AND G. ÖJTEG. Electrophysiology of renal capillary membranes: gel concept applied and Starling model challenged. *Am. J. Physiol.* 254 (Renal Fluid Electrolyte Physiol. 23): F364-F373, 1988.
 358. WRAIGHT, E. P. Capillary permeability to protein as a factor in the control of plasma volume. *J. Physiol. Lond.* 237: 39-47, 1974.
 359. YOSHIOKA, T., H. G. RENNKE, AND D. J. SALANT. Role of abnormally high transmural pressure in the permselectivity defect of glomerular capillary wall: a study in early passive Heymann nephritis. *Circ. Res.* 61: 531-538, 1987.
 360. YOUNG, G. A., A. M. BROWNJOHN, AND F. M. PARSONS. Protein losses in patients receiving continuous ambulatory peritoneal dialysis. *Nephron* 45: 196-201, 1987.